University of Calgary

PRISM Repository **https://prism.ucalgary.ca**

The Vault Open Theses and Dissertations

2019-08-09

Investigating groundwater recharge rates and seasonality under irrigated and dryland conditions at two agricultural sites near Lethbridge, Alberta

Hughes, Alexandra Therese

Hughes, A. T. (2019). Investigating groundwater recharge rates and seasonality under irrigated and dryland conditions at two agricultural sites near Lethbridge, Alberta (Master's thesis, University of Calgary, Calgary, Canada). Retrieved from https://prism.ucalgary.ca. http://hdl.handle.net/1880/110720

Downloaded from PRISM Repository, University of Calgary

UNIVERSITY OF CALGARY

Investigating groundwater recharge rates and seasonality under irrigated and dryland conditions at two agricultural sites near Lethbridge, Alberta

by

Alexandra Therese Hughes

A THESIS

SUBMITTED TO THE FACULTY OF GRADUATE STUDIES

IN PARTIAL FULFILMENT OF THE REQUIREMENTS FOR THE

DEGREE OF MASTER OF SCIENCE

GRADUATE PROGRAM IN GEOLOGY AND GEOPHYSICS

CALGARY, ALBERTA

AUGUST, 2019

© Alexandra Therese Hughes 2019

Abstract

In order to better understand the impacts of land use on groundwater resources, this study investigated the effects of irrigation on groundwater recharge at two study sites near Lethbridge, Alberta. Depression-focused and diffuse recharge rates were quantified beneath uplands, flatlands and depressions under irrigated and dryland conditions using the chloride mass balance, water table fluctuation and water balance methods. Seasonality of recharge was also considered (i.e., summer vs. overwinter). Results show long-term recharge rates of 88 ± 26 to 113 ± 31 mm/yr beneath depressions, 50 ± 21 to 29 ± 44 mm/yr beneath flatlands and -4 ± 5 to 4 ± 2 mm/yr beneath uplands. Overwinter (November 2017-April 2018) snowmelt recharge was the same for irrigated and dryland flatlands (between 33 ± 7 and 68 ± 113 mm). Recharge during the 2018 growing season was 42 ± 141 and 21 ± 122 mm beneath the irrigated and dryland flatlands, respectively. Numerical model simulations showed 3.1 times more summer recharge under irrigated versus dryland flatland conditions. Irrigation was shown to affect both the rate and seasonality of recharge at the two study sites.

Acknowledgements

Thank you first and foremost to my supervisor, Dr. Ed Cey, who provided unwavering guidance and support throughout this project. Also thank you to Dr. Masaki Hayashi for his contribution to the project in terms of both big picture goals and small but important details. The collaboration of the entire GRIP team at the U of C throughout this study was invaluable. Thanks to the many people who braved windy trips to LDF with me: Evan Sieben, Eric Mott and Brandon Hill, among many of the GRIP team members. This project could not have been possible without the cooperation and helpfulness of the LDF staff, Jim Parker, Mike Ellefson and Ward Henry, as well as the willingness of the Perry Family to allow studies on their land. Thanks to Willemijn Appels, Josh Bishop, Paul Fontaine and Kristyn Juergensen from Lethbridge College for useful discussions and help with snow survey data collection. Funding for this study was provided by the Natural Sciences and Engineering Research Council of Canada (NSERC), Alberta Innovates, and Alberta Environment and Parks. One of the eddy-covariance systems used in this study was graciously provided by Alberta Agriculture and Forestry. I am also grateful for funding and scholarships provided to me through the University of Calgary and the Government of Alberta.

I am forever thankful to my parents for supporting my decision to pursue grad school, even if it meant moving to Calgary. No worries Dad, I did not – and will never – become a Flames fan. Thanks to my awesome friends and sister for coming to visit me all the way down here and letting me ramble on about rocks whenever we're in the mountains. Finally, thank you to Grant for always making me smile even when the light at the end of the tunnel was faint, and for making sure I was the most well-fed grad student in the history of grad students.

Table of Contents

List of Tables

List of Figures

List of Symbols, Abbreviations and Nomenclature

Symbol	Definition
LDF	Lethbridge Demonstration Farm
PP	Perry Produce
SSRB	South Saskatchewan River Basin
ECC	Edmonton-Calgary Corridor
CLC	Calgary-Lethbridge Corridor
PPR	Prairie Pothole Region
DFR	Depression-Focused Recharge
CMB	Chloride Mass Balance
WTF	Water Table Fluctuation
Irr	Irrigated
Dry	Dryland
Dp	Depression
Fl	Flatland
Up	Upland
R	Recharge (mm/yr)
P	Precipitation (mm)
I	Irrigation (mm)
O	Overland flow (runoff) (mm)
C	Chloride concentration (mg/L)
ET	Evapotranspiration (mm)
VF	Vapour flux (mm)
K	Unsaturated hydraulic conductivity (m/s)
K_s	Saturated hydraulic conductivity (m/s)
bgs	below ground surface
asl	above sea level
θ	Volumetric water content
Ψ	Matric potential head
h	Hydraulic head
z	Elevation head

Chapter 1: Introduction

1.1 Motivation

Understanding, quantifying and managing water resources is crucial in order to sustain a growing human population, especially with global temperatures on the rise. Recent climate change projections predict significant reductions in renewable water resources by the mid-21st century, particularly in areas with dry climates (International Panel on Climate Change (IPCC), 2014). In the semi-arid region of southern Alberta, surface water resources are already under duress (Sauchyn et al., 2015). The South Saskatchewan River Basin (SSRB) provides water to much of southern Alberta including the cities of Calgary, Medicine Hat, Red Deer and Lethbridge, and the vast majority of agricultural activities in the region. However, virtually all of the rivers in the SSRB are considered over-allocated (Alberta Environment, 2005; Sauchyn et al., 2015) and new applications for licensed water allocations are no longer accepted in three of the four sub-basins (Bjornlund et al., 2014; Sauchyn et al., 2015). Groundwater resources are comparatively under-used in the region (Lemay & Guha, 2009), but may become crucial in response to surface water scarcity. As a result, there is an imminent need for knowledge about the state of groundwater resources in southern Alberta, as well as a definitive plan for developing sustainable groundwater management policies. Important factors that require investigation include the spatial distribution and quality of groundwater resources as well as the rate of replenishment, or groundwater recharge.

Groundwater recharge is defined in this study as any surface water which reaches the water table from above (recharge from lateral groundwater flow is not considered here). An accurate estimate of groundwater recharge and its spatiotemporal distribution is required in order to assess the sustainability of groundwater resources in southern Alberta (Sophocleous, 2000;

Zhou, 2009), as well as the potential impacts of long-term extraction. Recharge rates are controlled by several factors, including bedrock and surficial geology, topography, meteorological conditions and vegetation. Additionally, anthropogenic changes in land use can greatly alter natural recharge regimes. For example, increased recharge rates have been reported as a result of urbanization (Lerner, 1990; Foster et al., 1994; Hibbs & Sharp, 2010), deforestation (Bellot et al., 2001), conversion from grassland to cropland (Scanlon et al., 2005; Huang & Pang, 2011) and irrigation (Chiew & McMahon, 1991; Davisson & Criss, 1995; Willis & Black, 1996; Kendy et al., 2003;; Scanlon et al., 2005; Qin et al., 2011). Irrigation in particular is an important land use practice for Albertans, with sixty-seven percent of all irrigated land in Canada located in Alberta (Statistics Canada, 2011). Previous studies have found that recharge rates beneath irrigated fields were anywhere from 1.3 to 6.5 times higher than beneath dryland fields (Scanlon et al., 2005; Chiew & McMahon, 1991). This has implications for groundwater management policies, whereby sustainable groundwater extraction rates are typically determined based on the estimated natural recharge rate, among other factors (Sophocleous, 2000; Zhou, 2009). Irrigation in southern Alberta dates back to the early 1900s (Sauder, 1949) and covers approximately 625 000 hectares of land (Alberta Water Portal, 2018). However, the effects of irrigation on groundwater resources in southern Alberta have yet to be evaluated.

This study was part of a larger research initiative called Groundwater Recharge in the Prairies (GRIP), spearheaded by the University of Calgary. The GRIP project is aimed at evaluating how groundwater recharge is affected by factors such as topography, surficial geology, changes in land use, frozen soils and future climate change, focusing on the Edmonton-Calgary corridor (ECC) and Calgary-Lethbridge corridor (CLC). Results from the GRIP project will provide future policy makers with key information about how, when and where groundwater

resources are being replenished in southern Alberta. This information will form the basis for effective and sustainable groundwater management practices.

1.2 Groundwater recharge in the prairies

The Canadian prairies are underlain by glacial deposits of varying types and thicknesses (Fenton et al., 2013; Fenton et al., 1994). As a result, the low-permeability and hummocky terrain typical of glacial deposits is well-developed across much of the Canadian prairies and well into the United States, an area otherwise known as the Prairie Pothole Region (PPR, Figure 1.1) (Eisenlohr, 1972). Millions of topographical depressions, or "potholes", make up the PPR, creating a complex network of isolated surface water bodies with varying degrees of permanence and connection to the underlying groundwater (Eisenlohr, 1972; van der Valk, 2005; Hayashi et al., 2016). The continental climate of the region is characterized by a semi-arid climate where annual precipitation is exceeded by potential evaporation (Winter, 1989). In addition, a significant percentage of annual precipitation falls as snow, resulting in ponding of spring snowmelt runoff within the depressions, and subsequent infiltration of this water that can contribute to groundwater recharge (van der Valk, 2005; van der Kamp & Hayashi, 1998). This process is known as depression-focused recharge (DFR) (Lissey, 1968) and is an important mechanism for replenishing regional aquifer systems (van der Kamp & Hayashi, 1998). In contrast, diffuse recharge occurs across the landscape beneath uplands, depressions and flatlands as a result of infiltration and deep drainage (downward flow beneath the active rootzone) of snowmelt and/or summer precipitation.

In the PPR, DFR of spring snowmelt runoff is typically considered the primary recharge mechanism (Berthold et al., 2004), while diffuse recharge of summer precipitation contributes to

a lesser extent, primarily after large rainfall events (Freeze & Banner, 1970; Hayashi & Farrow, 2014). LeBlanc (2017) also suggested that dry soils on the uplands can contribute significant amounts of snowmelt infiltration through frozen ground if significant macropores (i.e., preferential flow paths) exist, contributing to enhanced recharge. These recharge mechanisms result in recharge rates which vary greatly both in time and in space within the PPR. Seepage rates measured beneath ponded depressions are typically high and represent short intervals of spring recharge: rates as high as 250-300 mm/yr have been reported in central Saskatchewan (Zebarth et al., 1989a) and 600 mm/yr (Rehm et al., 1982) and 950 mm/yr (Shjeflo, 1968) in North Dakota. However, it was noted by van der Kamp & Hayashi (1998) that the majority of this seepage is lost to evapotranspiration and does not make it to the water table.

In contrast, diffuse recharge rates beneath uplands are lower but can occur more frequently throughout the year (e.g., mid-winter snowmelt or summer storms). In order to account for relative areas of uplands and depressions in a given region, an average areal recharge rate can be reported. Previous studies have reported a wide range of recharge rates within the PPR: average areal estimates of 3-4 mm/yr (van Dijk, 2005) and 10-20 mm/yr (Hayashi & Farrow, 2014) have been reported near Calgary, Alberta, 5-40 mm/yr (van der Kamp & Hayashi, 1998) and 35 mm/yr (Zebarth et al., 1989a) in central Saskatchewan and 25-115 mm/yr (Rehm et a., 1982) in North Dakota. Although recharge rates have been found to increase as a result of irrigation (Chiew & McMahon, 1991; Davisson & Criss, 1995; Willis & Black, 1996; Kendy et al., 2003; Scanlon et al., 2005; Qin et al., 2011), no studies investigating the influence of irrigation on DFR rates within the PPR are known.

Recharge in the PPR is strongly seasonal, with the majority occurring in spring as a result of snowmelt and smaller amounts in summer in response to rainfall. Winter recharge can also

occur as a result of mid-winter melt events (Pavlovskii et al., 2019). However, it has been shown previously that increased fall soil water content leads to reduced infiltration capacity (Granger et al., 1984; LeBlanc, 2017), which has implications for spring recharge rates beneath irrigated fields. In other words, overwinter recharge (i.e., the combined winter + spring snowmelt recharge) may be reduced under irrigated conditions due to wetter soil conditions in fall. However, irrigated fields are subject to more frequent intense water input (i.e., rainfall + irrigation) events compared to dryland fields, which increases the potential for diffuse recharge during summer. As a result, irrigation may not only impact recharge rates, but also the seasonality and timing of recharge events. These dynamics have yet to be investigated.

1.3 Methods for quantifying recharge

The prominent spatial and temporal variability in groundwater recharge within the PPR makes the quantification of recharge rates a complex and challenging task. Several review papers exist that outline the many methods available for quantifying groundwater recharge (Scanlon et al., 2002; Gee & Hillel, 1988; Allison et al., 1994). The methods described here were chosen for their relevance to the study conditions; in other words, methods suitable for semi-arid climates and which focus on processes within the unsaturated and saturated zones of the subsurface (as opposed to surface-water methods such as baseflow analysis).

1.3.1 Physical techniques

1.3.1.1 Soil water balance

The soil water balance is typically considered the conventional method for estimating recharge (Rushton & Ward, 1979) according to the following equation:

$$P + I - ET \pm O - R = \Delta\theta \quad (1.1)$$

where P is precipitation, I is irrigation, ET is evapotranspiration, O is overland flow (or runoff), R is recharge, $\Delta\theta$ is the net change in soil water storage in the soil profile and all parameters are measured as rates (e.g., mm/yr). This method attempts to quantify all of the water inputs and outputs to the system over a specified time period, with recharge being equal to the residual component when all other components are known. The water balance method is applicable to a wide range of scales in both time and space, allowing for daily recharge estimates on small plots of land to regional recharge estimates over several decades (Scanlon et al., 2002). This method is limited by the precision of measurement and/or accuracy of estimation of each parameter in Equation 1.1, especially in arid regions where the magnitude of recharge is small relative to other variables (e.g., P and ET). In these cases, small uncertainties in the measured variables can result in rather large uncertainties in recharge estimates (Gee & Hillel, 1988). As such, recharge estimates obtained using the water balance method should be corroborated with estimates from other methods.

1.3.1.2 Lysimetry

Lysimeters are *in situ*, isolated blocks of disturbed or un-disturbed soil, used to measure components of the water balance directly (Allen et al., 1991; Gee et al., 1994; Young et al., 1996). They are typically heavily instrumented in order to monitor soil water tension, soil moisture and temperature conditions with depth within the soil profile, as well as changes in porewater characteristics via sampling access points. Non-weighing lysimeters include instruments for measurement and collection of drainage from the bottom of the soil column and can be used to estimate recharge rates. Weighing lysimeters are underlain by a sensitive scale capable of measuring small changes in soil water content which can be used to quantify

evapotranspiration. The areal scale of measurement using lysimeters generally ranges from several hundred cm^2 to several hundred m^2 (Scanlon et al., 2002). Very low recharge rates (e.g. 1 mm/yr) can be resolved with sufficiently precise instruments making this method applicable in arid climates. Recharge rates previously measured using lysimeters range from zero to over 400 mm/yr (Kitching et al., 1977; Kitching & Shearer 1982; Gee & Hillel, 1988) with even higher rates following snowmelt events (Jones & Skaggs, 1987). Although lysimeters are perhaps the best way to directly measure the components of the water balance (Gee & Hillel, 1988), they are expensive and difficult to install and maintain and thus are not commonly used for recharge studies.

1.3.1.3 Darcy's Law

Darcy's Law can be used to estimate recharge by quantifying the flux through the vadose (unsaturated) zone:

$$R = -K(\Psi)\left(\frac{dh}{dz}\right) \tag{1.2}$$

where R is recharge (m/s), K is the unsaturated hydraulic conductivity (m/s) as a function of the soil matric potential (Ψ, m), h is the total hydraulic head (m) and z is the elevation (m). Measurements of soil matric potential with depth within the soil profile are required in order to obtain the total hydraulic head gradient (i.e., $\frac{dh}{dz}$), since $h = \Psi + z$. Hydraulic conductivity as a function of soil matric potential ($K(\Psi)$) can be estimated using soil water retention ($\Psi(\theta)$)and unsaturated hydraulic conductivity ($K(\theta)$) curves. These relationships (i.e., K, Ψ, θ) can be difficult and time consuming (weeks to months) to determine. Small variations in θ can result in large (orders of magnitude) variations in K, and hysteresis results in different values of K for the same θ for wetting versus drying conditions. As a result, recharge estimates obtained using Darcy's Law in the vadose zone can have large errors. This method only provides point estimates

of recharge in space, but can be used over times scales of hours to years. Previous studies have used Darcy's Law in the vadose zone to quantify recharge rates ranging from 10 to 500 mm/yr (Enfield et al., 1973; Stephens & Knowlton, 1986; Kengni et al., 1994).

1.3.1.4 Water table fluctuation

The water table fluctuation (WTF) method estimates recharge based on the amount of groundwater level rise that occurs after a water input event (e.g. precipitation, snowmelt, irrigation). Recharge is calculated as outlined by Healy and Cook (2002):

$$R = \frac{S_y \Delta h}{\Delta t} \tag{1.3}$$

where R is recharge (mm/d), S_y is specific yield (unitless) and Δh (mm) is the change in groundwater level over some change in time, Δt, (days). This method is applicable to unconfined aquifers and is based on the assumption that an increase in groundwater level is due solely to recharging water arriving at the water table. It is best applied over short time scales (hours to days) in areas with shallow water tables that respond sharply to input events, however, in areas with large unsaturated zones it can also be applied if only seasonal water fluctuations occur (e.g. in direct response to spring snowmelt) (Healy & Cook, 2002). This method is limited by the difficulties associated with measuring/estimating S_y, and the fundamental assumption that water table fluctuations occur only as a result of recharge can break down if the aquifer is affected by other inputs/outputs (e.g. pumping, lateral groundwater flow, barometric pressure fluctuations, connection to surface water bodies, etc.). Measured recharge rates can represent areas from tens of square metres to thousands of square meters (Scanlon et al., 2002) and time scales from hours to months. Previous studies have used the WTF method to measure recharge rates ranging from several mm/yr to over 500 mm/yr (Abdulrazzak et al., 1989; Maréchal et al., 2006; Varni et al., 2013).

1.3.2 Tracer techniques

1.3.2.1 Applied tracers

Applied tracers are substances purposefully introduced into the system in order to detect, monitor and quantify water flow in the subsurface. These can include visual tracers such as dye (Flury et al., 1994), or chemical tracers such as bromide (Wang et al., 2008) or organic acids (Bishop et al., 2015), among many others. The tracer is applied to the ground surface and subsequently porewater, groundwater and soil samples can be analyzed at different depths to determine flow paths, calculate breakthrough curves and estimate downward flux through the vadose zone. Recharge (R) can be estimated as:

$$R = \frac{\Delta z}{\Delta t}\theta \tag{1.4}$$

where Δz is the distance from the ground surface to the peak tracer concentration (mm), Δt is the time between application (days) and sampling, and θ is the soil volumetric water content (m^3/m^3). Although applied tracers provide a fairly direct method for measuring flow, nearly all types of tracers are subject to some level of reaction, sorption or degradation within the soil profile, and diffusion with depth restricts this method to relatively thin vadose zones depending on the amount and concentration of tracer applied. In addition, Equation 1.4 functions under the assumption that flow is predominantly piston-like and that water mixing in the subsurface is negligible, although these assumptions are not always appropriate. The typical area represented by the applied tracer technique ranges from tens to hundreds of m^2 and the time scale of recharge rates is generally months to years (Scanlon et al., 2002).

1.3.2.2 Environmental tracers

Environmental tracers are substances that are present in the vadose and/or saturated zones as a result of either naturally-occurring processes or anthropogenic activities, but that were not introduced as part of an intended experiment. Only a subset of the most commonly used environmental tracers are included here.

1.3.2.2.1 Radioactive tracers

Compounds that have entered the atmosphere as a result of human activity during isolated, known time periods can be used as tracers. Examples are tritium (^{3}H) and chlorine (^{36}Cl) derived largely from nuclear weapons testing in the 1950s and 1960s (Cook et al., 1994). For example, water that recharged during or shortly after the nuclear testing will have high levels of nuclear ^{3}H and ^{36}Cl; these peaks can be located in the subsurface and the time of travel from the ground surface to the peak tracer concentration is used to estimate recharge rates according to Equation 1.4. The use of tritium is becoming less reliable due to its short half-life (12.3 yr) and relies on the detection limit of analysis instruments. While ^{36}Cl has a much longer half-life (300 000 yr), it can be taken up by plants, which can affect recharge estimates in vegetated areas with well-developed deep root zones. Recharge rates estimated using this method represent the average rate over the past few decades (i.e., since the time when the tracer pulse was initiated). The range of recharge rates that can be estimated using radioactive environmental tracers typically only ranges from 10 to 50 mm/yr (Scanlon et al., 2002; Allison et al., 1994).

1.3.2.2.2 Chloride

Meteoric chloride and the chloride mass balance (CMB) method is likely the most widely used technique for estimating recharge in semi-arid to arid climates (Scanlon et al., 2006). Naturally-occurring chloride within the atmosphere is deposited onto the ground surface via dry

fallout and precipitation. The CMB method is based on the principal of conservation of mass, and states that if the flux of chloride onto the ground surface as well as the concentration of chloride in the groundwater is known, recharge can be calculated as follows:

$$RC_R = PC_P \quad (1.5)$$

where R is recharge (mm/d), C_R is the chloride concentration of the recharging water (mg/L), P is the precipitation (mm/d) and C_P is the chloride concentration of precipitation (mg/L). C_P is usually taken to include both wet and dry fallout (Allison et al., 1994). Chloride is generally not taken up by plants and is thus concentrated within the root zone as a result of evapotranspiration. By Equation 1.5, higher chloride concentrations in the subsurface indicate lower recharge rates. Assuming chloride inputs are constant, chloride concentrations will increase within the rootzone to a maximum, constant value below the rootzone (Cook et al., 1989; Scanlon, 1991; Allison et al., 1994). However, more complex profiles can arise due to preferential flow, paleo-climatic changes in recharge rates or changes in land-use (Allison & Hughes, 1983; Scanlon, 2000). This method provides point-measurements of the long term (several years to thousands of years) average recharge rate, however, the time period represented by the recharge estimate must be carefully considered. The CMB method has been used to measure recharge rates as low as 0.05 mm/yr (Allison & Hughes, 1983) and is applicable to rates as high as 300 mm/yr (Scanlon & Goldsmith, 1997).

1.3.2.2.3 Stable isotopes of water

Stable isotopes of the water molecule (^{2}H and ^{18}O) have been used to study the rates, sources and seasonality of groundwater recharge (Allison et al., 1984; Maulé et al., 1994; Jasechko et al., 2014). Isotope ratios are measured relative to V-SMOW (Vienna-Standard Mean Oceanic Water) and reported using delta notation as a deviation from V-SMOW:

$$\delta_{sample} = \left[\frac{R_{sample}}{R_{V-SMOW}} - 1\right] \times 1000 \quad (1.6)$$

where R is the ratio of heavy to light isotopes, and δ is the deviation of the sample ratio from the V-SWOW ratio in per mill (‰). Temperature-driven fractionation processes lead to seasonal variations in the isotopic composition of precipitation and, as a result, infiltrating and recharging water. The distance between summer and winter peak signatures in the soil profile can be used to determine flow velocities in the vadose zone and potential recharge rates (Koeniger et al., 2016). This method requires soil samples from different depths in order to analyze the isotopic composition of the porewater, and is best applied in humid regions. Stable isotope analyses provide point estimates of recharge in space and the time-scale of estimates ranges from seasons in humid climates to decades in arid climates. Previously, recharge rates ranging from zero to approximately 300 mm/yr have been estimated (Koeniger et al., 2016). Stable isotopes can also be used to quantify the relative contribution of winter and summer precipitation to recharge using two-component mixing models (Maulé et al., 1994; Pavlovskii et al., 2018).

1.3.3 Numerical modeling

Numerical modeling of flow in the unsaturated zone can be used to estimate recharge using several different approaches (Scanlon et al. 2002). The two most common types of models for simulating recharge and vadose zone flow are bucket models (e.g. Noorduijn et al., 2018) and models that numerically solve the Richards equation (e.g. Šimůnek et al., 1998). While bucket models are generally considered the simpler of the two, requiring less data input and computational effort, models that solve the Richards equation provide a physical basis for simulating complex dynamics that affect flow, such as preferential flow and root growth. Models based on the Richards equation can require large amounts of input data (i.e. daily meteorological

and soil moisture conditions, soil properties, vegetation growth and water uptake information, etc.) which must be either measured or estimated. Ideally, the model is calibrated to a field-measured dataset. Recharge rates estimated using 1D flow simulations are point estimates in space, but can represent time scales from days to centuries depending on the availability of input data. Modeling results in recharge estimates that are subject to large uncertainty as a result of potentially inaccurate parameterization, unrepresentative boundary conditions and non-uniqueness of the calibrated solution. As such, recharge estimates should be verified using other methods.

1.4 Effects of irrigation on groundwater recharge

Previous studies from around the world have reported increased recharge rates and elevated water tables as a result of irrigation. Scanlon et al. (2005) compared recharge rates beneath grasslands (negligible), dryland agriculture (9-32 mm/yr) and irrigated agriculture (130-640 mm/yr) in the Amargosa Desert in Nevada and the High Plains of Texas using the CMB and tracer displacement methods (among others). Results also showed that conversion from grassland to either type of agriculture resulted in increased recharge rates (Scanlon et al., 2005). Another study in the High Plains of Kansas employed the use of tritium (H^3) and the CMB method and found that downward fluxes through the thick (> 40 m) vadose zone were 4 to 12 times higher beneath irrigated sites compared to grassland sites (McMahon et al., 2003). Chiew and McMahon (1991) used an integrated surface water and groundwater modeling approach to estimate regional recharge rates in the irrigated and dryland areas of a river basin in south eastern Australia. Simulated recharge was 1.3 to 6.5 times higher in the irrigated regions compared to dryland regions, values which were consistent with measured recharge rates reported by other

studies in the same basin (Chiew & McMahon, 1991). Also in south eastern Australia, Willis and Black (1996) found that irrigation agriculture resulted in deep drainage rates that have increased by 17 to 202 mm/yr compared to estimated drainage rates from before irrigation began. Results also indicated that groundwater level rise as a result of irrigation was between 37 and 524 mm/yr (Willis & Black, 1996). Kendy et al. (2003) used a 1D soil water balance model to show that recharge increased with increased irrigation in the North China Plain. No studies are known that have quantified recharge rates under irrigated conditions in southern Alberta.

The increased recharge caused by irrigation often leads to higher concentrations of agricultural contaminants in the underlying groundwater (Böhlke, 2002). Agricultural contaminants are chemicals linked to agricultural activity and can include inorganic compounds such as NO_3^-, N_2, Cl, SO_4^{2-}, H^+, P, C, K, Mg, Ca, Sr, Ba and Ra as well as other compounds from pesticides, fertilizers or organics (Böhlke, 2002). In particular, elevated nitrate concentrations in groundwater have been strongly correlated to irrigation in Kansas (McMahon et al., 2003), Nevada and Texas (Scanlon et al., 2005), Nebraska (Exner et al., 2014), and Northwest China (Qin et al., 2011). McMahon et al. (2003) also reported elevated concentrations of pesticides in groundwater beneath irrigated sites, and Qin et al. (2011) attributed high levels of chlorofluorocarbons (CFCs) in groundwater to deep drainage of irrigation water. In southern Alberta, Miller et al. (1995) confirmed herbicides in groundwater under irrigated fields near Lethbridge and Taber, while Chang and Entz (1996) and Rodvang et al. (2004) found leaching of nitrate to groundwater was higher beneath irrigated fields compared to dryland fields near Lethbridge.

Irrigation also leads to increased soil water content in fall, which reduces the amount of moisture that can be stored in the vadose zone during the overwinter period (e.g., snowmelt).

This has implications since spring water content is crucial for germination and early crop development, and crops are often planted soon after spring thaw. Hobbs & Krogman (1971) found that irrigated soils near Lethbridge stored a lower percentage (4-18%) of overwinter precipitation compared to a dryland soil (31%). Similarly, irrigated soils in the High Plains of Texas retained less than 10% of overwinter precipitation compared to 30-50% for dry soils (Musick, 1970). Increased soil moisture in fall also reduces the hydraulic conductivity of frozen soils by increasing the proportion of ice-blocked pores in the vadose zone (Granger et al., 1984; LeBlanc, 2017). This reduces infiltration and can inhibit recharge of snowmelt water until after the soil profile is thawed completely in spring (Hayashi et al., 2003; LeBlanc, 2017). Therefore, irrigation has the potential to affect both the timing and magnitude of overwinter recharge, something that has not yet been evaluated in southern Alberta.

1.5 Thesis objectives

The goal of this study was to investigate the effects of irrigation on groundwater recharge rates and processes in southern Alberta. There were two main objectives: first, to determine the influence of irrigation on both depression-focused and diffuse recharge rates at different topographic locations (e.g., depressions, uplands and flatlands); and second, to determine the effects of irrigation on the seasonality of recharge. Specifically, the latter objective was comprised of two questions: 1) does the increased fall water content of irrigated fields cause a reduction in overwinter snowmelt recharge?; and 2) does irrigation result in greater recharge beneath irrigated fields compared to dryland fields over the course of the growing season?

In order to fulfill these objectives, two field sites near Lethbridge, Alberta were instrumented, monitored and sampled from May 2017 to November 2018. Each site comprised

cropped fields under both irrigated and dryland conditions. Seasonal and long-term recharge rates were quantified for irrigated and dryland conditions beneath depressions, uplands and flatlands at both sites according to the WTF, CMB and water balance methods (Section 1.3). Lastly, vertical flow in the vadose zone was simulated using a numerical model in order to compare theoretical recharge rates under irrigated versus dryland conditions over the course of the growing season.

1.6 Thesis organization

This thesis is presented in three chapters. Chapter 1 explains the motivation for the study, provides background information in regards to groundwater recharge mechanisms in the prairies and a short review of methods for estimating recharge. Chapter 2 presents the methods, results and conclusions of the thesis in the format of a stand-alone manuscript, resulting in some redundancy in regards to topics covered in Chapters 1 and 3. Chapter 3 is a summary chapter which provides an overview of the study, the main limitations and suggestions for future work. Additional datasets are presented in a series of Appendices.

1.7 Figures

Figure 1.1. The location of the study area within the Prairie Pothole Region.

Chapter 2: The effects of irrigation on groundwater recharge rates and seasonality at two sites in southern Alberta

2.1 Introduction

Quantification of groundwater recharge rates is crucial for effective and sustainable water resource management, particularly in regions where surface water resources are stressed. Surface water allocations in southern Alberta have become increasingly restricted (Alberta Environment, 2005; Bjornlund et al., 2014) and, among predictions of continued population growth, groundwater resources may soon become an important alternative (Alberta Water Council, 2008; Government of Alberta, 2018). Groundwater recharge is affected by many factors including topography, geology, meteorological conditions and anthropogenic changes in land use (e.g., urbanization, agriculture, wetland drainage, etc.), all of which must be considered in order to accurately quantify recharge rates.

Natural recharge regimes can be greatly altered by changes in land use (Bellot et al., 2001; Scanlon et al., 2005; Lerner & Harris, 2009; Huang & Pang, 2011). In particular, increased recharge rates have been reported as a result of urbanization (Lerner, 1990; Foster et al., 1994; Hibbs & Sharp, 2010), conversion from grassland to cropland (Scanlon et al., 2005), and irrigation (Chiew & McMahon, 1991; Davisson & Criss, 1995; Willis & Black, 1996; Kendy et al., 2003; Scanlon et al., 2005; Qin et al., 2011). Sixty-seven percent of all irrigated land in Canada is found in Alberta, totaling approximately 625, 000 hectares (Statistics Canada, 2011; Alberta Water Portal, 2018) and, although irrigation is practiced throughout Alberta, most irrigation activity occurs within the 13 irrigation districts located in the southern part of the province (Alberta Agriculture and Forestry, 2000) (Figure 2.1). However, despite the large area

of irrigated cropland in southern Alberta, the effects of irrigation on groundwater recharge rates have scarcely been studied.

The Prairie Pothole Region (PPR) covers much of the Canadian prairies and extends well into the United States (Figure 1.1). It is characterized by millions of topographical depressions, or “potholes”, which are capable of storing water with varying degrees of permanence (van der Valk, 2005; Eisenlohr, 1972). Groundwater recharge in this region can generally be categorized as either focused or diffuse. Focused recharge of spring snowmelt runoff occurs beneath depressions and is referred to as depression-focused recharge (DFR) (Lissey, 1968), whereas diffuse recharge of summer and winter precipitation can occur across the landscape at various topographic positions (i.e., beneath depressions, uplands and flatlands). DFR is an important mechanism for replenishing regional aquifer systems (van der Kamp & Hayashi, 1998), and is generally considered the primary recharge mechanism throughout the PPR (Berthold et al., 2014). Diffuse recharge contributes to regional aquifers to a lesser extent, occurring primarily as a result of summer storms (Hayashi & Farrow, 2014), although mid-winter snowmelt infiltration through frozen upland soils can also contribute to recharge (Mohammed et al., 2019). The majority of the irrigated cropland in southern Alberta lies within the PPR (Figures 1.1 and 2.1), however, the impacts of irrigation on both depression-focused and diffuse recharge mechanisms have not been evaluated in this region.

Recharge in the PPR is strongly seasonal as a result of DFR of snowmelt runoff, however, there is evidence that irrigation may alter this seasonality. Irrigation increases the fall soil water content of cropped fields, reducing the infiltration capacity of frozen soils which has implications for reduced recharge of both mid-winter and spring snowmelt runoff (Granger et al., 1984; LeBlanc, 2017). In contrast, diffuse recharge rates during the growing season may be

greater on irrigated fields due to frequent and intense water inputs similar to summer storm events. As such, irrigation may affect the relative timing and amount of both overwinter (i.e., winter + spring) and summer recharge.

The purpose of this study was to investigate the effects of irrigation on groundwater recharge in southern Alberta. The first main objective of the study was to evaluate the effects of irrigation on depression-focused and diffuse recharge rates beneath depressions, uplands, and flatlands. The second main objective was to determine the effects of irrigation on the seasonality of recharge and was broken into two parts: first, to determine whether the increased fall soil water content of an irrigated field results in reduced overwinter snowmelt recharge; and second, to determine whether irrigation results in increased recharge rates on irrigated fields compared to dryland fields over the growing season. To achieve these research goals, hydrological monitoring and sampling was conducted at two study sites near Lethbridge, Alberta. Recharge rates on dryland and irrigated fields at both sites were estimated using the water table fluctuation (WTF) method, the chloride mass balance (CMB) method and the water balance method. Finally, a numerical model was developed using HYDRUS-1D to compare theoretical recharge rates under irrigated and dryland conditions.

2.2 Study sites

Investigations for this project were carried out from May 2017-November 2018 at two study sites located within the PPR (Figure 1.1), near the city of Lethbridge, Alberta (Figure 2.2a). The primary study site was located at the Lethbridge Demonstration Farm (LDF), situated less than 2 km east of the city limits (Figure 2.2c). A secondary site was located approximately 25 km northeast of Lethbridge on a quarter section of land owned by the Perry family; this site is

hereafter referred to as the Perry Produce site (PP) (Figure 2.2b). Both study sites are located within the St. Mary River Irrigation District (SMRID) (Figure 2.1), which receives water from the St. Mary, Waterton and Belly Rivers, ultimately fed from headwaters originating in the Rocky Mountains of Alberta and Montana (Mitchell & Prepas, 1990). Irrigation in southern Alberta dates as far back as 1901 (Sauder, 1949), but the exact irrigation history of the two study sites was difficult to determine due to changes in land ownership, land use (e.g., dryland to irrigated), and/or type of irrigation (e.g., wheel track to central pivot).

2.2.1 Lethbridge Demonstration Farm

The LDF site was acquired in 1998 by Alberta Agriculture under the Canada-Alberta Crop Development Initiative (CACDI) and was intended for field-scale research of irrigated crop production and irrigation efficiency (Rodvang, 2002). The LDF site consists of two 12-hectare (0.12 km^2) and one 27-hectare (0.27 km^2) central irrigation pivot systems as well as some dryland cropped fields (Figure 2.2c). The site is divided into ten fields numbered from west to east. Three sub-sites were instrumented at LDF: an irrigated depression in field 4 (denoted L_IrrDp), irrigated flatland in field 8 (L_IrrFl) and dryland flatland in field 10 (L_DryFl) (Figure 2.2c). In this report, "L_" and "P_" designate the LDF and PP study sites, respectively. "Irr" and "Dry" designate irrigated and dryland conditions and "Fl", "Up", "Dp" designate flatlands, uplands and depressions.

According to historical air photos, the LDF site has been irrigated at least since 1977, and possibly earlier considering the earliest irrigation in the Lethbridge area dates back to 1901 (Sauder, 1949). Wheel track irrigation at the LDF was converted to central pivot system around the year 2000. Although the dryland field used in this study (L_DryFl, Figure 2.2c) has not been

irrigated at least since the year 2000, it is unclear whether it has been irrigated at some other point in the past. Crops planted at the LDF site are rotated from year to year and include barley, alfalfa, corn, wheat, canola, peas, sugar beets, potato, and oats on irrigated fields, with barley, wheat, oats and canola grown on dryland fields. All three sub-sites were planted with barley for the 2017 growing season. In the following year (2018) L_IrrDp was planted with barley, L_IrrFl with sugar beets, and L_DryFl with canola.

The region surrounding the LDF is characterized by flat to gently undulating glaciolacustrine deposits to depths of up to 80 meters (Shetson, 1987; MacCormack et al. 2015). According to a previous study, the LDF site is directly underlain by a layer of medium-textured glaciolacustrine sediments that reaches a maximum thickness of 1.5 m and overlies clay till sediments up to 2.8 m thick (Rodvang, 2002). The colour of glacial sediments can be attributed to the degree of oxidation they have undergone. During the warmer and drier climate of the Altithermal period (about 8000 and 5000 years ago), the water table in North America dropped considerably, causing weathering and oxidation of the exposed glacial sediments above the water table (MacDonald, 1989; Hendry et al., 1986). These oxidation reactions caused the sediments to turn brown, whereas un-oxidized sediments below the water table retained their original grey colour. The boundary between oxidized and un-oxidized sediments is called the redoxcline and can be identified in the subsurface throughout North America, ranging from 3 to 17 m bgs. At the LDF site, Rodvang et al. (2002) concluded that a transition zone exists between the oxidized and un-oxidized zones, starting at approximately 6 m depth; the study did not sample deep enough to encounter the un-oxidized zone.

The soil in the region is categorized as Orthic Dark Brown Chernozem (Canadian System of Soil Classification, CSSC) consisting of fine-loamy to fine-silty glaciolacustrine material

(Kocaoglu & Pettapiece, 1980). Topography in this area is subtle, with slopes previously described as gentle or nearly flat (Kocaoglu & Pettapiece, 1980), with an average relief of 3 m (MacMillan & Pettapiece, 2000). Glacial deposits overlie the Oldman and Dinosaur Park bedrock formations of the Cretaceous Belly River Group (Prior et al., 2013).

Groundwater flow is from the southwest to the northeast of the site, following the gentle slope of topography (Rodvang, 2002). The average daily air temperatures recorded at the Lethbridge airport for July and January are 18.2°C and -6.0°C, respectively, and the annual average precipitation is 440 mm, approximately one-third of which is snowfall according to climate data from 1957 - 2007 (Government of Canada, 2017).

2.2.2 Perry Produce

A secondary site, the Perry Produce (PP) site, was included in the study in October, 2017. The PP site has one 80-hectare (0.8 km^2) central irrigation pivot system and four dryland corners (approximately 0.15 km^2 each). Four sub-sites were sampled: an irrigated upland (P_IrrUp), irrigated depression (P_IrrDp), dryland upland (P_DryUp) and dryland depression (P_DryDp) (Figure 2.2b). Personal communication with the Perry Family suggests that the field was not irrigated until they converted from dryland cultivation in 2004, and that the dryland corners have never been irrigated to their knowledge.

The geology surrounding the PP site is similar to LDF in that it is underlain by thick (50-60 m) glacial deposits, however these deposits are predominantly moraine till with isolated lenses of gravel, sand and silt (Shetson, 2005) as opposed to the glaciolacustrine deposits seen at LDF. Moraine till produces a much more hummocky terrain than glaciolacustrine sediments, resulting in an average local relief of 5 m, but ranging from 3-10 m (MacMillan & Pettapiece,

2000; Shetson, 1987). The soil is classified as Orthic Dark Brown Chernozem (CSSC) consisting of coarse-loamy and fine-loamy fluvial material overlying morainal deposits (Kocaoglu & Pettapiece, 1980). The shallowest bedrock is the Foremost Formation, a member of the Cretaceous Belly River Group (Prior et al. 2013). The long term climate data (average daily air temperature and precipitation) are assumed to be similar to the LDF site due to proximity.

2.3 Methods

The seven sub-sites indicated in Figure 2.2 were all instrumented, monitored and sampled at varying levels of detail: semi-permanent hydrological monitoring instruments were installed only at the LDF site, while drilling and soil, water and snow sampling occurred at both the LDF and PP sites. This section describes all of the instrumentation, monitoring and sampling conducted at each sub-site. The three recharge estimation methods are also described, as well as the numerical modeling approach.

2.3.1 Instrumentation

2.3.1.1 Meteorological measurements

Tipping bucket precipitation gauges were installed on May 8-9, 2017 at each of the three sub-sites at LDF to measure precipitation and irrigation. Winter precipitation data were obtained from an on-site Geonor T200B precipitation gauge (owned and operated by Alberta Agriculture and Forestry, see Figure 2.2c) and were corrected for wind-induced snow undercatch (Kochendorfer et al., 2017, Equation 3). On June 9, 2017, L_IrrFl was equipped with an eddy-covariance energy-balance system for measuring actual evapotranspiration (*ET*) using a sonic wind anemometer (Campbell Scientific, CSAT3) and a krypton hygrometer (Campbell

Scientific, KH20). The eddy-covariance system at L_DryFl was installed one year later on May 1, 2018. At both sub-sites, air temperature and relative humidity were also measured (Vaisala, HMP45C) as well as radiation using a four-component radiometer (Kip & Zonnen, CNR1 or CNR4). All meteorological measurements were made on a half-hourly basis.

Eddy-covariance data were corrected for: sensor tilt using a planar fit algorithm (Wilczak et al., 2001); temperature bias of the sonic anemometer due to humidity using the Webb-Pearman-Leuning correction (Webb et al., 1980); and, spatial separation of the krypton hygrometer and sonic anemometer (Oncley et al., 2007). Daily average turbulent heat fluxes (latent heat flux and sensible heat flux) were calculated from corrected data for days when at least 40 out of 48 half-hourly data points were recorded. Accuracy of turbulent flux data is typically evaluated on the basis of energy-balance closure:

$$Q_A = Q_H + Q_L \tag{2.1}$$

where Q_A is the total amount of available energy (i.e., net radiation minus ground heat flux), Q_H is the sensible heat flux and Q_L is the latent heat flux, all in W/m^2 (Twine et al., 2000). The eddy-covariance method has been shown to underestimate turbulent fluxes by 10-30% (Wilson et al., 2002). When averaged over the entire growing season, total turbulent fluxes at L_DryFl were 0.68 of available energy, which is similar to energy-balance errors observed by others (Hayashi et al., 2010; Wilson et al., 2002). While the cause of persistent energy-balance closure problem is still debated (e.g., Foken, 2008), it is imperative to account for the energy-balance error in water balance studies (Barr et al., 2012).

The krypton hygrometer at L_IrrFl malfunctioned throughout the entire 2017 growing season and much of the 2018 growing season due to a build-up of precipitate on the sensor following irrigation events. This prevented direct calculation of *ET* from latent heat flux data at

this sub-site, while sensible heat flux had few missing data. Therefore, the daily average latent heat flux at L_IrrFl was estimated from available energy and sensible heat flux from the energy balance. To account for the aforementioned energy-balance errors, a constant correction factor of 0.68 was applied in the energy balance calculation assuming that site conditions were similar and equipment was identical between L_DryFl and L_IrrFl sub-sites:

$$Q_{L\_EB} = Q_A - \frac{Q_H}{0.68} \quad (2.2)$$

where Q_{L_EB} is the latent flux corrected for energy balance error. Equation 2.2 also implicitly assumes that the energy-balance errors equally affect Q_L and Q_H (Twine et al., 2000), although such an assumption does not always hold (Foken, 2008; Charuchittipan et al., 2014). To compare *ET* at the two sub-sites in a consistent manner, Equation 2.2 was also used for L_DryFl, even though the hygrometer data were available during most of the growing season at this location. The latent heat flux estimated by Equation 2.2 (Q_{L_EB}) was similar to the corrected flux computed directly from eddy-covariance data (Q_{L_EC}) with daily energy-balance correction (instead of a constant factor of 0.68) at L_DryFl: $Q_{L\_EB} = 0.998 Q_{L\_EC}$, coefficient of determination (R^2) = 0.964. In previous studies conducted in similar environments using the same set of instruments, energy-balance-corrected *ET* has been found to overestimate true *ET* (Hayashi et al., 2010). The reason for this is unknown, but Charuchittipan et al. (2014) reported that the large-scale secondary circulation responsible for energy-balance errors affects sensible heat more than latent heat, implying that the method used in this study may over-correct for latent heat flux. Since raw *ET* (uncorrected for energy balance) often underestimates true *ET* and energy-balance-corrected *ET* overestimates true *ET*, the arithmetic average of *ET* values from before and after energy-balance correction was taken to be the best estimate of true *ET* (Hayashi et al. 2010).

Daily vapour flux values were required from November 1, 2017-April 30, 2018 in order to carry out water balance calculations (explained later in the text). However, since latent heat flux data from the L_IrrFl eddy-covariance system was unreliable due to malfunctioning equipment and the eddy-covariance system at L_DryFl had not yet been installed, daily vapour flux values were estimated using the Versatile Soil Moisture Budget (VSMB) model (Hayashi et al., 2010; Noorduijn et al., 2018). Hourly temperature, precipitation, wind speed, relative humidity and incoming shortwave radiation data from November 1, 2017-April 30, 2018 were used. Soil parameters (field capacity, permanent wilting point, porosity), and initial soil temperature and soil moisture conditions were obtained from L_IrrFl field data/soil samples. The model was run for bare ground conditions since no stubble was left over the winter period. Snowpack simulated using VSMB had good correlation with measured values ($R^2 = 0.75$). Daily vapour flux was taken as the sum of actual evapotranspiration and sublimation estimated by the model.

Weekly snow surveys were conducted at the LDF site from December 15, 2017 to April 9, 2018. Depth of the snowpack was measured every 1 m along 100-m long transects at each sub-site (Figure 2.2c). Snow density was measured every 50 m along the transect using an aluminum snow sampler tube. Average snow density along the transect was then multiplied by the mean snow depth to obtain the average snow water equivalent (SWE).

Time-lapse cameras and snow depth gauges were also installed at each of the three sub-sites at LDF to monitor daily changes in the snowpack in winter, ponding in spring, and crop growth in summer.

2.3.1.2 Vadose zone monitoring

Soil moisture, temperature, electrical conductivity and real dielectric permittivity were measured at each of the LDF sub-sites at depths of 20, 40, 60, 80, 100 and 150 cmbgs. Three soil pits were dug on May 8-9, 2017 and HydraProbe (Stevens) sensors were installed at each depth, connected to a data logger (Campbell Scientific, CR10X, CR1000 or CR3000) and set to record every 30 minutes. HydraProbe sensors measure soil temperature, electrical conductivity and real dielectric permittivity (ε_R), and then use ε_R to calculate volumetric water content (θ) using factory-derived equations for different soils (Bellingham, 2007). The default equation for loam soil is suggested for most soils (Bellingham, 2007) and was used in this study. Field-specific calibrations of HydraProbe sensors have been recommended by previous studies (Seyfried et al., 2005). However, laboratory experiments performed on soils taken from the LDF and other Alberta sites found that the default HydraProbe equation provided water content estimates with a root mean square error (RMSE) of 0.040 m^3/m^3 when compared to gravimetrically-determined water content (Muenchrath, 2018), which is close to the measurement accuracy of ± 0.03 m^3/m^3 reported for HydraProbe sensors (Bellingham, 2015). Additionally, deviations from true water content were significantly less for water contents below 0.30 (RMSE 0.022 m^3/m^3), compared to above 0.30 (RMSE of 0.055 m^3/m^3) (Muenchrath, 2018). Although a lab-calibrated equation did result in a lower average RMSE (0.028 m^3/m^3), the improvements were only significant above a water content of about 0.40 (Muenchrath, 2018). Such wet conditions occurred only at the L_IrrDp sub-site during periods of ponding. As such, the HydraProbe data presented in this study are the raw values, obtained using the default equation for loam soil.

Six intact soil samples were collected in 100 cm^3 metal soil rings from each soil pit at 20, 40, 60, 80, 100 and 150 cmbgs. Samples were taken as close as possible to HydraProbe sensor

locations. Rings were hammered horizontally into the soil profile and removed carefully to ensure the soil remained as intact as possible. The entire soil ring was capped, sealed and stored in a cooler until refrigeration upon return to the lab.

Over several weeks in June 2018, nested tensiometers (Soil Moisture Equipment Corp., Jet Fill) were installed at 30, 60, 90 and 150 cmbgs at each LDF sub-site. Holes were made using a 2.5 cm diameter hand-auger to the desired depth, the pre-wetted tensiometers were inserted, and a slurry made from DI water and sieved soil (fines only) was poured down the hole to improve contact between the ceramic cup and the soil. The holes were then backfilled around the tensiometer tubes with bentonite up to about 15 cmbgs and then backfilled to ground surface with native soil. Each tensiometer assembly included a pressure transducer (Transducers Direct, TDH31) attached to the tube above ground surface. Pressure transducers were connected to a data logger (Campbell Scientific, CR1000) and soil matric potential was recorded every 30 minutes. Matric potential values were later converted to hydraulic heads using the ground surface as the zero elevation head datum, and corrected to the value measured at the centre of the ceramic cup. Tensiometer tubes were re-filled with water about every two weeks but dried out completely within a matter of days at L_DryFl, causing sensor failure and resulting in large data gaps for this location. Soil water retention curves based on field data were attempted to be made using the matric potential measured with tensiometers and the approximately co-located soil water content measured by HydraProbes. These curves were largely incomplete due to large gaps in the tensiometer data as well as the fact that some depths had minimal variability in both water content and matric potential over the course of the growing season. This resulted in field soil water retention curves being only a small “snapshot” of the entire curve. As such, only the more

complete curves generated using the pressure plate method (described in a later section) are included here.

2.3.2 Drilling and well installation

2.3.2.1 Borehole soil samples

Eight boreholes ranging from 4 to 16 m deep were drilled at the LDF site on May 8-9 2017. Two boreholes were drilled at L_IrrDp, three at L_IrrFl and three at L_DryFl (Table 2.1). Boreholes at each sub-site are designated 1, 2 or 3 from shallowest to deepest, respectively (Table 2.1). The deepest borehole at each sub-site (i.e., L_IrrDp-2, L_IrrFl-3 and L_DryFl-3) was drilled using a truck-mounted hollow stem auger system to allow for continuous coring and soil sampling at discrete, known depths. The remaining five boreholes were drilled for well installation purposes using a solid stem auger and no samples were taken. At the PP site, four boreholes were drilled and sampled on October 31-November 1, 2017 using the same truck-mounted hollow stem auger system, one at each of the sub-sites indicated in Figure 2.2b. Boreholes at the PP site were 7.6 m deep in depressions and 9.1 m deep on the uplands (Table 2.1). The sampling procedure was the same for each borehole and is described as follows.

Sediment cores were photographed and soil properties (i.e., texture, colour, moisture, competency, relative clay content, etc.) were logged. Cores were sampled every 0.30 m (1 ft) for the first 1.52 m (5 ft), and then every 0.61 m (2 ft) below that. Two sediment samples were taken from each sampling location along the core: the first was extracted using 100 cm^3 metal soil rings and then deposited into sealable bags (“bagged samples”), the second was hand-filled into glass jars (“jarred samples”). Nitrile gloves were worn in order to prevent contamination of the sediment. Samples were stored in a cooler until refrigeration upon return to the lab.

2.3.2.2 Monitoring wells

Monitoring wells were installed in each borehole at the LDF site. All wells were completed using 5 cm diameter PVC casing with threaded couplings and slotted screens with 0.03 cm wide slots (0.01 in). Well completion details, including depths and screened intervals, are listed in Table 2.1. Each borehole annulus was backfilled with sand around the screened interval to a height of approximately 30 cm above the top of the screen. The remaining borehole annulus above the filter sand was filled with bentonite up to ground surface. All wells were equipped with non-vented pressure transducers (Solinst, Levelogger) to record water levels every 30 minutes. Manual water level readings were also taken using a water level tape about every 2-4 weeks. Barometric compensation to account for non-vented sensors was done using a separate transducer (Solinst, Barologger) hanging above the water column and the automatic barometric compensation application offered with Solinst Levelogger version 4.3 software.

In order to obtain *in situ* hydraulic conductivity estimates of native sediments, bail tests were conducted for each monitoring well on July 27, 2017 by quickly removing a known volume of water from the wells and analysing the subsequent recovery to static water level using pressure transducers. Wells took anywhere from five minutes to five months to recover. Recovery data was analysed according to the Bouwer & Rice (1976) method using the AQTESOLV Pro version 4.0 software (Duffield, 2007).

2.3.3 Soil properties

Dry bulk density (ρ_b) was determined for intact soil ring samples and bagged borehole samples by oven-drying at 105°C and weighing daily until sample weights did not change. This was used to calculate volumetric water content (θ). Porosity (ϕ) was determined for intact soil

ring samples by saturating the rings for 48 hours and weighing before oven-drying. The gravity-drained water content (θ_{gd}) was then determined by weighing the samples again after 24 hours of gravity drainage. Grain size analysis was performed on select borehole samples and all intact soil ring samples using a laser diffraction particle size analyser (Malvern Mastersizer2000). Grain size and soil texture classification were characterized according to the Wentworth scale (Wentworth, 1922). Clay mineralogy was determined for intact soil ring samples from 20, 60 and 150 cmbgs using X-ray diffraction (Rigaku Multiflex X-Ray Diffractometer).

Soil water retention characteristics were determined for all intact soil ring sensors using the pressure plate extractor method according to Klute (1986) over the matric head range of approximately -0.01 m to -50 m. Additional measurements were made using the dewpoint potentiometer (Decagon, WP4C) method described by Hayashi et al. (2012) to a minimum matric head of approximately -1000 m. Resultant soil water retention data was fitted to the van Genuchten (1980) model to determine soil water retention parameters.

2.3.4 Water sample collection

2.3.4.1 Surface water samples

In this study, "surface water samples" refers to all precipitation (snow and rain) samples, as well as irrigation water samples and samples taken from ponded water in the depressions in spring. All water samples were filtered through a 0.45 μm membrane into scintillation vials and placed in a cooler until refrigeration upon return to the lab.

Weekly snow samples were collected every 50 m along the three snow survey lines at the LDF site (Figure 2.2c) using an aluminum snow sampler tube and clean, dry, sealable bags. A total of 152 snow samples were collected from LDF between January 3 and April 9, 2018. Ten

snow samples were also taken from the borehole locations at PP on March 8, 2018. Samples were double-bagged to prevent leakage and placed in the refrigerator to melt before filtering. Only five rain events occurred at LDF in July-August, 2018 and rain from each event was collected using a custom-built sampler. Samples were transferred from the outdoor sampler to the refrigerator on the same day or the day after the rain event by LDF staff. The first rain event was omitted from any calculations due to suspected evaporation before analysis (as indicated by stable isotope analysis results).

Irrigation water at the LDF site was sampled once in July 2017 as well as six times in 2018 from June-September. Samples were collected directly from the primary irrigation pipeline located on the western edge of the LDF property. For the PP site, irrigation samples were taken on June 13, 2018 from the open irrigation canal, located approximately 800 m south of the site, which supplies the PP irrigation system. Additional samples were collected from open irrigation canals at three locations between the PP and LDF sites (all within the SMRID) on the same day to determine whether any spatial trends in irrigation water chemistry could be observed. The locations and results from irrigation canal sampling can be found in Appendix A. All irrigation samples were collected in clean, 50 mL (or similar) plastic vials and stored in a cooler until refrigeration upon return to the lab.

Snowmelt runoff samples were collected from ponded depressions at the LDF and PP sites on March 23, 2018 and again at LDF on April 24, 2018. Multiple samples were taken from different locations within each ponded depression in an attempt to capture any spatial variability in the pond water. Samples were collected in clean, 50 mL (or similar) plastic vials and stored in a cooler until refrigeration upon return to the lab.

2.3.4.2 Groundwater samples

Groundwater samples were collected from the eight monitoring wells at the LDF site in July and October of 2017 and May and September of 2018. Sampling methods varied for each well depending on the rate of recovery of the well. Typically, since stagnant water in the well can be unrepresentative of formation water, three to five well volumes should be purged before sampling (American Society for Testing and Materials, ASTM # D4448-01). However, only one well (L_IrrDp-2) recovered quickly enough (i.e., within minutes) for three well volumes to be purged prior to sampling. Three of the wells (L_IrrDp-1, L_IrrFl-2, and L_DryFl-1) recovered in 5 hours or less and were purged dry and then sampled several hours later on the same day, after sufficient water level recovery. The remaining four wells (L_IrrFl-1, L_IrrFl-3, L_DryFl-2 and L_DryFl-3) took anywhere from three days to several months to recover. It has been shown that groundwater typically moves horizontally across the well screen and maintains little interaction with the stagnant water column above (Powell & Puls, 1993) which can allow for discrete sampling of water from the within the screened interval. Therefore, the slow-recovering wells at LDF were sampled by lowering a bailer slowly to the middle of the screened interval and pulling up quickly in an attempt to sample only that part of the water column. It should also be noted that both stagnant and formation waters were sampled when possible (in wells that were purged) and results from both samples were always within 1 mg/L (chloride analyses) or 1 ‰ (stable isotope analyses) of each other. This indicates that chloride concentrations and isotopic conditions in the stagnant water in the wells did not differ significantly from the formation waters. All groundwater samples were collected using a single valve bailer; water was transferred directly from the bailer to clean, 50 mL plastic vials and stored in a cooler until refrigeration upon return to the lab.

2.3.5 Water sample analyses

Chloride concentration in porewater of all borehole samples was determined via the aqueous extraction method described by Rhoades (1982). A subsample of 100 g was taken from each of the bagged borehole samples and placed in an Erlenmeyer flask with 120 mL of deionized water. The flasks were placed on an orbital shaker for four hours to homogenize the slurry, and then transferred to centrifuge tubes and centrifuged for about one hour. The resultant supernatant was filtered through a 0.45 μm membrane and analysed using ion chromatography (Dionex, ICS-1000). The dilution factor of the supernatant to the original porewater was calculated using the subsample wet weight, the gravimetric water content (from oven-drying) and the volume of water added to the slurry, and was then used to calculate the concentration of chloride in the porewater. Chloride concentrations of melted snow, rain, irrigation water, snowmelt runoff and groundwater samples were also determined using ion chromatography (Dionex, ICS-1000) after filtering through a 0.45 μm membrane.

Stable isotopes of the water molecule (^{2}H and ^{18}O) were analysed for all water samples. Isotope ratios are measured relative to V-SMOW (Vienna-Standard Mean Oceanic Water) and reported in delta notation:

$$\delta_{sample} = \left[\frac{R_{sample}}{R_{V-SMOW}} - 1\right] \times 1000 \quad (2.3)$$

where R is the ratio of heavy to light isotopes. All surface and groundwater samples were analysed at the University of Calgary Isotope Science Laboratory (ISL) using an off-axis integrated-cavity laser spectroscopy isotope analyser (LosGatosResearch, DLT-100). Porewater of borehole samples was analysed using the direct equilibrium method described by Koehler et al. (2000). A subsample of about 4 g was taken from each jarred borehole sample and placed in a

12 mL vial with a hokko bead (a platinum catalyst required for hydrogen-water equilibrium). The subsample was then flushed with H_2 for ten minutes and left to equilibrate for 4 hours for ^{2}H analysis; for ^{18}O analysis it was flushed with CO_2 and equilibrated for 12 hours. Samples were then analysed using continuous flow isotope ratio mass spectrometry (CF-IRMS). The ISL set up consisted of an on-line gas preparation system (Thermo Scientific, Finnigan II Gasbench) coupled to a mass spectrometer (Thermo Scientific, Delta V Plus).

2.3.6 Quantifying recharge

2.3.6.1 Water table fluctuation method

The water table fluctuation (WTF) method described by Healy and Cook (2002) was used to estimate recharge at the three LDF sub-sites (Figure 2.2). This method uses the increase in groundwater level in response to water input events (i.e., rainfall and irrigation) to calculate the resultant groundwater recharge. Specific yield (S_y) of the formation must also be known. It is applicable to unconfined aquifers and assumes that all water level rise is due to water arriving at the water table. Healy and Cook (2002) state that although this method is most suitable in areas with shallow water tables and short (hours to days) periods of water level rise, it can also be applied to aquifers with thick unsaturated zones if the system displays only seasonal fluctuations in water level. The latter is the case at LDF, where there is typically only one period of water level rise per year following spring snowmelt, and sometimes a second rise related to irrigation. Recharge, R (mm/d), was calculated using the following equation:

$$R = \frac{S_y \Delta h}{\Delta t} \tag{2.4}$$

where S_y is specific yield (unitless), Δh is the change in water level (mm), and Δt is the time period over which the water level rise occurs (d). A specific yield of 0.083 was previously

determined for a nearby site with similar soil and surficial geology, located approximately 2 km to the north west of the LDF site (Kyte, 2018). Specific yield is dependent on the depth of the water table. This dependency is especially important in areas with fine-grained sediments, such as glacial till, due to the effects of capillary rise above the water table. Therefore, S_y was determined based on the method described by Cheng et al. (2015), which relies on soil water retention curve data to approximate the soil water content in the profile above the water table. To estimate S_y, Kyte (2018) assumed a water table depth of 3.0 m which is similar to depths measured at the three LDF sub-sites (ranging from 1.4 to 4.1 m bgs on average over the duration of the study period). For this reason, as well as the proximity of the Kyte (2018) study to the LDF site and reported similar soil conditions (Dark Brown Chernozem) and surficial geology (glacial deposits), the value obtained by Kyte (2018) was deemed appropriate to use for LDF WTF calculations. Additionally, this value is within the range of reported values for fine-grained sediments such as clay till (Johnson, 1967). As such, the value of 0.083 was used for all WTF calculations at the LDF site.

The uncertainty in WTF calculations was estimated assuming an accuracy of ± 0.05% for water level readings reported by Solinst pressure transducers (according to published instrument specifications), and ± 0.02 days (30 minute transducer reading frequency). Since no uncertainty values for S_y estimates were reported by Kyte (2018) or Johnson (1967), an estimated uncertainty of ± 20% was used.

2.3.6.2 Chloride mass balance method

The chloride mass balance (CMB) method is often cited as the most widely used approach for estimating ground water recharge in arid and semi-arid climates (Scanlon et al., 2006). It is based on the principle of conservation of mass, where the mass of chloride deposited

onto the ground surface is equal to the mass of chloride entering the groundwater (Allison & Hughes, 1978; Scanlon et al., 2002), and is described by the following equation:

$$RC_R = PC_P \quad (2.5)$$

where R is recharge (mm/yr), C_R is the chloride concentration in groundwater (mg/L), P is precipitation (mm/yr), and C_P is the chloride concentration in precipitation (mg/L). Measurements of C_P typically include both wet and dry fallout (Allison et al., 1994). Equation 2.5 shows that recharge is inversely proportional to the chloride concentration in groundwater.

The standard CMB method described above does not account for other anthropogenic chloride inputs to the system, such as fertilizer, cattle salt blocks or road salt, nor does it account for the lateral transfer of chloride via runoff from uplands to depressions or subsurface cycling from depressions to uplands. Pavlovskii (2019) recently addressed these concerns and suggested a modified CMB method that is more appropriate for application in the prairies of Alberta where hummocky terrain and agriculture are ubiquitous. The modified CMB method used in this study is based on the work done by Pavlovskii (2019), and is described by the following equation:

$$RC_R = PC_P + IC_I + Q_{in} \pm OC_O \quad (2.6)$$

where I is the amount of irrigation applied to the field (mm/yr), C_I is the chloride concentration of the irrigation water (mg/L), Q_{in} is the amount of chloride applied via anthropogenic inputs (fertilizer in this case) (mg/m^2/yr), O is the lateral overland flow subtracted from uplands and added to depressions (mm/yr), and C_O is the chloride concentration of the overland flow (mg/L). Figure 2.3 shows a schematic depicting the differences between the standard CMB method and the modified approach used in this study. The modified CMB method was used to estimate long-term annual recharge rates in mm/yr for all seven sub-sites at the LDF and PP sites (Figure 2.2). In this study, the “long term” recharge rate determined for a sub-site refers to the average

recharge rate since irrigation began at that location. A brief description of how each parameter in Equation 2.6 was quantified follows below, and parameter inputs used for each CMB calculation are shown in Table 2.2. The uncertainty estimated for each parameter is also described and reported in Table 2.2.

Chloride concentration of the groundwater (C_R) was estimated as the average chloride concentration in porewater extracts from borehole samples from 1.5 to 7.5 mbgs. Chloride concentrations of groundwater sampled from monitoring wells at LDF were typically identical to concentrations in porewater sampled from the same depth; as such the porewater was considered representative of groundwater conditions. Samples above 1.5 mbgs were excluded since chloride concentrations in the root zone are affected by evapotranspiration and solutes in the first 1-2 mbgs have been found to be partially excluded from the recharge flux (Gaye and Edmunds, 1996). Only chloride concentrations from borehole samples above 7.5 mbgs were included in CMB calculations since three of the seven sampled boreholes did not exceed this depth (Table 2.1) and a consistent measurement interval was desired for comparing recharge rates between locations. Uncertainty in C_R for each borehole was estimated as the standard deviation of the chloride concentration of samples from 1.5 to 7.5 mbgs in that borehole.

Precipitation (P) was taken as the 50-year average annual precipitation value of 440 mm/yr recorded at the Lethbridge airport weather station from 1957-2007 (Government of Canada, 2017). Uncertainty in precipitation was estimated as the standard deviation of annual precipitation records over the same time period (1957-2007). Summers and Hitchon (1973) found that the average chloride concentration in year-round precipitation (C_P) was 0.36 mg/L for central Alberta, whereas the weighted average value recorded at the Lethbridge Airport by the Canadian Air and Precipitation Monitoring Network (CAPMoN) from 1976-1985 was 0.27 mg/L

(Government of Canada, 2018). The weighted average chloride concentration of all precipitation samples collected at the LDF site was 0.57 mg/L and 0.45 mg/L at the PP site. However, the precipitation sampling method used in this study was not ideal for accurate chloride analysis due to the potential for contamination. Previous studies in the Canadian prairies have used values up to an order of magnitude lower for CMB calculations, ranging from 0.04 mg/L to 0.07 mg/L (Hayashi et al., 1998; Pavlovskii et al., 2019), recorded at weather stations located over 300 km to the northeast of Lethbridge (eg., Esther, Alberta). As such, the value of 0.27 mg/L obtained from CAPMoN data was used for CMB calculations in this study since it was determined from samples collected at the Lethbridge airport, much nearer to the study sites than other reported values. Although the value of 0.27 mg/L is larger than values previously used for CMB calculations in the prairies, the region northeast of Lethbridge has the highest density of livestock in Alberta (Beaulieu et al., 2001) which could contribute to the elevated chloride in the atmosphere. The uncertainty in the C_P value was chosen to be ± 0.20 mg/L in attempt to span the range of values reported by the aforementioned studies.

The average annual irrigation (I) was determined by consulting annual reports published by the SMRID from 1969-2017. The volume of water delivered to each "water coordinator" as well as the total area irrigated within the district were reported annually, giving an estimate of the irrigation applied on average throughout the SMRID each year. Resultant yearly irrigation amounts were averaged over the past 40 years (1977-2017) for the LDF site and 15 years (2002-2017) for the PP site based on knowledge of the irrigation history at each site (Section 2.2). This resulted in an average long-term irrigation amount of 292 mm/yr for LDF and 213 mm/yr for PP. These values are similar to irrigation amounts recorded at LDF during the study period (Table 2.3), keeping in mind that irrigation amounts vary significantly from year to year depending on

meteorological conditions (including precipitation) and crop type. Uncertainty in annual irrigation rates was estimated as the standard deviation of yearly irrigation calculated from 1969-2017. C_I was determined by taking the average chloride concentration of LDF irrigation water samples (0.48 mg/L) for LDF locations, and the average of irrigation samples from canals near PP (0.64 mg/L) for PP locations. Uncertainty in C_I was estimated as the standard deviation of the chloride concentration of all irrigation samples collected in 2018.

The anthropogenic chloride input (Q_{in}) was difficult to determine due to scarce information about typical application rates and conventions for reporting fertilizer application that are not conducive to estimating Cl^-. For example, reports typically only present the amount of nutrient (e.g., nitrogen, potassium, phosphate) applied, with little information provided about the chemical composition of the fertilizer blend. Additionally, the variability of application rates between years, crops and farmers is significant. The method for determining Q_{in} in this study was based on the method used by Pavlovskii et al. (2019). For this method, yearly shipments of potassium chloride (KCl^-) fertilizer to Alberta (available since 2010), and the area of land in crops and pastures (available for 2011 and 2016, Statistics Canada) were determined. The assumption employed for this method is that most imported fertilizer would likely be applied to areas with these land use classifications, although this presents a large degree of uncertainty. Since fertilizer application is typically greater for irrigated crops compared to dryland crops, relative rates of fertilizer application reported for each land use type (Alberta Agriculture and Forestry,) and relative areas of irrigated, dryland and pastured land in Alberta (Statistics Canada) were used to determine the average yearly application rate for irrigated and dryland crops. The calculated annual Q_{in} values were 420 mg/m^2 for irrigated fields and 368 mg/m^2 for dryland fields (Table 2.2). This method relies on many additional assumptions (e.g., that all KCl^-

shipments to Alberta are used as fertilizer, that no other source of Cl^- in fertilizer is added, that application rates for irrigated, dryland and pasture fields are the same throughout the province, etc.), and thus there is a large uncertainty associated with the resultant application rates. The uncertainty in the Q_{in} values was estimated using the standard deviation of the fertilizer shipments since 2010, the standard deviations of the area of cropped and pastured land from 2011 and 2016, and the standard deviations of the areas of irrigated, dryland and pasture from 2014 and 2016, and applying the standard error propagation analysis during calculations.

It should be noted that information about fertilizer application since 2005 at the LDF site was provided, however, the analysis of these data suggested chloride application rates an order of magnitude higher than the rates presented above for irrigated fields, which seemed unlikely. Furthermore, no data were provided for the dryland field. This method (i.e., to estimate local rates at the LDF rather than regional rates) also requires many assumptions. In particular, it assumes that all of the potassium reported in fertilizers applied to the fields was sourced from KCl^-, which is likely but not necessarily always the case. Additionally, other nutrients in fertilizer (e.g. nitrogen and phosphorus) can be associated with Cl^- but could not be accounted for based on the information provided. Lastly, because the information provided only allowed for estimates of fertilizer application for the irrigated fields at the LDF site, using the regional rates determined above was deemed to be more representative of both the LDF and PP sites as a whole, despite the associated error.

The amount of overland flow (O) estimated for each upland and depression was determined using fine-resolution (< 5 m) elevation maps and the volume-area-depth relationship method described by Hayashi and van der Kamp (2000). There were two melt events in 2018 that produced significant ponding, but re-freezing, precipitation and evaporation/sublimation

occurred between and during the two events, making it difficult to accurately quantify the exact amount of additional overland flow added during the second event. As such, the uncertainty in overland flow was estimated as the amount of overland flow produced from the first melt event ± the amount estimated from the second melt event. The chloride concentration of overland flow (C_O) was determined using the average chloride concentration of snowmelt runoff sampled from each depression. Only overland flow as a result of snowmelt (i.e., spring snowmelt runoff) was considered for CMB calculations, and was assumed to be negligible on flatlands. The uncertainty in C_O values for each depression was estimated as the standard deviation of chloride concertation of samples from that depression.

2.3.6.3 Water balance method

The water balance method attempts to quantify all water inputs and outputs to the system, making groundwater recharge the residual in a water budget equation where all other parameters are known (Scanlon et al, 2006). Recharge was calculated at all three of the LDF sub-sites (Figure 2.2) using the following water budget equation:

$$P + I - ET \pm O - R = \Delta\theta \quad (2.7)$$

where P is precipitation, I is irrigation, ET is evapotranspiration, O is overland flow (or runoff), R is recharge, $\Delta\theta$ is the net change in soil water storage in the soil profile and all parameters are measured in rates (e.g., mm/d).

In this study, $\Delta\theta$ was determined by measuring the net change in water content using HydraProbe sensors at depths of 20, 40, 60, 80, 100 and 150 cmbgs and integrated over the soil profile from 0-2 mbgs. Therefore, recharge was defined as any residual water that was available for drainage below 2 m depth. Precipitation, irrigation and ET were quantified using

meteorological measurements and overland flow was quantified using the volume-depth-area relations according to Hayashi and van der Kamp (2000). The water balance calculation was always done over some known time period and all parameters were cumulative measurements over that period with the exception of $\Delta\theta$, which was a net change calculated using the initial and final soil water contents from the beginning and end of the period. Two time periods are of interest for water balance calculations in this study: the "overwinter" period was defined as November 1, 2017 to April 30, 2018 in order to estimate snowmelt recharge in mid-winter and spring, whereas the "growing season" period was from seeding date to harvest date to estimate recharge from irrigation and summer precipitation. Uncertainty in water balance calculations was quantified using standard error propagation analysis. Details about error analysis can be found in Appendix G.

2.3.7 Numerical model

A numerical model was constructed in order to compare recharge rates and processes under irrigated and dryland conditions, specifically during the growing season. The model was calibrated using data collected from L_IrrFl during part of the 2018 growing season. The full growing season was then simulated under both irrigated and dryland conditions. The following section will describe in detail the model construction, calibration and simulations.

2.3.7.1 Governing equations

The numerical model was constructed using the HYDRUS 1D version 4.17 software (Šimůnek et al., 1998; Šimůnek et al., 2013). In order to account for the potential role of preferential flow in the subsurface, a dual-porosity flow model was chosen for all simluations in this study (Šimůnek et al., 2003), with mass transfer driven by differences in pressure head. The

dual-porosity flow model describes water flow using two domains: the matrix (subscript *m*) and the macropores (subscript *f*). Water flow is restricted to the macropore domain; water in the matrix is stagnant and does not flow. As a result, the total water content (θ_t) is partitioned into the matrix and macropore regions:

$$\theta_t = \theta_m + \theta_f \tag{2.8}$$

where θ_m is the water content of the matrix domain and θ_f is the water content of the macropores, all in m^3/m^3. Exchange of water and solutes is permitted between the two domains and described using first-order transfer terms (Šimůnek et al., 2003). Water movement and storage within the dual-porosity model is described using the Richards equation (Equation 2.9) for the macropore domain and a mass balance equation that describes moisture dynamics in the matrix domain (Equation 2.10):

$$\frac{\partial \theta_f}{\partial t} = \frac{\partial}{\partial z}\left[K(\Psi)\left(\frac{\partial \Psi}{\partial z} + 1\right)\right] - S_F - \Gamma_w \tag{2.9}$$

$$\frac{\partial \theta_m}{\partial t} = -S_m + \Gamma_w \tag{2.10}$$

where Ψ is the soil matric potential (cm), *t* is time (d), *z* is the depth within the soil column (cm), *K* is the unsaturated hydraulic conductivity (cm/d), and S_f and S_m are sink terms (root-water uptake) for each domain (1/d). Γ_w (1/d) is the mass transfer rate between matrix and macropore domains and is assumed to be proportional to the difference in pressure heads between the two domains (Gerke & van Genuchten, 1993; Šimůnek et al. 2003):

$$\Gamma_w = \omega(h_f - h_m) \tag{2.11}$$

where ω is a first-order mass transfer coefficient (1/cm·d). In order to compute heads for each domain (i.e., h_f and h_m), soil water retention characteristics are described using six parameters for the macropores ($\theta_{s\text{-}f}$, $\theta_{r\text{-}f}$, α_f, n_f, K_s, and *l*) and four for the matrix ($\theta_{s\text{-}m}$, $\theta_{r\text{-}m}$, α_m, n_m) (van

Genuchten, 1980; Mualem, 1976). The governing flow equations are solved numerically in HYDRUS-1D using Galerkin-type linear finite element schemes (Šimůnek et al., 2013).

ET in HYDRUS 1D is divided into two independent processes: evaporation from the soil surface and transpiration from the soil profile (i.e., root-water uptake). In the dual-porosity model, root-water uptake is restricted to the macropore domain (since water in the matrix cannot flow) and is distributed within the soil profile depending on the root distribution/root depth. Thus, in Equations 2.9 and 2.10, $S_m = 0$ (Jiang et al., 2010), and S_f was specified based on published root water uptake and water stress response functions available in HYDRUS for different crops (Feddes et al., 1978). Additionally, HYDRUS requires input of daily potential evaporation and transpiration rates, and actual rates are calculated based on the availability of water in the soil profile.

2.3.7.2 Calibration

One-dimensional, vertical water flow at L_IrrFl was simulated for a soil column with a length of 250 cm over a period of 52 days from August 10 to September 30, 2018. Large gaps in tensiometer data prevented a longer calibration period. The column was discretized into 150 nodes and divided into three layers (Figure 2.4) based on both field and laboratory observations of soil texture, grain size and soil water retention characteristics. The top of the soil column (ground surface) was set to a time-variable atmospheric boundary condition to allow for input of daily precipitation, irrigation and actual *ET* measurements. It should be noted that HYDRUS requires potential ET values, but only actual ET was measured at the LDF site. This introduces some uncertainty in water balance calculations derived from model simulations, where the usage of actual ET in place of potential ET will cause ET to be underestimated by the model.

The water table at L_IrrFl was approximately 250 cm bgs for the duration of the calibration period; the bottom of the soil column was therefore represented using a constant pressure head boundary condition of Ψ=0 cm. Any downward flux across the lower model boundary was considered recharge (i.e., water that reached the water table). The sugar beet crop was considered mature for the duration of the calibration period since it spanned the late growth crop stage (Allen et al., 1998) and therefore a constant maximum rooting depth of 90 cm was used (Allen et al., 1998). Root-water uptake was described using the Feddes et al. (1978) water stress response function; the default root-water uptake parameters for sugar beets were selected from the HYDRUS-1D database (Šimůnek et al., 2013).

Initial conditions were set to hydraulic head values measured at 30, 60, and 90 cmbgs at L_IrrFl on August 10. Data from the 150 cm deep tensiometer showed evidence of a compromised seal around the tensiometer cup (i.e., measured pressure heads approximately equal to atmospheric pressure) and were thus omitted from the modeling exercise. A spin-up period was simulated in order to achieve equilibrated initial conditions, using the daily *ET*, precip and irrig measured at L_IrrFl during the first 5 days of the calibration period (August 10-August 14). This spin up period was chosen because it included an irrigation event on August 11, and the hydraulic head conditions were similar on August 10 and August 14. The 5 days of input data were repeated 50 times, for a total spin up simulation period of 250 days. Initial estimates for soil water retention parameters ($\theta_{s\text{-}f}$, $\theta_{r\text{-}f}$, α_f, n_f, K_s, l, $\theta_{s\text{-}m}$, $\theta_{r\text{-}m}$, α_m, and n_m) were obtained from lab measurements (pressure plate analysis, oven-drying) and literature review (Šimůnek et al., 2003, Bishop et al., 2015; Jiménez-Martínez et al., 2009). The simulated hydraulic head values at 30, 60, and 90 cmbgs the end of the spin up period were within 5% of the field-measured values

on August 10. The resultant hydraulic head distribution within the soil profile was used as initial head conditions for the calibrated model described below.

The model was calibrated by modifying soil water retention parameters for both the macropore and matrix domain to reproduce daily field measurements of pressure head and soil moisture at L_IrrFl. Hydraulic head measured at 30, 60 and 90 cmbgs and water content measured at 20, 40, 60, 80, 100 and 150 cmbgs were used (Figure 2.4). The observed amount of recharge produced at L_IrrFl during the calibration period was estimated using the water balance method, and the flux out of the bottom of the model was set to this value in order to further constrain the calibrated model. The inverse solution function in HYDRUS-1D allows for optimization of a maximum of 15 parameters. As such, the following five parameters were optimized for each of the three layers: n_f and K_s, (macropores), α_m and n_m (matrix) and ω. The remaining soil water retention parameters were estimated from pressure plate analyses or determined from the literature (Šimůnek et al., 2003, Bishop et al., 2015; Jiménez-Martínez et al., 2009).

2.3.7.3 Irrigated field simulation

The calibrated model was modified slightly in order to simulate the entire L_IrrFl growing season. Seeding occurred at L_IrrFl on May 24 and harvest was on October 31 (Table 2.3). However, the irrigated simulation period was chosen to begin several weeks prior to seeding to allow for model spin up, resulting in a simulation period of 184 days from May 1 to October 31, 2018. The soil column, boundary conditions and layering are shown in Figure 2.4 (the same as for the calibration period) and each layer was assigned the soil water retention parameters obtained during calibration. Daily meteorological measurements for the entire simulation period were used for the top boundary condition. A root-growth curve was developed

based on data collected by Fitters et al. (2018), who measured sugar beet rooting depth in the early crop stages under irrigated conditions (Figure 2.5). Daily values for rooting depth were determined based on Figure 2.5 and the maximum rooting depth was maintained at 90 cmbgs (Allen et al., 1998).

Simulated hydraulic head and water content values were compared to field data from L_IrrFl to determine whether the model could reproduce realistic conditions within the soil profile. Additionally, a water balance calculation was done for the simulation period to estimate simulated recharge, using the simulated *ET* and net changes in water content. The simulated and measured components of the water balance calculation were then compared.

2.3.7.4 Dryland field simulation

Ideally, hydraulic head data from L_DryFl tensiometers would have been used to construct a fully calibrated dryland model, such as the one described above for the irrigated simluations. However, the dry conditions at L_DryFl resulted in tensiometers drying out, causing sensor failure and very few days of reliable tensiometer data, preventing the construction of a calibrated dryland model. As an alternative, the calibrated model from irrigated field simulations was modified in order to simulate dryland conditions. Although this prevents the direct comparison of simulated outputs to field data measured at L_DryFl, comparing the irrigated and dryland field simluations allows for analysis of vadose zone dynamics under both irrigated and dryland conditions.

The model developed for the irrigated field simulations was modified slightly in order to simulate a theoretical dryland field scenario. The soil column, boundary conditions, layering and soil water retention parameters were the same as for the irrigated field simulation (Figure 2.4). The daily meteorological measurements were modified by excluding irrigation events (i.e., using

only precipitation events) and using actual *ET* values obtained from L_DryFl as opposed to L_IrrFl. Again, the use of actual ET rather than potential ET introduces uncertainty into the water balance calculations derived from model results (see section 3.2). The dryland field simulation period was the same as for the irrigated field simulation (May 1 to October 31, 2018), however, since dryland crops have shorter growth stages and are harvested earlier (Allen et al., 1998), the seeding and harvest dates from the L_DryFl canola crop in 2018 were used (Table 2.3). Since sugar beets would likely not be grown under dryland conditions, the root water uptake and water stress response parameters were changed from sugar beets to wheat (canola was not listed in the HYDRUS-1D database and wheat and canola display similar growth patterns (Allen et al., 1998)). The root growth function in Figure 2.5 was also modified to reflect canola under dryland conditions using an approximate rooting depth of 5 cm at emergence (Canola Council of Canada, 2017) and a maximum rooting depth of 100 cm (Allen et al., 1998).

Just as for the irrigated field simluations, hydraulic head and water content values from the dryland simluations were compared to field-measured values from L_DryFl. However, since the model was not calibrated to L_DryFl field measurements, these data are only included to provide an example of possible dryland conditions and direct comparisons between simulated and observed measurements cannot be drawn. A water balance calculation was also done for the dryland field simulation to estimate simulated recharge using simulated *ET* and net changes in water content. Lastly, the water balance results from the irrigated and dryland field simluations were compared.

2.4 Results

2.4.1 Soil properties and lithology

Lithological well logs were developed for each borehole drilled at the LDF and PP sites and can be found in Appendix B. At LDF, glaciolacustrine sediments (e.g., silty clay) were observed from ground surface to a maximum depth of 2.5 m, below which clay till with sporadic sand stringers (sand beds a few centimeters thick) and abundant shield clasts was observed. The sediments were brown or brownish-grey to a depth of about 13.5 m, becoming medium grey below that. This is consistent with observations made by Rodvang et al. (2002), who suggested brown sediments represent the oxidized zone above the regional redoxcline (Hendry et al., 1986), while brownish-grey sediments represent a transition zone to the grey, unoxidized zone below (they did not sample deep enough to encounter grey sediments). At the PP site, silty-clay or fine-grained sand was observed to depths of 7.6 mbgs beneath both depressions and to approximately 5 m depth below P_IrrUp. Below the sand at P_IrrUp, clay till was observed. At P_DryUp, silty clay was observed to approximately 1 mbgs, with clay till below that.

Porosity, dry bulk density, grain size and clay mineralogy obtained from laboratory analyses of intact soil ring samples are presented in Table 2.4. Grain size analyses indicate that soil texture ranged from loamy sand to sandy loam (Canadian System of Soil Classification), with loamy sand only occurring at L_DryFl, and a clay fraction of less than ten percent in all samples. On average, clay, silt and sand fractions were 7.5 %, 25.3 % and 63.7 %, respectively, at L_IrrDp, 7.3 %, 21.8 % and 67.3 % at L_IrrFl, and 6.3 %, 18.2 % and 72.8 % at L_DryFl. Clay mineralogy is presented as a percentage of total clay fraction by weight and results indicate that the clay fraction was predominantly made up of smectite, with smaller proportions of illite and kaolinite for all samples (Table 2.4). Soil hydraulic parameters obtained from fitting pressure

plate and dewpoint data to the van Genuchten (1980) model are also included in Table 2.4. Soil water retention curves showing data points and fitted van Genuchten curves are included in Appendix C.

Volumetric water content (θ) profiles measured on borehole samples from the LDF and PP sites are shown in Figure 2.6. Both sites showed greater variability in water content between sub-sites above 1.5 to 2.0 m depth (i.e., the active rootzone for most mature crops), and then became more consistent below the water table. Figure 2.6 shows that, when comparing all boreholes, the average water content in the active root zone was greater for irrigated sub-sites (0.26 to 0.37) than for dryland sub-sites (0.11 to 0.22). Specifically, at the LDF site (Figure 2.6a), the average water content in the active root zone at L_IrrDp was slightly wetter (0.29) than L_IrrFl (0.26) and both were significantly wetter than L_DryFl (0.18). Deeper in the profile, the average water content below approximately 3 m depth remained relatively stable around 0.3 beneath all sub-sites at LDF. Similarly, at the PP site (Figure 2.6b), the average water content in the active root zone was extremely variable: P_IrrDp was the wettest of all sub-sites at 0.37, followed by P_IrrUp (0.31), P_DryUp (0.22) and P_DryDp (0.11). The average water content below approximately 4 m depth at PP hovered around 0.44 beneath all sub-sites except P_DryUp, which was significantly drier (0.28) from about 2 to 6 m depth, increasing to 0.37 below that.

2.4.2 Snow surveys

SWE obtained from weekly snow surveys at each LDF sub-site are presented in Figure 2.7. All three sub-sites at LDF displayed similar SWE values throughout the winter except on

February 25 and March 4, when L_IrrDp SWE was significantly higher than the other two sub-sites, possibly due to accumulation of windblown snow within the topographic low.

Mid-winter melts have been shown to play an important role in the timing and amount of overwinter recharge in regions where complete snow depletion occurs in mid-winter due to *foehn* winds, or "Chinooks" (Pavlovskii et al., 2019), which are common in the Lethbridge area (Nkemdirim, 1996). Several mid-winter snowmelt events occurred at the LDF site during the study period; however, only three mid-winter melt events resulted in complete snowpack depletion *and* increased soil moisture in the profile. For simplicity, in this study, any melt event that occurred prior to the final spring melt is considered a "mid-winter" melt, even those that occurred in later winter/early spring when meteorological conditions may have been more spring-like than winter. The three mid-winter melt events at the LDF site each consisted of a "melt period" that occurred over several days, from the start of snowpack depletion to complete snowpack depletion as determined by time-lapse photos. The first mid-winter melt event occurred from November 21-23, 2017 and is not shown in Figure 2.7 as snowpack data collection did not begin until January 2018. The other two events occurred in 2018 from January 5-8 and March 19-22 (Figure 2.7). The final spring melt occurred on Apri1 11. These four melt events will be referred to later in the text as the November, January, March and April melt events, respectively. Note that no snow survey was conducted at L_IrrDp on April 9 since ponding occurred on March 19, followed by several freezing and snowfall events, making it difficult to delineate snow, liquid water and ice areas.

2.4.3 Groundwater monitoring

Saturated hydraulic conductivity (K_s) results obtained from bail tests performed at LDF monitoring wells are shown in Figure 2.8. Measured K_s values varied over four orders of magnitude, from 1.3×10^{-6} to 3.6×10^{-10} m/s, which is slightly larger than the range previously measured by Rodvang et al. in 2002 (1.9×10^{-6} to 6.3×10^{-9} m/s). However, tills often exhibit a wide variation in K_s, especially in the area above and near the redoxcline due to extensive fracturing produced by weathering (Hendry et al., 1986) and the variable number of fractures intersected by each well screen. K_s decreased significantly in the deepest well (Figure 2.8), which is likely below the fractured, oxidized zone.

Water levels from monitoring wells at LDF for the duration of the study period can be found in Appendix D. Figure 2.9 shows the water levels in the two shallowest wells from each sub-site at LDF from March to September 2018 (the deep wells at L_IrrFl and L_DryFl took months to recover and were therefore omitted). The water table at L_IrrDp (Figure 2.9a) rose above the ground surface following the March melt event, producing a pond in the depression with a maximum depth of 0.24 m. There was an average upward hydraulic gradient at L_IrrDp for most of the year of approximately 0.08 between the two well screens. Both sets of flatland wells (Figures 2.9b and 2.9c) showed an increase in water level rise around April 19, about one week after the final snowmelt event on April 11. Water levels at L_IrrFl showed a second increase in water level rise after July 5, in response to two large, back-to-back irrigation events on July 5 and 6. The post-harvest period at L_DryFl (i.e., after August 16) showed a transition to a slight upward hydraulic gradient.

The WTF method was used to estimate groundwater recharge from the water level responses described above. The recharge calculated from the snowmelt response in the

shallowest well at each sub-site indicated in Figure 2.9 was 170 ± 34 mm for L_IrrDp and 33 ± 7 mm for both L_IrrFl and L_DryFl. The recharge calculated from the irrigation response at L_IrrFl was 42 ± 9 mm. Uncertainty in recharge estimates using the WTF method is likely conservative due to lack of information about error in the S_y value (section 2.3.6.1).

2.4.4 Soil moisture and temperature

Complete daily soil moisture data from LDF for the duration of the study period can be found in Appendix E. To demonstrate the variability between growing seasons, daily soil moisture data from 20, 60 and 150 cmbgs for July and August is shown for 2017 and 2018 in Figure 2.10. Recall that in 2017 all three sub-sites were seeded with barley, while in 2018 L_IrrDp was barley, L_IrrFl was sugar beets and L_DryFl was canola. L_IrrDp was the wettest and L_DryFl was the driest consistently in both years. In 2017, L_IrrDp showed a soil moisture response to most irrigation events at 20 cmbgs, with smaller magnitude responses seen at 60 cmbgs, however, no response to irrigation was seen in L_IrrFl despite the generally drier soil conditions. Comparatively, in 2018 L_IrrFl showed increases in soil moisture after irrigation events, but L_IrrDp did not. At L_DryFl, soil moisture in 2017 gradually declined over the month of July at 20 and 60 cm depths, but the drying front did not reach 150 cm, whereas in 2018 drying occurred much earlier and reached depths of at least 150 cm (maximum depth of measurement). Irrigation events in 2018 were generally more frequent but lower magnitude than in 2017.Total irrigation in 2017 was 287 mm for L_IrrDp and 190 mm for L_IrrFl and 217 mm for L_IrrDp and 308 mm for L_IrrFl in 2018 (Table 2.3). Summer precipitation (May 1-October 31) was 175 mm in 2017 and 150 mm in 2018.

To analyze the soil profile during the overwinter period (November 1, 2017 to April 30, 2018), Figure 2.11 shows the daily soil moisture data at 20, 60 and 150 cmbgs. The term "overwinter recharge" will herein refer to the recharge that occurred as a result of both mid-winter melts and spring snowmelt, between November 1, 2017 and April 30, 2018. Temperature data is also shown at each depth in Figure 2.11 to help determine whether changes in soil moisture are coincident with freezing and thawing, since soil moisture probes essentially measure liquid water rather than total water content (i.e., liquid + ice). In fall, prior to freezing, the wettest conditions were at L_IrrDp (0.35), L_IrrFl was moderately wet (0.26) and the driest conditions were at L_DryFl (0.22). These relative trends in soil moisture persisted through the winter and into spring.

Figure 2.11 shows increases in soil moisture and temperature in response to the snowmelt events that were discussed previously (Section 2.4.3). November and January melt events resulted in increases in soil moisture at L_IrrFl and L_DryFl only. The March melt event resulted in ponding and saturated conditions at L_IrrDp as well as significant increases in soil moisture at L_IrrFl and L_DryFl. The final melt event in April only caused an increase in soil moisture at L_IrrFl and L_DryFl since conditions were already saturated at L_IrrDp. Note that increases in soil moisture related to melt events typically represent some combination of thawing of existing water plus infiltration of new water from above. Freezing occurred at each sub-site to a depth of at least 20 cmbgs from approximately December 28-January 6 causing slight decreases in soil moisture, although freezing occurred more rapidly and more completely in the flatlands compared to L_IrrDp. The profiles at both flatland sub-sites became frozen to 60 cmbgs from approximately February 15-March 23, whereas the profile at L_IrrDp only froze to 20 cmbgs during that time.

2.4.5 Soil Porewater: chloride and stable isotope profiles

Chloride concentration of porewater extracts from borehole samples are shown in Figure 2.12. At the LDF site (Figure 2.12a), chloride concentration in the top 4 mbgs was lower at L_DryFl (2.5 mg/L) than the two irrigated sub-sites, and then increased with depth to about 60 mg/L at 7 mbgs. In contrast, the two irrigated sub-sites had higher chloride concentrations above 4 mbgs (L_IrrDp at 10.6 mg/L and L_IrrFl at 18.6 mg/L) that decreased with depth and then stabilized around 6.6 mg/L between 4-5 mbgs. Both P_IrrDp and P_DryDp showed consistently low chloride concentration with depth with an average of 10.0 mg/L from 0-7.5 m bgs. In comparison, both uplands showed greater chloride concentrations: P_DryUp reached a maximum of 237 mg/L around 3.7 m bgs while P_IrrUp reached a maximum of 130 mg/L at 4.9 m bgs. Chloride concentrations beneath both P_DryUp and P_IrrUp hovered around 100 mg/L below 5 m bgs. Overall, chloride concentrations in the profiles were much higher at PP than at LDF (note the different x-axis ranges in Figure 2.12).

The $\delta^{18}O$ profiles from stable isotope analyses of porewater extracts from borehole samples are shown in Figure 2.13. Surface water samples (rain, snow, irrigation water, and runoff from two snowmelt events at LDF) are shown, as well as groundwater samples taken from monitoring wells at LDF. Spatial trends and relative isotopic ratios were similar for $\delta^{2}H$ profiles, and are provided in the Appendix F. The volume weighted average $\delta^{18}O$ value for snow samples was -26.7 ‰ at LDF and -24.8 ‰ at PP, which is typical for winter precipitation. The March runoff event had an average of -23.1 ‰ at LDF and -25.1 ‰ at PP. Runoff was sampled a second time at LDF in April after the final melt, and had a much more positive $\delta^{18}O$ value of -14.7 ‰ due to evaporation of the pond water. The average rain and irrigation samples were -15.4 ‰ and

-17.1‰, respectively. At both study sites, the isotope profiles beneath the depressions were consistently more negative than the uplands/flatlands, except for the irrigated depression at PP.

2.4.6 Chloride mass balance

Figure 2.14 shows the long-term annual recharge rates calculated for each study location using the modified CMB method. These results represent point estimates taken at each borehole location and have not been normalized for relative upland/depression/flatland areas of contribution. Depressions at PP had the highest recharge rates, with P_IrrDp and P_DryDp at 113 ± 31 mm/yr and 94 ± 45 mm/yr, respectively, and the LDF irrigated depression was slightly lower at 88 ± 26 mm/yr. The irrigated and dryland flatlands at LDF had comparatively moderate rates of 50 ± 21 mm/yr and 29 ± 44 mm/yr, respectively. The uplands at PP had very low rates, with P_IrrUp at -4 ± 5 mm/yr and P_DryUp at 4 ± 2 mm/yr. When comparing irrigated versus dryland sub-sites, CMB results suggest slightly increased recharge rates on irrigated depressions and flatlands compared to their dryland counterparts, however, this is not true for the uplands (Figure 2.14). It should be noted that the negative recharge rate calculated for P_IrrUp is a byproduct of Equation 2.6 used in the CMB method, where runoff is subtracted from the total input to the upland, and in this case does not necessarily imply upward migration of groundwater from the water table. Recharge estimates using the CMB method have large uncertainties associated with estimating long-term rates for each parameter in Equation 2.6 (see section 2.3.6.2).

2.4.7 Water balance

A water balance was performed for the overwinter season (November 1, 2017 to April 30, 2018) and growing season (seeding to harvest of 2018, Table 2.3) for the three LDF sub-sites (Figure 2.15). An overwinter water balance for L_IrrDp was omitted, however, for several reasons: 1) vapour flux data for L_IrrDp was unavailable, and using values from the other sub-sites as an estimate proved unreliable since L_IrrDp was the only location with standing water; 2) uncertainty in runoff calculations associated with catchment delineation; 3) multiple freezing/melting/snowfall cycles in the pond made it difficult to determine relative amounts of liquid water, snow and ice; and 4) a significant amount of ponded water was pumped out of the depression by landowners near the end of April and, although they provided a rough estimate of the water removed, it was not considered accurate enough to apply to a water balance calculation.

Figure 2.15a shows that overwinter recharge was the same beneath both flatland sub-sites at LDF: 68 ± 113 mm beneath L_IrrFl and 67 ± 113 mm beneath L_DryFl. The similarity in recharge at these two sub-sites is partially due to the fact that a single weather station was used to estimate vapour flux (-37 mm) and precipitation (171 mm) at both sub-sites, since the eddy-covariance system had not yet been installed at L_DryFl. However, net changes in soil moisture content were identical at each site (66 mm) indicating that other fluxes might also have been similar.

The growing season water balance is shown in Figure 2.15b. Precipitation (140 mm) and ET (-448 mm) for L_IrrFl were used for L_IrrDp since no weather station was installed at that sub-site. Precipitation (91 mm) and ET (-246 mm) were significantly less for L_DryFl due to the shorter time period between seeding and harvest (Table 2.3) over which the calculation was

performed. Irrigation for L_IrrFl (350 mm) was greater than for L_IrrDp (217 mm). The net change in water content in the profile was -20 mm for L_IrrDp, 0 mm for L_IrrFl and -176 mm for L_DryFl. These inputs resulted in a negative recharge for L_IrrDp (-39 ± 141 mm), and (42 ± 141 mm) for L_IrrFl which was twice the amount as L_DryFl (21 ± 122 mm).

Recharge estimates obtained using the water balance method have large uncertainty associated with the large magnitude of uncertainty in many of the parameters in Equation 2.7. Values for input into the water balance equation as well as the estimated uncertainty in each parameter are presented in Table 2.5. Detail about error analysis can be found in Appendix G.

2.4.8 Recharge estimates at LDF and PP

A summary of recharge estimates obtained using the WTF, CMB and water balance methods at each study location is shown in Table 2.6. Results from all three methods show that, of the seven sub-sites (Figure 2.2), depressions had the highest recharge rates, followed by flatlands which had moderate recharge and uplands which had very low (if any) recharge. Both the water balance and WTF methods showed that overwinter recharge was nearly identical for both flatlands at LDF, although the water balance method estimated almost double the amount (68 ± 113 and 67 ± 113 mm) compared to the WTF method (33 ± 7 mm). During the growing season at LDF, the water balance and WTF method estimated the same amount of recharge at L_IrrFl (42 ± 9 mm), which is double the amount estimated at L_DryFl using the water balance method (21 ± 122 mm). The water balance method resulted in negative recharge values at L_IrrDp over the summer months, which is consistent with monitoring well data (Figure 2.9) that indicated an upward hydraulic gradient during this time period.

2.4.9 Numerical modeling

2.4.9.1 Calibration results

Model input parameters used for all simulations are shown in Table 2.7. Bolded values were obtained via inverse modeling during the calibration exercise and non-bolded values were determined from laboratory measurements (θ_s) or literature estimates (θ_r, α, l). Values for n were initially estimated by fitting the van Genuchten (1980) model to laboratory-measured soil water retention data (section 2.3.3). However, due to the long time periods required to reach equilibrium for fine-grained soils, water content values under drier conditions were considered uncertain. As a result, *n*-values were determined via inverse modeling during the calibration period. The resultant *n*-values were similar to lab-measured values with the exception of Layer 2, for which the *n*-value determined via inverse modeling was higher than was determined in the pressure plate analysis (Tables 2.4, 2.7). This is consistent with the suspected presence of a "hard-pan" layer at that depth, which would be susceptible to fractures and therefore larger *n*-values than perhaps would have been captured by the *in-situ* soil ring samples.

Hydraulic head results from the calibration period are shown in Figure 2.16, plotted alongside measured tensiometer data from L_IrrFl. The tensiometer cup is in contact with the soil matrix and should therefore, in theory, represent the matric potential of the matrix domain. However, analysis of tensiometer data indicated macropore-like features such as sharp changes in water content in response to irrigation events. Additionally, Šimůnek et al. (2003) suggested that matric potential measurements using tensiometers are "often dominated by the wetter fracture domain that reaches equilibrium relatively quickly". As a result, any hydraulic head data presented for the modeling portion of this study is representative of the macropore domain. The Nash-Sutcliffe (NS) coefficient (Nash & Sutcliffe, 1970), root mean squared error (RMSE) and

mean absolute error (MAE) were used as measures of goodness of fit of simulated heads to observed heads. The model was deemed calibrated when the NS coefficient neared 0.5 and when the RMSE and MAE were less than 10% of the total range in measured heads. Values of goodness of fit were calculated for each layer and then averaged resulting in a NS coefficient of 0.47, a RMSE of 10.0 cm and a MAE of 7.7 cm. The RMSE and MAE are 9.7% and 7.5% of the total range of measured heads, respectively. The calibrated results in Figure 2.16 show reasonably good model fit to measured hydraulic head data, and daily ET outputs were almost identical to measured values.

Figure 2.17 shows the simulated and measured water content for each layer. Note that henceforth in the modeling portion of this study, any water content data presented represents the total water content in the profile (i.e., the sum of macropore and matrix water contents). The model reproduced both the timing and magnitude of changes in water content reasonably well; however, the absolute value of water content was often either over- or underestimated. In other words, for some measurement depths, the model predicted a different water content for a given matric potential than was observed in the field, but the timing and magnitude of changes in soil water content are consistent with field observations. This is in part due to the way soil water retention parameters were estimated, using small sub-samples that are likely not representative of larger scale soil characteristics (e.g., macropores). This was also noted when comparing the partial soil water retention curves generated from field data (section 2.3.1.2) with lab-generated soil water retention curves from pressure plate analysis: for a measured matric potential in the field, the observed field water content was not always consistent with the predicted water content from the pressure plate curves. However, since the model reproduced the timing and magnitude of changes in water content well, the discrepancy between absolute estimates of water content

was deemed acceptable for the purposes of the model (the water balance equation used to estimate recharge from the model requires only the use of $\Delta\theta$).Therefore, in order to better compare the relative timing and magnitude of changes in observed and simulated water content, the mean observed and simulated water content was calculated at each depth (Table 2.8) and the relative offset from the mean water content was calculated. Figure 2.17 shows the observed and simulated water content plotted as the offset from the mean observed or simulated water content, respectively, at each depth.

The simulated water content matched observed values in Layer 1 (20 cm) quite well, while simulated values in Layer 2 (40, 60 and 80 cm) were less well matched (Figure 2.17). Layer 3 (100 and 150 cm), showed very little variability in both simulated and observed water contents. During calibration, matching the absolute value of measured water contents was deemed less important than matching timing and magnitude of soil moisture responses. As such, goodness of fit calculations were calculated based on the absolute deviation from the mean water content, and are also shown in Table 2.8. The average NS coefficient was 0.75, while the average RMSE and MAE were both less than 0.01 (Table 2.8). The absolute values of simulated water content and raw observed water content for the simulated period are included in Appendix H.

A water balance calculation for the calibration period was also used to compare field-measured parameters to model outputs (Table 2.9). Precipitation and irrigation amounts were manual inputs to the model, while evapotranspiration, net change in volumetric water content in the profile and recharge were model outputs. Table 2.9 shows that the model estimated 152.5 mm of ET, a net change in soil moisture of -16.1 mm and 31.6 mm of recharge, compared to 153.9 mm of ET, a net change in soil moisture of -15.6 mm and 29.7 mm of recharge, in the

field-measured water balance. The calibrated model slightly underestimated ET and slightly overestimated recharge but, overall, reproduced field observations at L_IrrFl reasonably well.

2.4.9.2 Irrigated field simulations

The simulated hydraulic heads for the irrigated field are shown in Figure 2.18 plotted with hydraulic heads measured in tensiometers at L_IrrFl. Recall that seeding was May 24 and harvest was October 31(Table 2.3), whereas the simulation period was May 1 to October 30 to allow for model spin-up prior to seeding. Reliable tensiometer data was only available between August 10 and September 30 (i.e., the calibration period). Measured precipitation, irrigation and ET are also shown as well as simulated ET. The model did a reasonably good job reproducing measured heads within each layer. The simulated ET is only slightly underestimated near the beginning and end of the simulated period; this is caused by the use of actual ET in place of potential ET, as described in section 2.3.7.2. During the final two weeks (October 15 – October 31), the simulated heads decreased relatively quickly, which is not consistent with field observations of water content over this same period (Figure 2.19). The suspected reason for this will be discussed in more detail along with Figure 2.19 below.

The measured and simulated water contents in each layer are presented in Figure 2.19. Similar to the calibrated model, the field data was well-reproduced in the top layer in terms of absolute values of water content and timing of responses. However, the model did show slightly larger magnitude fluctuations in water content after each irrigation event, meaning the profile is wetting-up and draining more readily than is observed. Timing and magnitude of fluctuations in water content in Layer 2 were reasonably well-reproduced by the model, but again, like the calibrated model, they were either over- or underestimated. There was a significant increase in measured soil moisture in Layers 2 and 3 following two back-to-back irrigation events on July 6

and 7. This increase was reproduced by the model in Layer 2, but the layer drains too quickly and moisture is not retained in the profile as seen in the field. The model failed to reproduce similar water content increases observed in Layer 3.

Lastly, the soil moisture and hydraulic head in all layers declined steeply during the last two weeks of the simulation period after irrigation stopped on October 5 (Figures 2.18, 2.19). This is another example of the model's tendency to drain the profile too quickly and inability to retain moisture without frequent water inputs. The observed water content did decline after irrigation ceased, since the crop was still taking up water, but the rate of soil moisture decrease in the simulation was much more rapid (Figure 2.19). Additionally, in 2018, sugar beets were not seeded directly above the sensors for fear of damaging cables during seeding, which had occurred in 2017. Instead, weeds occupied the soil directly above the sensors, with the nearest sugar beet plants approximately 40 cm away. Although the soil moisture conditions directly surrounding the sensors would be strongly affected by the sugar beet plants and root systems, the different vegetation growing directly above the sensors could explain some of the discrepancies between observed and simulated water contents. These discrepancies might be more noticeable late in the growing season due to differences in crop behaviour to water stress.

A water balance calculation using simulated and observed data was completed for the period from May 15 to October 15 and is indicated by the shaded region in Figure 2.19. This shortened time interval (compared to the entire simulated period) was chosen to account for the model spin up at the beginning of the simulation period, as well as the discrepancies in the final two weeks mentioned above. The results from the water balance are shown in Table 2.10. The model overestimated recharge (105.6 mm) compared to the field water balance (46.9 mm) and underestimated ET (402.5 mm) compared to measured data (427.9 mm). There is a measured net

increase in water content in the profile (24.0 mm) compared to a simulated net decrease (-9.2 mm).

Overall, the irrigated model reproduced hydraulic head conditions in the profile reasonably well, and matched timing and magnitude of fluctuations in water content reasonably well in the top two layers. However, the simulated water contents (Figure 2.19) suggest that the model was allowing too much drainage through the profile. This results in a net loss in water content in the profile over the simulation period as well as an overestimation of recharge. ET is underestimated during periods of infrequent irrigation. This is because HYDRUS assumes ET inputs are potential rates (as opposed to actual) and the potential for ET decreases with decreased water input.

2.4.9.3 Dryland field simulations

Simulated hydraulic heads for the dryland model are shown in Figure 2.20, plotted with measured tensiometer, ET and precipitation data from L_DryFl. Recall, the "theoretical" dryland model was set up identical to the irrigated model, with the exception of the ET inputs (data from L_DryFl was used), crop type (wheat), and seeding and harvest date (May 17 and August 16, respectively). As such, the primary purpose of the dryland simulations was for evaluating vertical fluxes relative to the irrigated field simulations; however the simulated dryland hydraulic head and water content responses are compared to L_DryFl field data as a point of reference.

The simulated hydraulic heads in Layer 2 dried out to a minimum of -560 cm as the crop matured, and then increased after harvest on August 16. Overall, this pattern is similar to observed heads at L_DryFl, which dried out to a minimum of -800 cm as the crop matured, and increased after harvest (Figure 2.20). Layer 3 also showed drying, although simulated heads only reach a minimum of -400 cm whereas measured heads reached approximately -710 cm. The

simulated head in Layer 1 dried out to a minimum value of -400 cm and then plateaued for most of the growing season, which is not realistic behaviour. This is likely due to the van Genuchten parameters that represent the macropore domain in the uppermost layer of the model and will be discussed with Figure 2.21 below.

Between July 15 and Aug 16, when the most frequent tensiometer data was available, the average observed hydraulic head was -740 cm in Layer 2 and -600 cm in Layer 3. The resultant average observed hydraulic gradient over this period was approximately 4.7 cm/cm (flow from Layer 3 to Layer 2). Comparatively, the average simulated hydraulic head was -460 cm in Layer 2 and -340 cm in Layer 3. The resultant average simulated hydraulic gradient was approximately 4.0 cm/cm (flow from Layer 3 to Layer 2). Therefore, there was a similar hydraulic gradient, in terms of both direction and magnitude, between the bottom two layers for both observed and simulated data. The suggested flow upwards from Layer 3 to Layer 2 is consistent with dryland field conditions, where the majority of water would be extracted from Layer 2 by root uptake and water from below would be drawn upwards to replenish it.

Lastly, Figure 2.20 shows that the dryland model significantly underestimated daily evapotranspiration during most of the growing season. Again, this is because HYDRUS assumes ET inputs are potential rates as opposed to actual rates, causing the greatest underestimation to occur during dry periods between rainfall events.

Simulated water contents are shown in Figure 2.21 with field data from L_DryFl included as a reference. Similar to simulated heads, the water contents in Layer 2 behaved realistically, drying out as the crop matured and recovering slowly after harvest. Data from L_DryFl shows the distinct propagation of a drying front with depth in the entire profile from the end of June to the start of August; a similar front is somewhat represented in Layer 2 of the model but not

nearly as strongly. Layer 3 of the model experienced only a slight decline in soil moisture. Layer 1 dried out to a water content of 0.29 and then plateaued in a manner that was similar to the head behaviour shown in Figure 2.20, and is likely a result of how the dual-porosity model manages water storage and transmission through the profile. Layer 1 has a large macropore n-value (5.9) which suggests large macropores that drain quickly, and since the dual-porosity model only allows for flow in the macropores, any water in the matrix is isolated at that depth once the macropores dry out. The water isolated in the matrix manifests as plateauing head and water content values, until the profile wets up again and transfer between the two domains can resume. Vertical flow within the soil matrix is not possible in dual porosity simulations, even in the presence of large vertical gradients in pressure head (and, by association, water content). Although this feature of the top model layer does not represent realistic field conditions very well, it still suggests very dry conditions in the top two layers from the end of June until the start of September, which is realistic for a dryland crop. The post-harvest data from L_DryFl show that the bottom of the profile is the first to recover moisture, suggesting upward migration of water from below, likely via the finer-grained soil matrix; this is not the case in the model since flow in the matrix cannot be simulated.

Water balance calculations were done for the two shaded box intervals shown in Figure 2.21. The “pre-harvest” calculation is for the period between May 15 and August 15, which represents the period from seeding to harvest, whereas the “post-harvest” calculation represents the time from harvest to the end of the 2018 growing season (August 16 to October 15). These intervals were also chosen to allow for direct comparison to the water balance results from the irrigated field simulations, which were taken between May 15 and October 15 (Figure 2.19). The results from the water balance calculations are shown in Table 2.10. The L_DryFl recharge from

May 15 to August 15 is 19.5 mm, while the dry model estimated 34.3 mm for the same time period. For the post-harvest window, the results are -21.4 mm for the field water balance and -47.5 mm for the dry model. The model significantly underestimated ET during the pre-harvest period, at 152.4 mm compared to a measured ET of 238.8 mm. However, ET was well-reproduced during the post-harvest period, likely due to reduced root water uptake and more frequent rain events, with simulated and field values of 54.8 and 56.9 mm, respectively.

Overall, the theoretical dryland model produced plausible head and water content profiles in the bottom two layers. The uppermost layer did not produce optimal results due to the limitations of the dual-porosity model under such dry conditions; likely the result of having calibrated to much wetter conditions. The water balance calculations show that, like the irrigated model, the dryland model is still overestimating recharge and underestimating ET, especially during the pre-harvest period. However, changes in water content, ET and recharge during the post-harvest period were reasonably well reproduced.

2.4.9.4 Modeling summary

The water balance results from the modeling exercise (Table 2.10) allow for comparison of recharge estimates beneath irrigated fields versus dryland fields during the growing season. When comparing the irrigated and dryland recharge calculated from field observations (46.9 and 19.5 mm, respectively), we see that the irrigated flatland produced 2.4 times greater recharge than the dryland flatland. Comparatively, modeling results showed that the irrigated flatland produced 105.6 mm of recharge compared to 34.3 mm in the dryland, or 3.1 times more recharge under irrigated conditions. The model underestimated ET in all cases and therefore the water balance calculations are subject to uncertainty.

2.5 Discussion

2.5.1 Influence of topography on recharge

It is well known that topography plays an important role in groundwater recharge processes, especially in the PPR where DFR is ubiquitous (Zebarth & De Jong, 1989; van der Kamp & Hayashi, 1998). Results from all three recharge estimation methods (Table 2.6) consistently showed increased recharge rates beneath depressions compared to moderate rates beneath flatlands and low rates beneath uplands. This is consistent with our understanding of DFR, but a more detailed analysis is required to understand how DFR is affected by the addition of irrigation. Characteristics of each topographic element (i.e., uplands, depressions and flatlands) will be discussed below.

2.5.1.1 Uplands

Uplands typically do not contribute significantly to recharge (Rehm et al., 1982; Zebarth et al., 1989a), and any diffuse recharge that does occur has been shown using stable isotope signatures to be primarily sourced from summer precipitation (Pavlovskii et al., 2018). At the PP site, CMB results (Figure 2.14) indicated that recharge was very low beneath the uplands compared to depressions. However, it should be noted that these are point estimates only, and when taking into consideration the relative area of uplands versus depressions in a given catchment, the contribution to recharge from the uplands can increase significantly and perhaps even be comparable to depressions in some cases. Due to the lack of high-resolution elevation data for the entire catchment at the PP site, relative areal contributions of recharge from uplands and depressions could not be calculated.

From isotope profiles at the PP site (Figure 2.13b), we can see that the volume weighted average $\delta^{18}O$ values for summer precipitation (-15.4 ‰) and irrigation water (-17.1‰) were

close to the average values in the upland profiles for both P_IrrUp (-14.8 ‰) and P_DryUp (-16.8 ‰). Therefore, any diffuse recharge occurring beneath the uplands is likely sourced primarily from either summer precipitation or irrigation water, or both on P_IrrUp. However, the addition of water to the uplands through irrigation does not appear to lead to increased recharge on the uplands: P_IrrUp actually showed lower recharge (-4 ± 5 mm/yr) than P_DryUp (4 ± 2 mm/yr) according to CMB results, although both numbers are very low. Instead, the increased water input on P_IrrUp may lead to increased summer runoff, which would then end up in the depressions.

2.5.1.2 Depressions

In contrast to uplands, depressions have been shown to contribute significantly to groundwater recharge via ponding and subsequent infiltration of snowmelt runoff (van der Kamp & Hayashi, 1998; Rehm et al., 1982; Zebarth et al., 1989). Both study sites indicated higher recharge rates beneath depressions compared to uplands or flatlands (Table 2.6). Stable isotope profiles beneath depressions typically represent a long-term average of contributions from winter precipitation and snowmelt runoff (Pavlovskii et al., 2018). Isotope profiles of $\delta^{18}O$ at both study sites (Figure 2.13) suggest that snowmelt is contribuing to recharge in the depressions.

2.5.1.2.1 LDF depressions:

At LDF, both the WTF and the CMB method indicated higher recharge rates beneath L_IrrDp compared to the flatlands (Table 2.6). The overwinter recharge of 170 ±34 mm at L_IrrDp is especially high compared to 33 ± 7 mm for the flatlands (Table 2.6), suggesting DFR of snowmelt is indeed a primary recharge mechanism in the depression. The weighted average $\delta^{18}O$ value for snow at LDF was -26.7‰, whereas the two LDF runoff events sampled in March and April have values of -23.1 ‰ and -14.7 ‰, respectively. This indicates an evolution of

ponded water with time towards a more positive isotope signature, as evaporation from the surface of the pond causes fractionation of the pond water (Pavlovskii et al., 2018). The result is that the average $\delta^{18}O$ value of the profile beneath L_IrrDp (-18.2 ‰) appears similar to warm-season precipitation, when in reality it is strongly affected by infiltration of enriched snowmelt pond water (Pavlovskii et al., 2018). During the summer months, vertical flow beneath L_IrrDp flow is predominantly upwards as indicated by the hydraulic gradient in the monitoring wells (Figure 2.8) as well as the negative recharge value obtained from the water balance calculation (Figure 2.15, Table 2.6). As such, recharge during the summer months is unlikely at L_IrrDp and DFR of snowmelt runoff is the dominant contributor to recharge at this location.

2.5.1.2.2 PP depressions:

At the PP site, the CMB results showed significantly higher recharge rates beneath both irrigated and dryland depressions compared to the uplands (Figure 2.14, Table 2.6). The average $\delta^{18}O$ value of PP snow samples was -24.8 ‰ and the March runoff event was -25.1 ‰ (Figure 2.13). Only one runoff event was sampled at PP, but it is reasonable to assume the evolution of the ponded water would be similar to that of the LDF depression due to similar isotopic compositions of March runoff and proximity of the two sites, suggesting similar weather conditions. Therefore, if DFR of snowmelt is a primary recharge mechanism beneath the depressions, isotope profiles should represent a long term average of contributions from snow and snowmelt runoff (Pavlovskii et al., 2018). This appears to be the case for P_DryDp (-20.5 ‰), however, P_IrrDp (-15.3 ‰) did not show the negative isotopic shift one would expect from DFR of snowmelt. There are several possibilities that might explain the lack of shift at this location: 1) a more positive isotopic source is contributing to recharge, offsetting the negative contribution from snowmelt, 2) infiltration of snowmelt is less significant than one would expect

under DFR conditions, causing little to no negative shift in the profile or 3) the isotopic profile is strongly affected by groundwater mixing and/or cycling from the uplands. These three possibilities will be examined below.

First, recall from the above discussion of the PP uplands that irrigation might result in increased runoff from the uplands on irrigated fields. If P_IrrDp is in fact receiving runoff from irrigation events, and these events cause enough ponding to lead to DFR, there is potential for a more isotopically positive source of recharge to infiltrate and offset the negative contribution of snowmelt, which would reduce the negative shift in the $\delta^{18}O$ profile as seen in Figure 2.13b. However, in order for the negative shift due to snowmelt DFR to be offset as strongly as is shown in Figure 2.13b, a significant amount of summer DFR would need to occur at P_IrrDp. Personal communication with other researchers working on the site has indicated that summer ponding is a regular occurrence in P_IrrDp (W. Appels, personal communication, April 23, 2018). Additionally, to further investigate the possibility of summer ponding, near-infrared satellite imagery (Planet Team, 2017) was used to determine whether liquid water could be identified in the irrigated depression in the middle of the growing season. High resolution (< 10 m) satellite imagery were analyzed using ArcMap in order to extract near-infrared bands, which are useful for delineating water bodies since water absorbs most light in this wavelength range. Although no examples were found for 2018 due to sporadic daily imagery, Figure 2.22 shows a clear example of summer ponding from June 28, 2012. It is likely that this ponding event was caused by irrigation and not a summer rainstorm, since no liquid water was detected in the dryland depression (Figure 2.22). The ponded area was roughly 580 m^2, which corresponds to 52 mm of standing water in the depression according to volume-area relationship calculations (Hayashi & van der Kamp, 2000). Not all of this water would have been available for recharge

due to evapotranspiration and soil water storage, but it is likely that some of this isotopically positive water recharged beneath the depression. Multiple, recurring summer ponding events could potentially offset the isotopically negative contribution from snowmelt. This would result in an isotopic profile with a less prominent negative shift due to DFR of snowmelt, similar to the P_IrrDp profile in Figure 2.13b. Additionally, if P_IrrDp is receiving DFR of both snowmelt and irrigation water, this would suggest increased overall recharge rates beneath irrigated depressions compared to dryland depressions. This is demonstrated at PP where CMB results suggest a slightly higher recharge rate (113 ± 31 mm/yr) at P_IrrDp compared to P_DryDp (94 ± 45 mm/yr) (Figure 2.14). Previous studies have shown that winter precipitation is overwhelmingly the dominant contributor to recharge via DFR (Maulé et al., 1994; van der Kamp & Hayashi, 1998; Pavlovskii et al., 2018), however, these data suggest that DFR of irrigation water may also contribute to recharge on irrigated fields in hummocky terrain.

The second possible explanation for the lack of negative shift in the isotopic profile is a reduction in snowmelt contribution at P_IrrDp. This is certainly plausible, since depressions have elevated soil moisture compared to uplands, and fall water content has been shown to be inversely related to infiltration of overwinter precipitation due to reduced infiltration capacity and water storage efficiency of wet soils (LeBlanc, 2017; Granger et al., 1984). It then follows that an irrigated depression would have an even greater reduction in winter/spring infiltration compared to a dryland depression, as a result of the increased near-surface soil moisture of an irrigated field (Musick, 1970; Hobbs & Krogman, 1971; Wight & Black, 1978). The soil moisture in the active root zone beneath P_IrrDp is near saturation (0.37), which would significantly reduce soil water storage potential and inhibit infiltration of overwinter recharge. Additionally, if macropores are present in the soil beneath P_IrrDp, they are likely to become

blocked by ice upon freezing, further reducing potential infiltration pathways for mid-winter snowmelt (LeBlanc, 2017). As such, P_IrrDp may be experiencing reduced DFR of snowmelt runoff compared to P_DryDp, preventing the typical shift towards a winter precipitation signature in the isotopic profile (Figure 2.13b).

The third possible explanation for the lack of negative shift in the isotopic profile beneath P_IrrDp (Figure 2.13b) is that groundwater mixing and/or cycling of water from the uplands to depressions (or vice versa) is occurring beneath the depression, making it difficult to discern an isotopic winter signature (Pavlovskii et al., 2018). Since no data was collected on the depth or fluctuation of the water table at the PP site, nor on the isotopic composition of the groundwater, it is unclear whether mixing or cycling are occurring at this location.

In summary, it seems reasonable to conclude that DFR of snowmelt is likely contributing to recharge in both depressions at the PP site, but that other mechanisms attributed to irrigation (e.g., DFR of irrigation water and/or reduction of DFR of snowmelt runoff) are affecting recharge processes at P_IrrDp.

2.5.1.3 Flatlands

The DFR model does not directly allow for consideration of flatland contribution to recharge. However, one can infer that it would likely be a value somewhere between the upland and depression end-members since the lack of topography results in very little run-off (compared to an upland) or run-on (compared to a depression). The CMB results suggest that this is indeed the case: the recharge rates beneath the two flatlands at LDF were intermediate to the depression and upland rates (Figure 2.14). The isotope profiles beneath L_IrrFl and L_DryFl had average $\delta^{18}O$ values of -17.0 ‰ and -15.9 ‰, respectively, suggesting that flatland recharge is primarily sourced from summer precipitation (-15.4 ‰) and that irrigation water (-17.1‰) likely

contributes to recharge at L_IrrFl (Figure 2.13). Both water balance and WTF results showed more summer recharge beneath L_IrrFl compared to L_DryFl, which also suggests that irrigation is contributing to recharge (Table 2.6). Further influence of irrigation on summer recharge beneath flatlands is explored in a later section.

The water balance and WTF method also indicated that overwinter recharge is significant at both flatlands (Table 2.6). Curiously, overwinter recharge estimates appeared to be nearly identical for both flatland sub-sites, although the water balance method estimated a greater magnitude (68 ± 113 mm at L_IrrFl and 67 ± 113 mm at L_DryFl) compared to the WTF method (33 ± 7 mm for both). The true overwinter recharge is likely closer to the WTF estimates, since the water balance method can result in larger errors in recharge estimates for arid climates (Gee & Hillel, 1988; Appendix G). Since similar overwinter recharge was estimated for both flatland sub-sites using two independent estimation methods, however, this similarity is likely not coincidental. It is worth noting that the delayed increase in water levels in response to snowmelt seen beneath the flatland fields (Figure 2.9) may be in part due to lateral transfer of the large "pulse" of recharge that occurred beneath L_IrrDp.

2.5.2 Influence of fall water content on overwinter recharge

Previous studies have shown that increased soil moisture leads to reduced infiltration in frozen soils, due to a reduction in hydraulic conductivity caused by blockage of flow paths by ice-filled pores (LeBlanc, 2017; Granger et al., 1984). As such, the wetter conditions in fall (i.e., November 1, 2017) at L_IrrFl should, in theory, have resulted in less overwinter recharge compared to L_DryFl. However, according to the results from both the WTF and water balance methods, the net overwinter recharge appeared to be the same for L_IrrFl and L_DryFl (Table 2.6). The main reason for this is likely that the average soil moisture in the profile in fall was

only 0.26 at L_IrrFl (Figure 2.11), which is wetter than the average fall soil moisture at L_DryFl (0.22), but significantly drier than the “wet” conditions of 0.40 and 0.35 reported by LeBlanc (2017) and Granger et al., (1984), respectively. Therefore, it is likely that the conditions at L_IrrFl were not wet enough compared to L_DryFl to significantly reduce infiltration, since a comparable number of pores would have remained ice-free at both sub-sites upon freezing (both have similar porosity, see Table 2.4). As a result, similar overall inputs (SWE) and outputs (vapour flux) at both sub-sites would have produced a comparable amount of infiltration, causing similar net changes in water content in the profile for the overwinter period, and, consequently, similar overwinter recharge (Figure 2.15a). Comparatively, the high average fall water content of L_IrrDp (0.35) would have led to a greater proportion of ice-blocked flow paths upon freezing compared to the flatlands, resulting in reduced infiltration throughout the overwinter period. The overwinter recharge calculated for L_IrrDp using the WTF method (170 ± 34 mm) was greater than for the flatlands (33 ± 7 mm), however, this is only a result of higher overall inputs (e.g., runoff) to the system resulting in DFR.

Although the infiltration and net overwinter recharge were similar at both L_IrrFl and L_DryFl, Figure 2.11 provides insight into the dynamics of this infiltration throughout the overwinter period. Recall that three mid-winter melts occurred at the LDF site in November, January and March, followed by the final spring melt in April (Figure 2.9). These four melt events correspond to increases in soil moisture in the profile as a result of infiltration of snowmelt water (Figure 2.11). Using the magnitude of soil moisture increase at 20 cmbgs after each melt event as a rough proxy for infiltration, Figure 2.11 shows that wet frozen soils do indeed experience reduced infiltration compared to dry frozen soils. For example, in response to the January melt event, L_IrrDp showed zero increase in soil water content at 20 cmbgs

compared to an increase of 0.04 at L_IrrFl and 0.09 at L_DryFl, keeping in mind that exact liquid water contents are difficult to interpret in partially frozen soils. Figure 2.11 supports the notion that, while L_IrrFl was slightly wetter in fall than L_DryFl, it was still dry enough to allow for infiltration of mid-winter snowmelt. Meanwhile, fall conditions at L_IrrDp were wet enough to significantly reduce mid-winter snowmelt infiltration since the only significant increase in soil moisture occurred after the March melt event, which resulted in thawing of the soil column and ponding in the depression.

It is worth noting that increases in soil moisture at L_IrrFl and L_DryFl were only detected at 20 and 60 cmbgs, while the soil moisture remained constant at 150 cmbgs at both sub-sites until after the final melt in April (Figure 2.11). This suggests that infiltrating snowmelt water became frozen and was stored in the profile until the soil thawed completely in April, after which deep drainage occurred to at least 150 cmbgs. Previous studies have reported re-freezing of infiltrating water under frozen-soil conditions (Watanabe & Kugisaki, 2017; Mohammed et al., 2019).Therefore, it is plausible that infiltrating water from early mid-winter melt events was stored in the profile as ice, with deep drainage only occurring after the soil profile had thawed completely following the final April melt.

To further investigate the possibility of infiltrating water being stored in the profile, the soil water storage capacity was calculated for the profiles at L_IrrFl and L_DryFl. It has been shown that fall water content is inversely related to soil water storage capacity (Musick, 1970; Hobbs & Krogman, 1971; Wight & Black, 1978). Soil water storage capacity in fall (SWS_{fall}) was determined for the top 2 m of the soil profile at the LDF sub-sites by:

$$SWS_{fall} = \left(\theta_{gd} - \theta_{fall}\right) \times 2000\, mm \qquad (2.12)$$

where θ_{gd} is the average water content of the soil samples after 24 hrs of gravity drainage post saturation (Section 2.3.3), and θ_{fall} is the average water content of the profile in fall, both in m^3/m^3.

L_IrrFl has a fall soil water storage capacity of 380 mm in the top 2 m of the profile compared to 580 mm at L_DryFl. Although L_DryFl had a greater soil water storage capacity in fall, the magnitude of soil water storage at both fields was significantly greater than the total input to the system of 134 mm over the overwinter period (171 mm precipitation minus 38 mm vapour flux, Figure 2.15a). Therefore, it seems possible that most of the infiltrating snowmelt water could be retained at both sub-sites in the soil profile and become frozen, effectively remaining stored in the soil profile until thawing and deep drainage occurred in April.

Although it seems counterintuitive to suggest that the overwinter infiltration dynamics were so similar for both a dryland and irrigated field, the key point is that although L_IrrFl was irrigated, the soil moisture conditions in fall 2017 were not significantly wetter than at L_DryFl. As a result, only slight differences in infiltration rates and timing were observed at each flatland sub-site and net overwinter recharge was the same. This was the case for the 2017-2018 overwinter period, however, in years with different crops, different amounts of precipitation and different irrigation routines, it is possible that soil moisture conditions at L_IrrFl would be wet enough to reduce infiltration and thus overwinter recharge compared to L_DryFl. Therefore, although irrigation did not significantly affect the amount of overwinter recharge at the LDF site during this study period, it certainly has the potential to do so in other years.

2.5.3 Contribution of irrigation to summer recharge

2.5.3.1 Field-derived evidence

Irrigation increases the total amount of water input to the system, and has previously been found to contribute to and increase groundwater recharge (Chiew & McMahon, 1991; Davisson & Criss, 1995; Willis & Black, 1996; Kendy et al., 2003; Scanlon et al. 2005; Qin et al., 2011). Scanlon et al. (2005) found that while diffuse recharge did occur beneath dryland fields, recharge rates beneath irrigated fields were four to five times higher. Chiew and McMahon (1991) found that modeled regional recharge rates were anywhere from 1.3 to 6.5 times higher for irrigated regions compared to dryland regions, which was consistent with observed rates measured in the field. The present study found that, according to water balance calculations, diffuse recharge beneath L_IrrFl (42 ± 141 mm) was approximately twice the amount beneath L_DryFl (21 ± 122 mm) during the 2018 growing season (Table 2.6). Additionally, results from the WTF method suggest that recharge during the growing season at L_IrrFl (42 ± 9 mm) exceeded overwinter recharge (33 ± 7 mm). CMB results (Figure 2.14, Table 2.6) also show a slightly higher annual recharge rate for L_IrrFl (50 ± 21 mm/yr) compared to L_DryFl (29 ± 44 mm/yr), and isotope profiles suggest irrigation water contributes to recharge at L_IrrFl (Figure 2.13).Therefore, it is highly likely that irrigation is contributing to increased recharge rates at L_IrrFl compared to L_DryFl.

At the PP site, we can compare irrigated versus dryland recharge rates for uplands and depressions. CMB results (Figure 2.14, Table 2.6) show slightly higher recharge rates beneath P_IrrDp compare to P_DryDp. It is possible that irrigation contributes to increased recharge in the depression via DFR of irrigation water (Section 2.5.1.2). In contrast, irrigation does not seem to result in increased recharge on the uplands: P_IrrUp has slightly lower recharge rate than

P_DryUp, and both are small compared to rates in the depressions (Figure 2.14, Table 2.6). The increased recharge rate in the irrigated depression is only 1.1 times the rate in the dryland depression (Table 2.6), which is lower than the irrigated/dryland ratios calculated on the LDF flatlands and reported by others (Chiew & McMahon, 199;1Scanlon et al. 2005).

2.5.3.2 Numerical model evidence

Numerical modeling of the unsaturated zone has been employed successfully in the past to estimate recharge under irrigated conditions (Jiménez-Martínez et al., 2009; Jiang et al., 2010; Lu et al., 2011; Li et al., 2014). However, recharge estimates obtained using vadose zone modeling are wrought with uncertainty, especially in arid climates where recharge is typically small compared to errors in other estimated hydrological parameters (e.g., ET) (Gee & Hillel, 1988; Scanlon et al., 2002). Despite their inherent uncertainty, numerical models can be useful in helping to understand flow processes and fluxes within the vadose zone (Scanlon et al., 2002). Moreover, understanding the reasons behind "poor" model performance can provide important insights into how the system is functioning within the model, and this can allow seemingly inadequate models to be interpreted and useful.

As such, although both the irrigated and dryland models developed for this project estimate far more recharge than is observed in the field (Table 2.10), the overall ability of the models to represent realistic soil moisture and head dynamics in the profile is reasonably good (Section 2.4.9). This allows for a reasonably reliable comparison of modeled recharge rates under irrigated and dryland conditions. During the growing season, the irrigated field simulation produced 3.1 times more recharge than the dryland field simulation (Table 2.10), an irrigated/dryland ratio which is higher than measured ratios at LDF (Table 2.6) but lower than ratios reported by Scanlon et al. (2005) and Chiew and McMahon (1991). As such, despite the

limitation of the models developed in this study, they help to solidify our conclusions drawn from field observations (i.e., that summer recharge is higher on irrigated fields compared to dryland fields) and to support conclusions made by previous studies that irrigation leads to increased recharge.

2.5.4 Implications of increased recharge due to irrigation

This study confirms previous findings that irrigation can lead to increased groundwater recharge (Chiew & McMahon, 1991; Davisson & Criss, 1995; Willis & Black, 1996; Kendy et al., 2003; Scanlon et al., 2005; Qin et al., 2011). This has several implications for the irrigated regions of Alberta, particularly where groundwater quality is concerned. Previous studies have found that increased recharge associated with irrigation has been linked to a degradation in shallow groundwater quality (Böhlke, 2002; McMahon et al., 2003; Scanlon et al., 2005; Qin et al., 2011; Exner et al., 2014). Böhlke (2002) found that agricultural contaminants (chemicals in groundwater found to have higher concentrations linked to agricultural activity) can be affected by increased downward flux of water through the profile; these can include inorganic compounds such as NO_3^-, N_2, Cl, SO_4^{2-}, H^+, P, C, K, Mg, Ca, Sr, Ba and Ra as well as other compounds from pesticides, fertilizers or organics. Qin et al. (2011) found that increased recharge in irrigated areas led to CFCs and high nitrate concentrations in groundwater, while Exner et al. (2014) and McMahon et al. (2003) also found a correlation between irrigation and high nitrate levels in groundwater.

Although the glacial till sediments in the Lethbridge area typically have very low hydraulic conductivities, preferential flow through the oxidized weathered zone is permitted via fractures (Hendry, 1982; Hendry et al., 1986), allowing for deep drainage much faster than usual

through such fine-grained sediments. As a result, the ubiquitous, long-term irrigation in the region and inevitable resulting increase in groundwater recharge has likely degraded the quality of shallow groundwater, a trend which several studies have already observed in southern Alberta (Miller et al., 1995; Chang & Entz, 1996; Rodvang et al., 2004; Kyte, 2018). Luckily, at present, groundwater is not significantly used for domestic or agricultural purposes in this area due to the abundance of surface water and relatively low hydraulic conductivity of shallow water-bearing units. However, by 2005, virtually all of the rivers in the South Saskatchewan River Basin (SSRB), which sustains much of southern Alberta, were highly or over-allocated (Alberta Environment, 2005), and by 2014 new applications for licensed water allocations were no longer accepted (Bjornlund et al., 2014). As such, there is an increased need for groundwater resources, which will continue to grow as population increases and agriculture intensifies (Alberta Water Council, 2008), making groundwater quality a primary concern. Further studies are needed to develop ways to mitigate deterioration in groundwater quality if irrigation is to remain a sustainable agricultural practice.

On the other hand, increased recharge associated with irrigation provides shallow unconfined aquifers with replenishment they would not have otherwise received. Although irrigation-return recharge can degrade shallow groundwater quality, it can also provide a buffer for stressed aquifers by increasing water inputs (Kendy et al., 2003; Scanlon et al., 2005). In light of recent government strategies set out to increase water efficiency and productivity in Alberta (Alberta water Council, 2008), many studies have considered the impacts of improved irrigation efficiency on Alberta's water resources (Bjornlund et al., 2009; Ali & Klein, 2014). However, since more efficient irrigation practices will potentially reduce groundwater recharge rates, improved irrigation efficiency is unlikely to counteract groundwater level declines in areas where

groundwater resources are already stressed (Kendy et al., 2003). This demonstrates the importance of land-use analysis before regional assessments of groundwater recharge are undertaken. Overlooking increased recharge on irrigated lands could result in significant underestimation of the actual recharge an area receives. This has implications for water management and policy makers: if groundwater is being replenished more than was previously thought, the sustainability of the resource might increase. Improvement of irrigation efficiency must also be considered as a type of land-use change, since it will have effects on groundwater recharge rates as well.

2.6 Conclusions

Irrigation is a crucial part of the thriving agriculture sector in Alberta, but little research has been completed on the impacts of large-scale, long term irrigation on our province's groundwater resources. Groundwater recharge in the prairies occurs as both DFR of snowmelt runoff and diffuse recharge of summer precipitation, mechanisms which have been well-studied and documented (Lissey, 1971; van der Kamp & Hayashi, 1998; Berthold et al., 2004; Hayashi & Farrow, 2014). However, the effects of irrigation on these recharge mechanisms have not been investigated in southern Alberta, despite the fact that irrigation has been shown to affect groundwater recharge in other parts of the world (Qin et al., 2011; Scanlon et al., 2005). As such, the goal of this study was to investigate the effects of irrigation on groundwater recharge rates and seasonality in southern Alberta. Three recharge estimation methods (WTF, CMB and water balance) were employed to assess both depression-focused and diffuse recharge rates beneath three topographic elements (uplands, depressions and flatlands) for irrigated and dryland cropped

fields at two study sites near Lethbridge, Alberta. A numerical model was also developed to compare theoretical recharge rates under irrigated and dryland conditions.

Results show that, regardless of irrigated or dryland conditions, recharge rates were consistently highest beneath depressions, moderate beneath flatlands and lowest beneath uplands. The CMB method indicated that depressions at both study sites had the highest long term recharge rates: 88 ± 26, 113 ± 31, and 94 ± 45 mm/yr. Flatlands had moderate recharge rates of 50 ± 21 and 29 ± 44 mm/yr and uplands had very low recharge rates of -4 ± 5 and 4 ± 2 mm/yr. Overwinter recharge (i.e., recharge from November 1, 2017 to April 30, 2018) at the main study site was calculated to be 170 ± 34 mm in the irrigated depression compared to 33 ± 7 mm for both the irrigated and dryland flatland. These results are consistent with our previous understanding of the DFR model (i.e., recharge rates are highest beneath depressions and lowest beneath uplands). However, while most DFR is comprised of snowmelt runoff at both study sites, isotope profiles and satellite imagery suggest irrigation runoff may also contribute to DFR beneath irrigated depressions during the summer months. This leads to slightly increased recharge beneath irrigated depressions (113 ± 31 mm/y) compared to dryland depressions (94 ± 45 mm/yr), whereas recharge rates beneath both irrigated and dryland uplands was very low (-4 ± 5 and 4 ± 2 mm/yr, respectively) and did not appear to be altered by irrigation.

This study also confirmed previous findings that increased soil water content in fall leads to reduced infiltration rates in frozen soils (Granger et al., 1984; LeBlanc, 2017). Daily soil moisture data from November 2017-April 2018 indicated that the irrigated depression at the main study site, which had the highest fall soil water content (0.35), had reduced infiltration of mid-winter snowmelt. However, the fall water content of the irrigated flatland (0.26) was only slightly greater than the fall water content of the dryland flatland (0.22). This resulted in similar

snowmelt infiltration and, consequently, nearly identical amounts of overwinter recharge calculated for each flatland (33 ± 7 mm using the WTF method and 68 ± 113 mm using the water balance method). However, since irrigation schedules differ greatly from year to year depending on crop type and precipitation, such similar fall water contents for the irrigated and dryland fields may not be a common occurrence.

Lastly, field and numerical model results show that irrigation does indeed contribute to increased recharge over the course of the growing season in southern Alberta. This was shown at the main study site using the WTF method which indicated 42 ± 9 mm of recharge on the irrigated flatland between seeding and harvest. The water balance method also estimated 42 ± 141 mm of recharge over the same period for the irrigated flatland, compared to 21 ± 122 mm over the growing season for the dryland flatland. Numerical modeling also showed 3.1 times more recharge over the growing season period for an irrigated field simulation compared to a dryland field simulation. Additionally, long term recharge rates estimated using the CMB method suggest elevated rates beneath the irrigated flatland (50 ± 21 mm/yr) compared to 29 ± 44 mm/yr for the dryland flatland. The ratios of irrigated to dryland recharge rates are within the range of values estimated by previous studies (Chiew & McMahon, 1991; Scanlon et al., 2005). Increased recharge associated with agricultural practices has been found to degrade groundwater quality in shallow unconfined aquifers, but may help mitigate declining groundwater levels in areas of groundwater stress (Böhlke, 2002; Kendy et al., 2003; Scanlon et al., 2005).

2.7 Figures and Tables

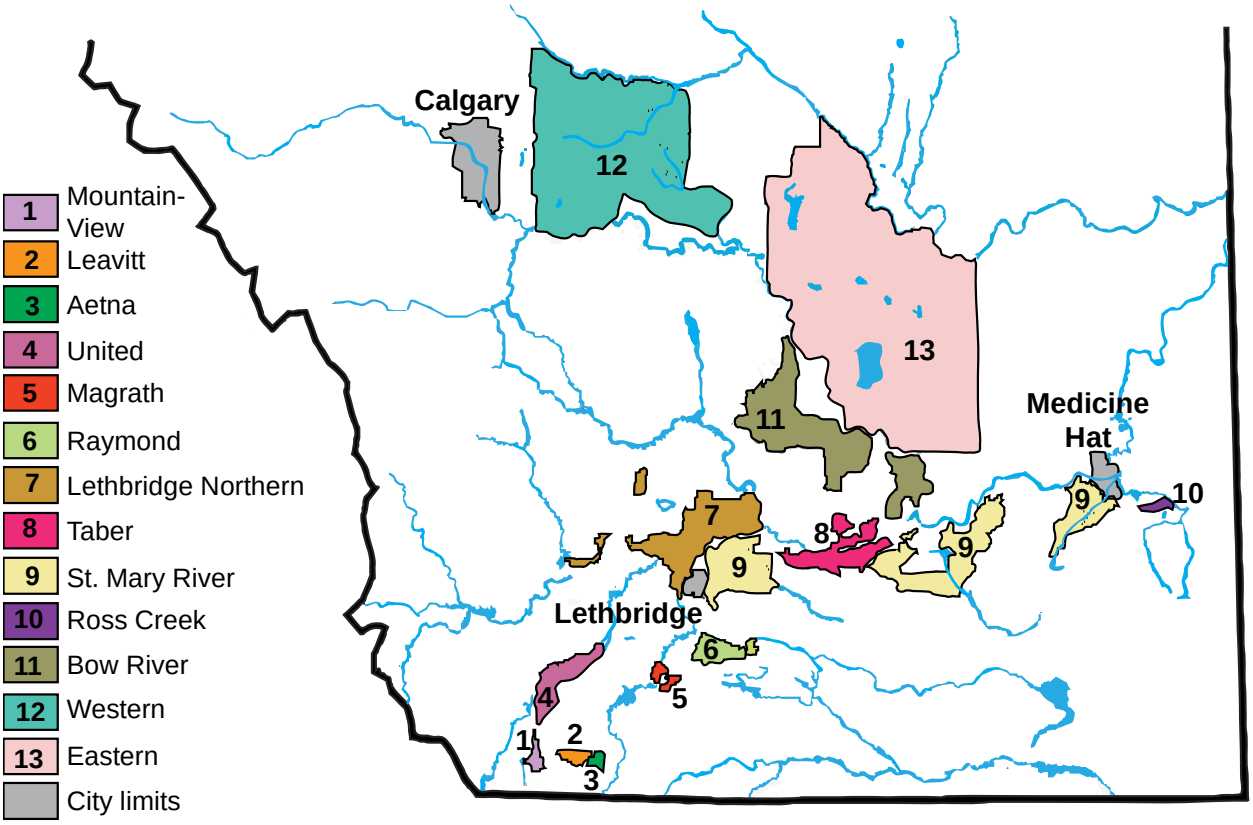

Figure 2.1. The location of Alberta's 13 irrigation districts. The study area is located in district 9, the St. Mary's Irrigation District (SMID), directly east of the City of Lethbridge, AB. Modified from the Government of Alberta, Alberta Agriculture and Forestry (URL: https://www1.agric.gov.ab.ca/$department/deptdocs.nsf/all/irr12911)

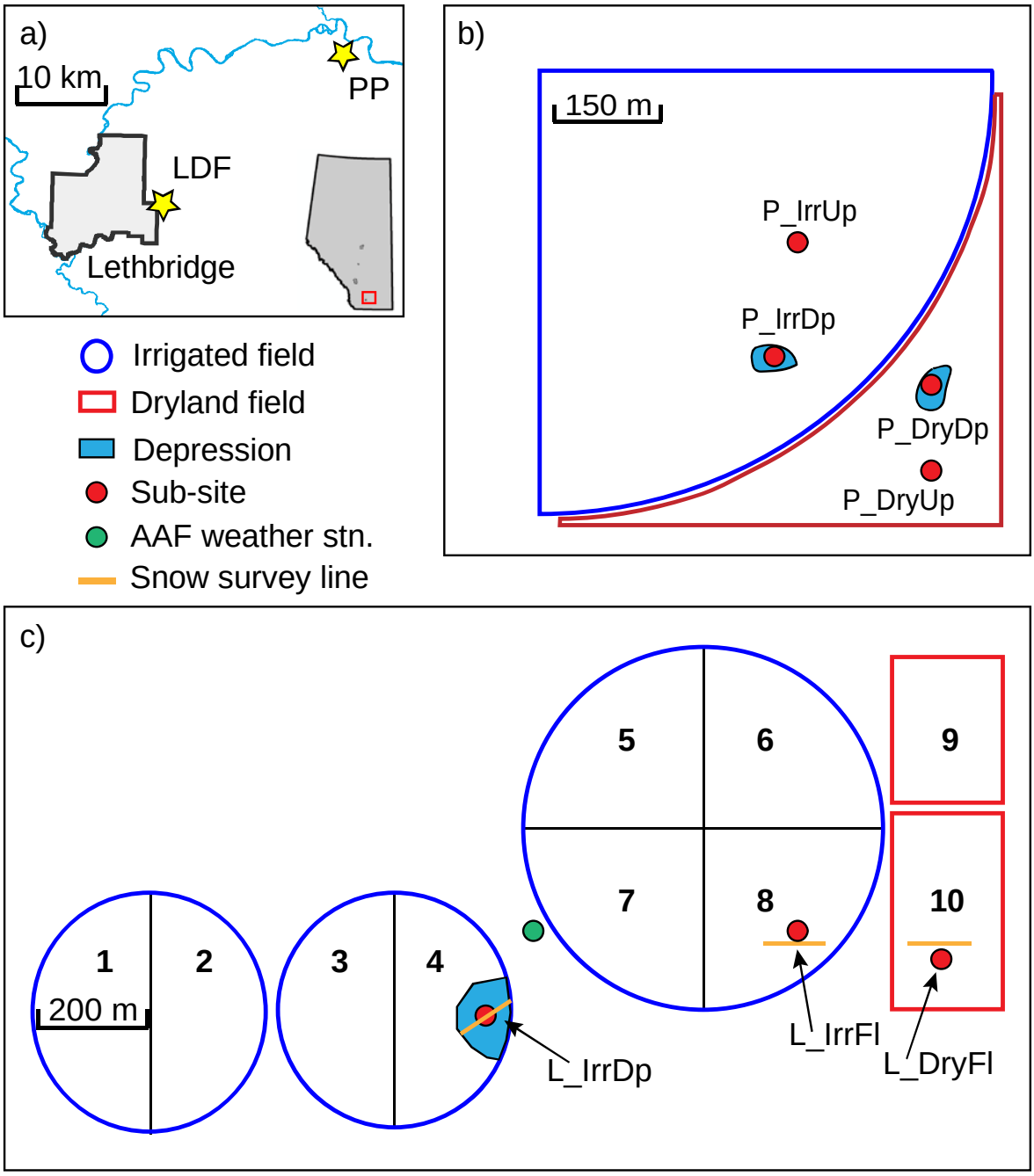

Figure 2.2. Location and layout of main study sites and sub-sites. Lethbridge Demonstration Farm (LDF) consisted of three sub-sites (a); Perry Produce (PP) site consisted of four sub-sites (c). Location of LDF and PP are shown relative to Lethbridge (b). AAF = Alberta Agriculture and Forestry; stn. = station.

Table 2.1. Drilling and well completion information for monitoring wells and boreholes at LDF and PP.

Well ID	Date drilled	Drilling method	Depth to bottom	Depth to mid-screen	Screen length	Top of casing elevation
			mbtoc	mbtoc	m	masl
LDF boreholes/monitoring wells:						
L_IrrDp-1	9-May-17	solid stem	4.1	3.7	0.76	906.99
L_IrrDp-2	9-May-17	hollow stem	8.0	7.3	1.52	907.00
L_IrrFl-1	8-May-17	solid stem	4.5	4.1	0.76	906.66
L_IrrFl-2	8-May-17	solid stem	6.9	6.5	0.76	906.61
L_IrrFl-3	8-May-17	hollow stem	15.9	15.2	1.52	906.71
L_DryFl-1	9-May-17	solid stem	4.7	4.4	0.76	904.31
L_DryFl-2	9-May-17	solid stem	7.0	6.6	0.76	904.26
L_DryFl-3	9-May-17	hollow stem	9.6	9.2	0.76	904.34
PP boreholes:						
P_IrrDp	31-Oct-17	hollow stem	7.6	n/a	n/a	n/a
P_IrrUp	31-Oct-17	hollow stem	9.1	n/a	n/a	n/a
P_DryDp	31-Oct-17	hollow stem	7.6	n/a	n/a	n/a
P_DryUp	1-Nov-17	hollow stem	9.1	n/a	n/a	n/a

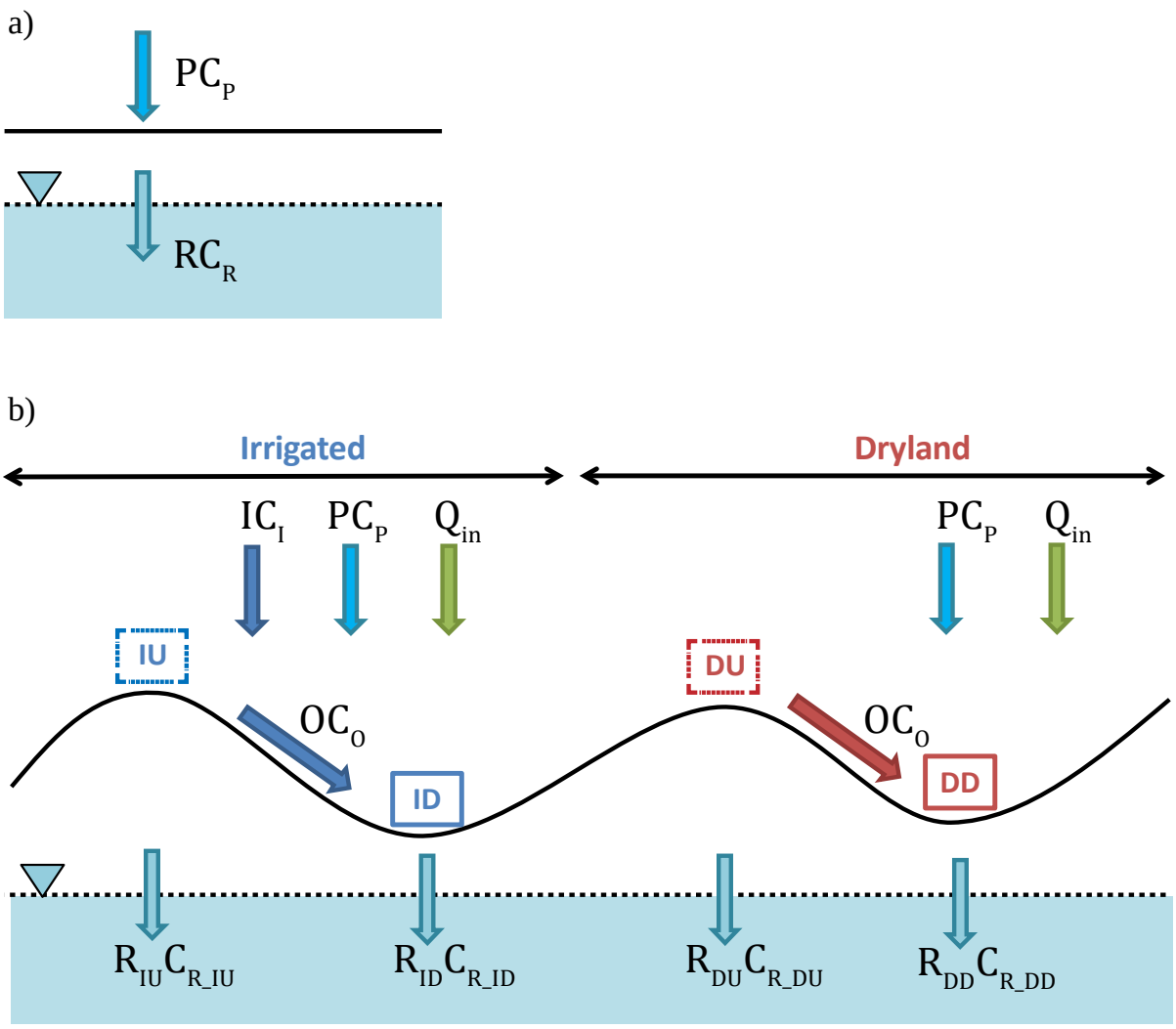

Figure 2.3. A schematic showing the conceptual framework for the chloride mass balance (CMB) method. The standard CMB method (a) is for diffuse recharge on flatlands with chloride inputs solely from precipitation. The modified CMB method used in this study (b) accounts for chloride inputs from irrigation water, anthropogenic inputs (e.g., fertilizer), and lateral transfer of chloride via runoff from uplands to depressions resulting in different recharge rates for each landscape position (upland and depression).

Table 2.2. Parameter inputs for chloride mass balance (CMB) method for estimating recharge. The uncertainty estimated for each parameter is shown in brackets.

Location	C_R mg/L	P mm/yr	C_P mg/L	I mm/yr	C_I mg/L	Q_{in} mg/m^2/yr	O mm/yr	C_O mg/L
LDF:								
L_IrrDp	8.7 (± 2.7)	440 (± 123)	0.27 (± 0.2)	292 (± 95)	0.48 (± 0.23)	420 (± 82)	17 (± 4)	5 (± 0.1)
L_IrrFl	13.7 (± 6.3)	440 (± 123)	0.27 (± 0.2)	292 (± 95)	0.48 (± 0.23)	420 (± 82)	0	0
L_DryFl	16.7 (± 18.9)	440 (± 123)	0.27 (± 0.2)	0	0	368 (± 72)	0	0
PP:								
P_IrrUp	69.5 (± 39.2)	440 (± 123)	0.27 (± 0.2)	213 (± 53)	0.64 (± 0.23)	420 (± 82)	-28 (± 6)	33 (± 5)
P_IrrDp	14.1 (± 4.5)	440 (± 123)	0.27 (± 0.2)	213 (± 53)	0.64 (± 0.23)	420 (± 82)	28 (± 6)	33 (± 5)
P_DryUp	121.8 (± 64.8)	440 (± 123)	0.27 (± 0.2)	0	0	368 (± 72)	-5 (± 1)	6 (± 4)
P_DryDp	5.5 (± 2.7)	440 (± 123)	0.27 (± 0.2)	0	0	368 (± 72)	5 (± 1)	6 (± 4)

C_R=chloride concentration in groundwater; P=precipitation; C_P=chloride concentration in precipitation; I=irrigation; C_I=chloride concentration in irrigation water; Q_{in}=anthropogenic input of chloride; O=overland flow (runoff); C_O=chloride concentration in overland flow

Table 2.3. Crop type, seeding and harvest dates and total annual irrigation applied to each field at LDF in 2017 and 2018.

Location	Crop	Seed date	Harvest date	Irrigation (mm)
2017*:				
L_IrrDp	barley	15-May	15-Aug	287
L_IrrFl	barley	15-May	16-Aug	190
L_DryFl	barley	15-May	16-Aug	0
2018:				
L_IrrDp	barley	19-May	2-Aug	217
L_IrrFl	sugar beets	24-May	31-Oct	350
L_DryFl	canola	17-May	16-Aug	0

*2017 seeding date is approximate for all fields.

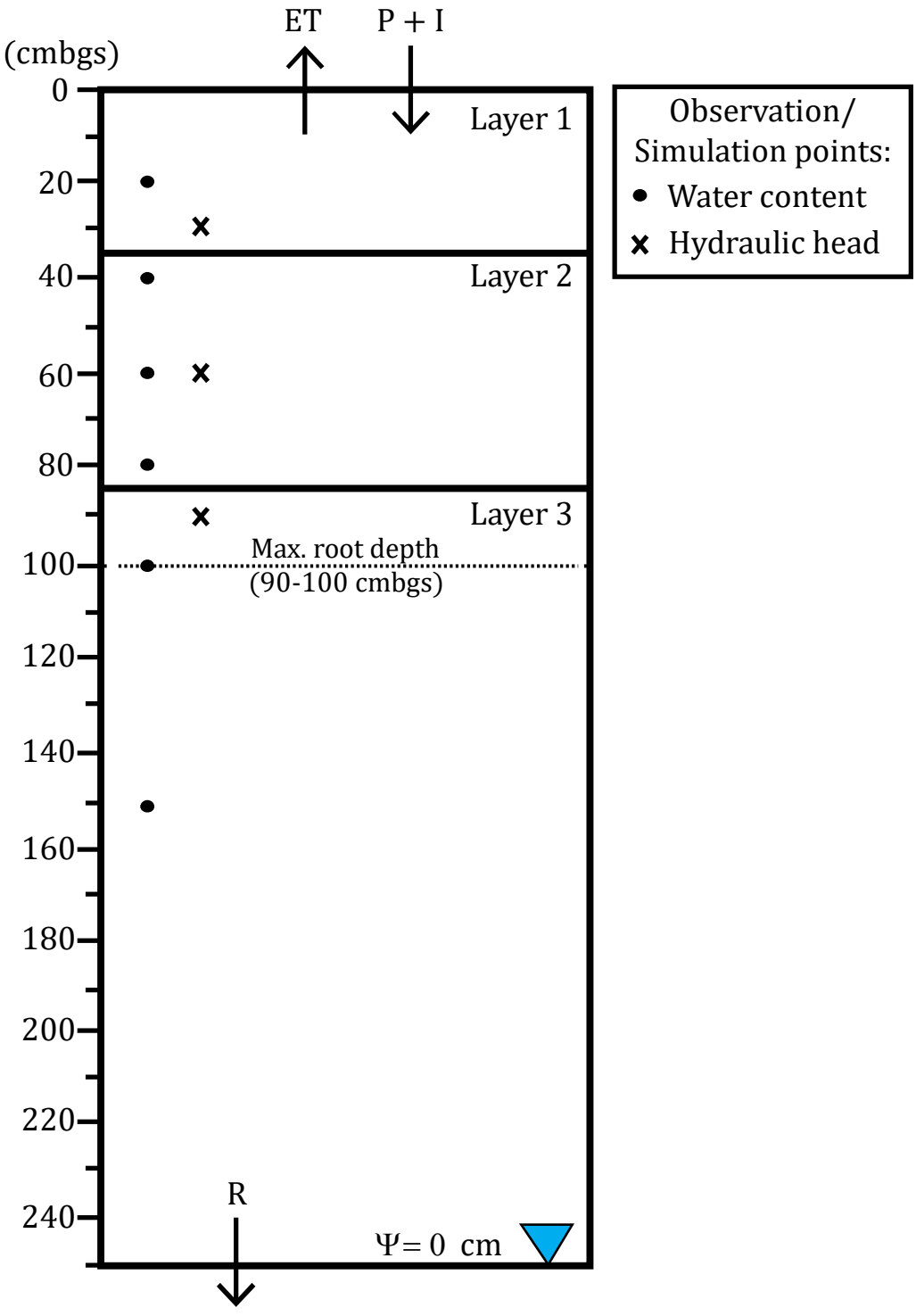

Figure 2.4. A diagram showing the soil layering scheme, boundary conditions and location of field measurements/simulation outputs used to simulate 1D vertical groundwater flow at L_IrrFl using HYDRUS-1D. Ψ = pressure head; *ET* = evapotranspiration; *P* = precipitation; *I* = irrigation; *R* = recharge.

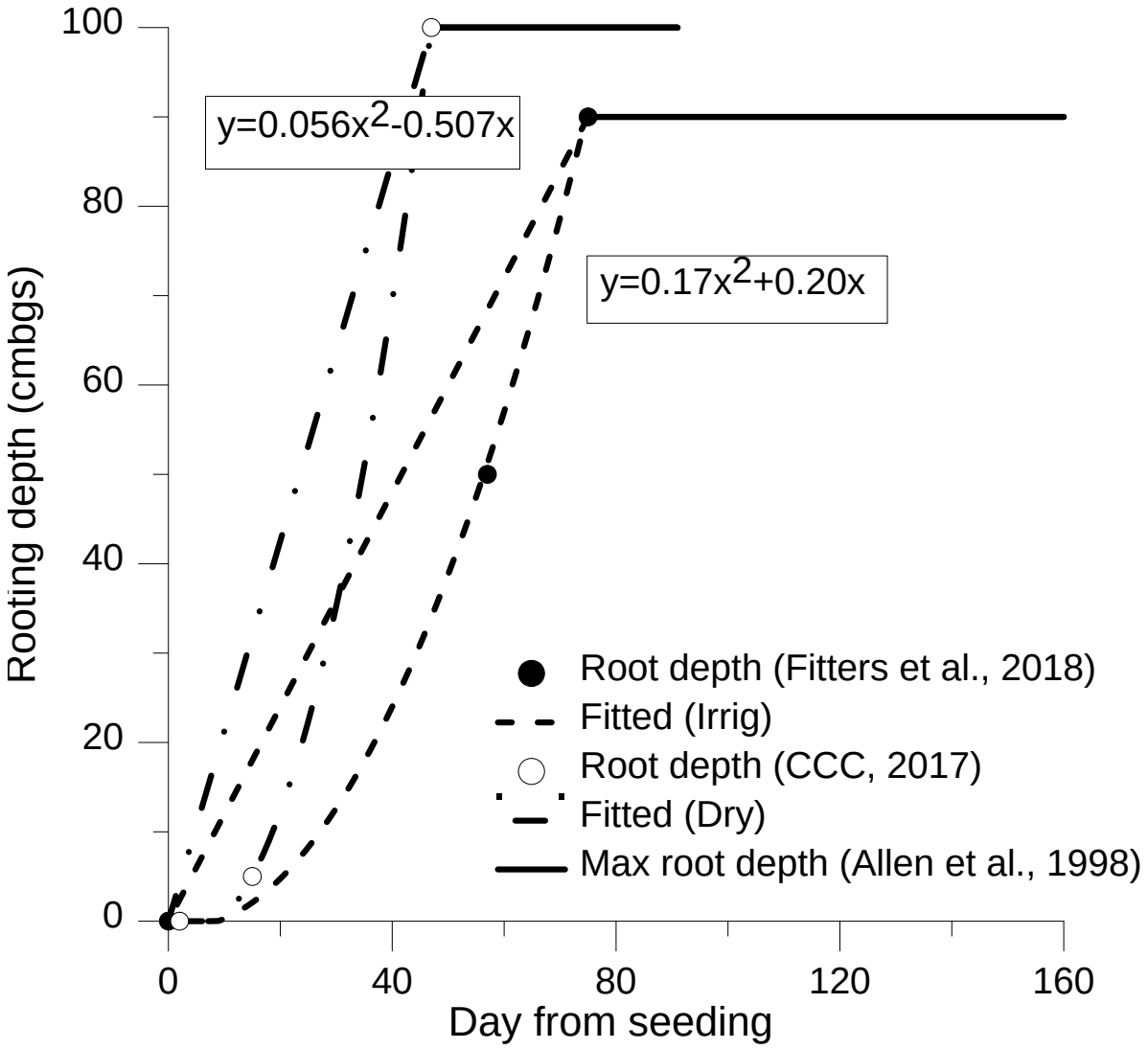

Figure 2.5. Root growth curve used to determine daily rooting depth for the irrigated field simulation (sugar beets) and dryland field simulation (canola). Rooting depth of sugar beets during the early growth stages under irrigated conditions was measured by Fitters et al. (2018) and resulting data was fitted using a second order polynomial function. Canola root depth in early growth stages was reported by the Canola Council of Canada (CCC, 2017). Maximum rooting depth of sugar beets and canola was assumed to remain constant at 90 cm and 100 cm, respectively, during the mid and late growth stages (Allen et al., 1998).

Table 2.4. Soil properties measured on intact soil ring samples from each instrumented location at LDF. Note that the 80 cm soil ring sample from L_DryFl was destroyed and could not be used for pressure plate analysis. SL = sandy loam; LS = loamy sand

Field	Depth (cm)	Porosity	Dry bulk density (g/cm^3)	Grain size analysis (%)			Soil text.	Clay mineralogy wt % of clay			Water retention parameters* (pressure plate analysis)			
				Clay	Silt	Sand		smectite	illite	kaolinite	θ_r	θs	α (1/cm)	n
L_IrrDp	20	0.56	1.44	9	32	55	SL	70	21	8	0.01	0.50	0.023	1.21
	40	0.55	1.67	9	28	58	SL	n/a	n/a	n/a	0.01	0.51	0.012	1.21
	60	0.49	1.70	7	28	61	SL	65	20	15	0.01	0.42	0.006	1.26
	80	0.47	1.71	7	22	68	SL	n/a	n/a	n/a	0.01	0.43	0.012	1.24
	100	0.49	1.63	5	21	72	SL	n/a	n/a	n/a	0.01	0.45	0.005	1.30
	150	0.44	1.77	8	21	68	SL	65	15	20	0.01	0.40	0.001	1.38
L_IrrFl	20	0.49	1.63	6	18	73	SL	69	16	15	0.01	0.43	0.018	1.20
	40	0.55	1.57	7	18	72	SL	n/a	n/a	n/a	0.01	0.48	0.033	1.26
	60	0.60	1.54	8	33	55	SL	69	13	18	0.01	0.50	0.019	1.37
	80	0.57	1.54	9	21	66	SL	n/a	n/a	n/a	0.01	0.49	0.032	1.29
	100	0.45	1.82	7	20	70	SL	n/a	n/a	n/a	0.01	0.40	0.027	1.20
	150	0.49	1.76	7	21	68	SL	67	12	21	0.01	0.42	0.047	1.18
L_DryFl	20	0.48	1.62	5	16	76	LS	71	16	13	0.01	0.46	0.043	1.22
	40	0.55	1.47	5	11	82	LS	n/a	n/a	n/a	0.04	0.50	0.039	1.37
	60	n/a	1.47	7	15	75	SL	68	13	19	0.01	0.64	0.027	1.21
	80	n/a	n/a	7	26	64	SL	n/a	n/a	n/a	n/a	n/a	n/a	n/a
	100	0.55	1.67	5	12	81	LS	n/a	n/a	n/a	0.03	0.49	0.042	1.42
	150	0.58	1.66	9	29	59	SL	72	12	16	0.01	0.49	0.040	1.27

*Water retention parameters are based on the van Genuchten (1980) model; soil water retention curves are shown in Appendix C.

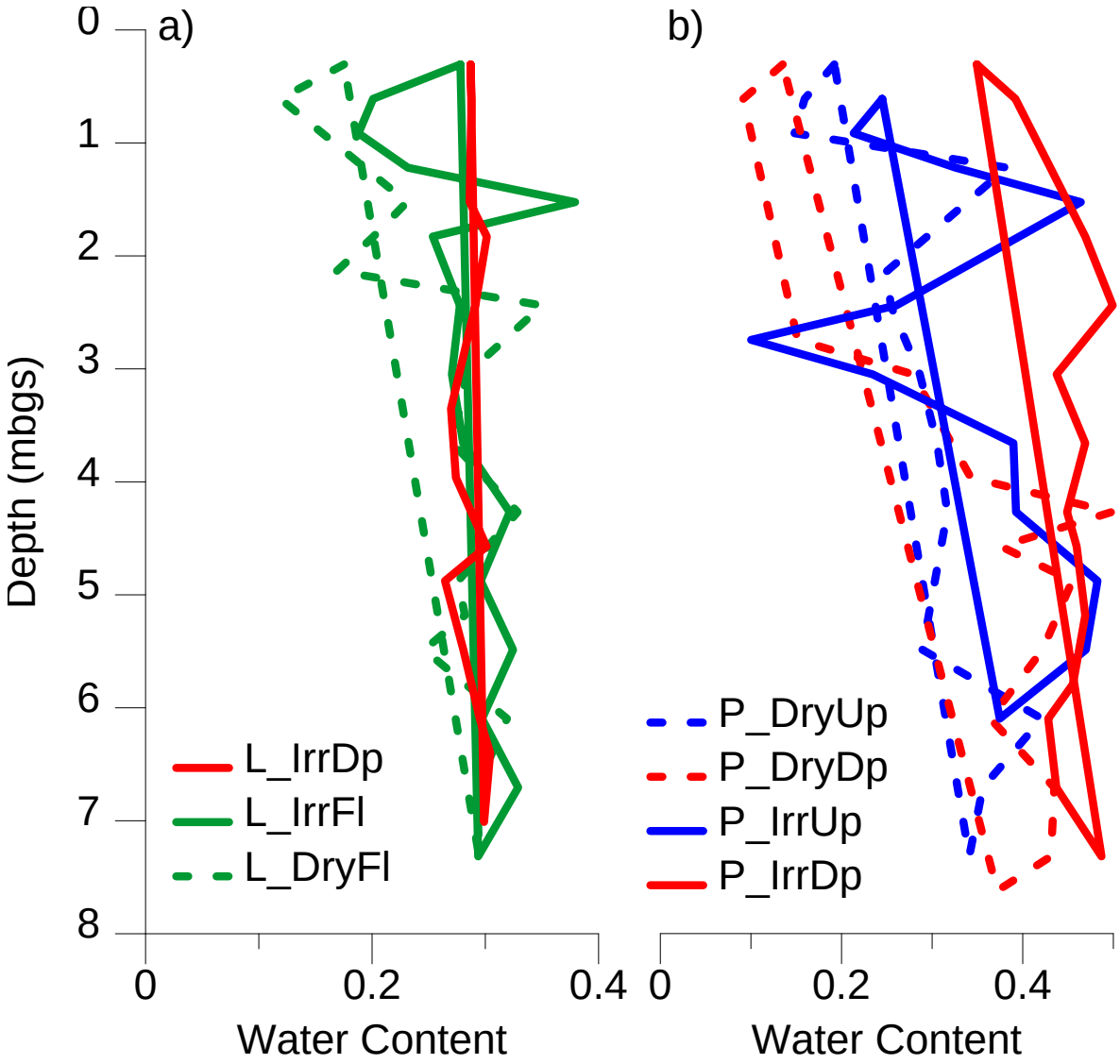

Figure 2.6. Volumetric water content (θ) of oven-dried borehole samples from a) Lethbridge Demonstration Farm and b) Perry Produce. Depressions are red, uplands are blue and flatlands are green. Dryland fields are shown with dashed lines while irrigated fields are shown with solid lines.

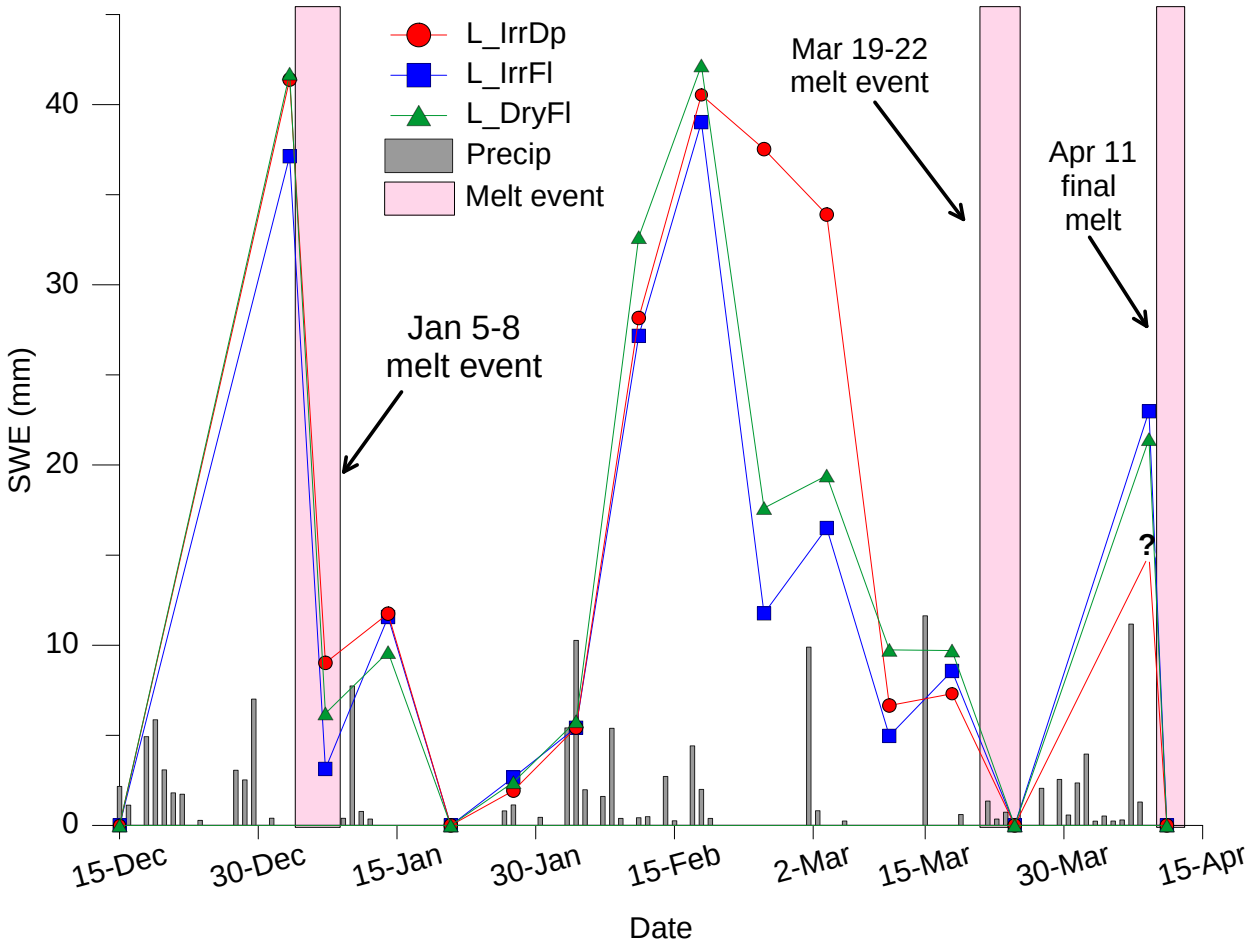

Figure 2.7. Snow survey data showing weekly average snow water equivalent (SWE) for survey lines on each field at LDF. Surveys were conducted from December 15, 2017 until April 9, 2018. No survey was conducted at L_IrrDp on April 9 due to ponding in the depression, making it difficult to delineate snow, liquid water and ice. Two significant mid-winter melt event periods are indicated that resulted in both complete snowpack depletion *and* increases in soil moisture in the profile; the final spring melt occurred on April 11, 2018.

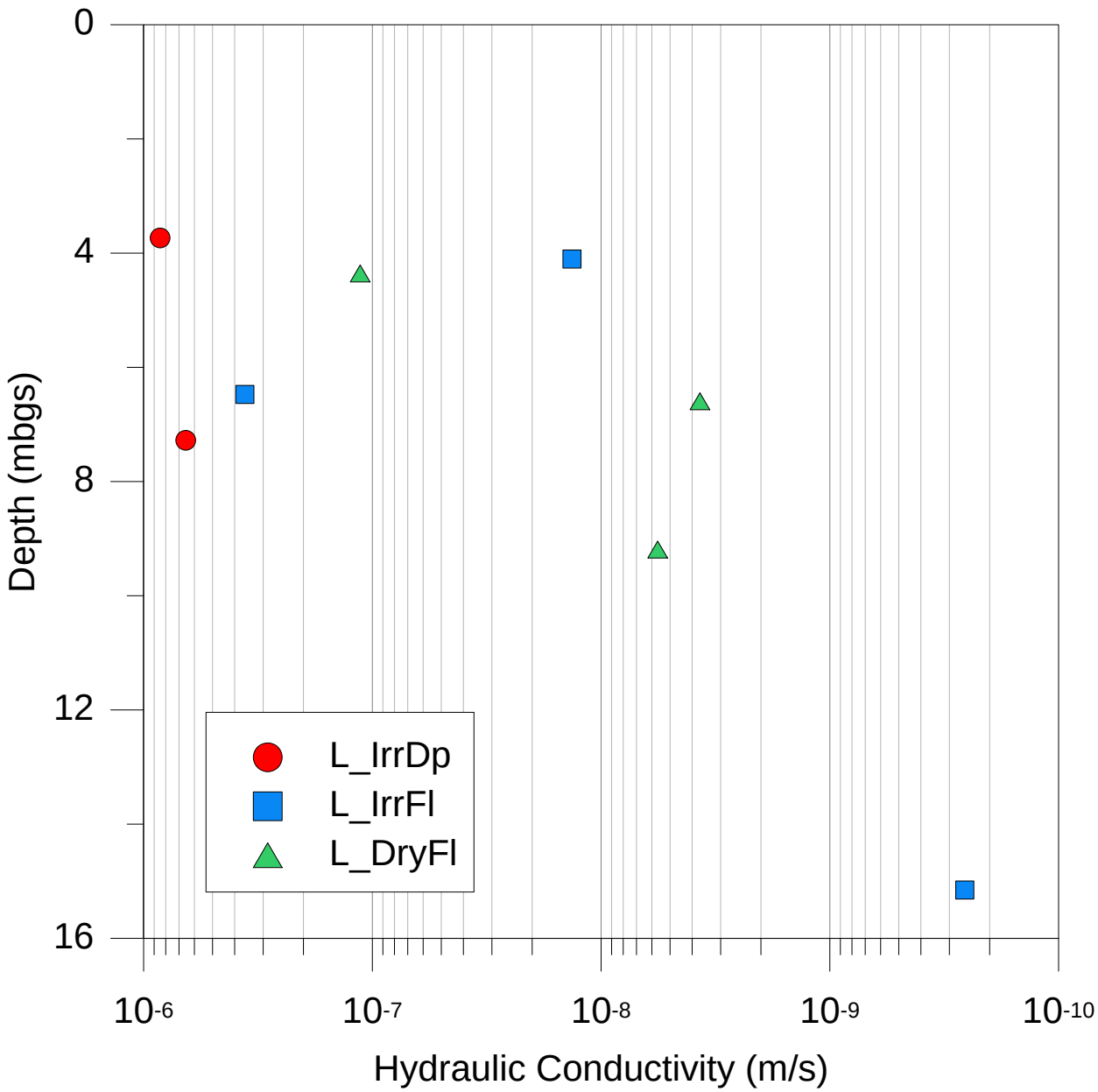

Figure 2.8. Hydraulic conductivity (K_s) results from July 2017 bail tests at Lethbridge Demonstration Farm monitoring wells. Water level recovery data was analyzed using the Bower and Rice (1976) solution in AQTESOLV. Note that K_s is likely underestimated for the deep well at L_IrrDp.

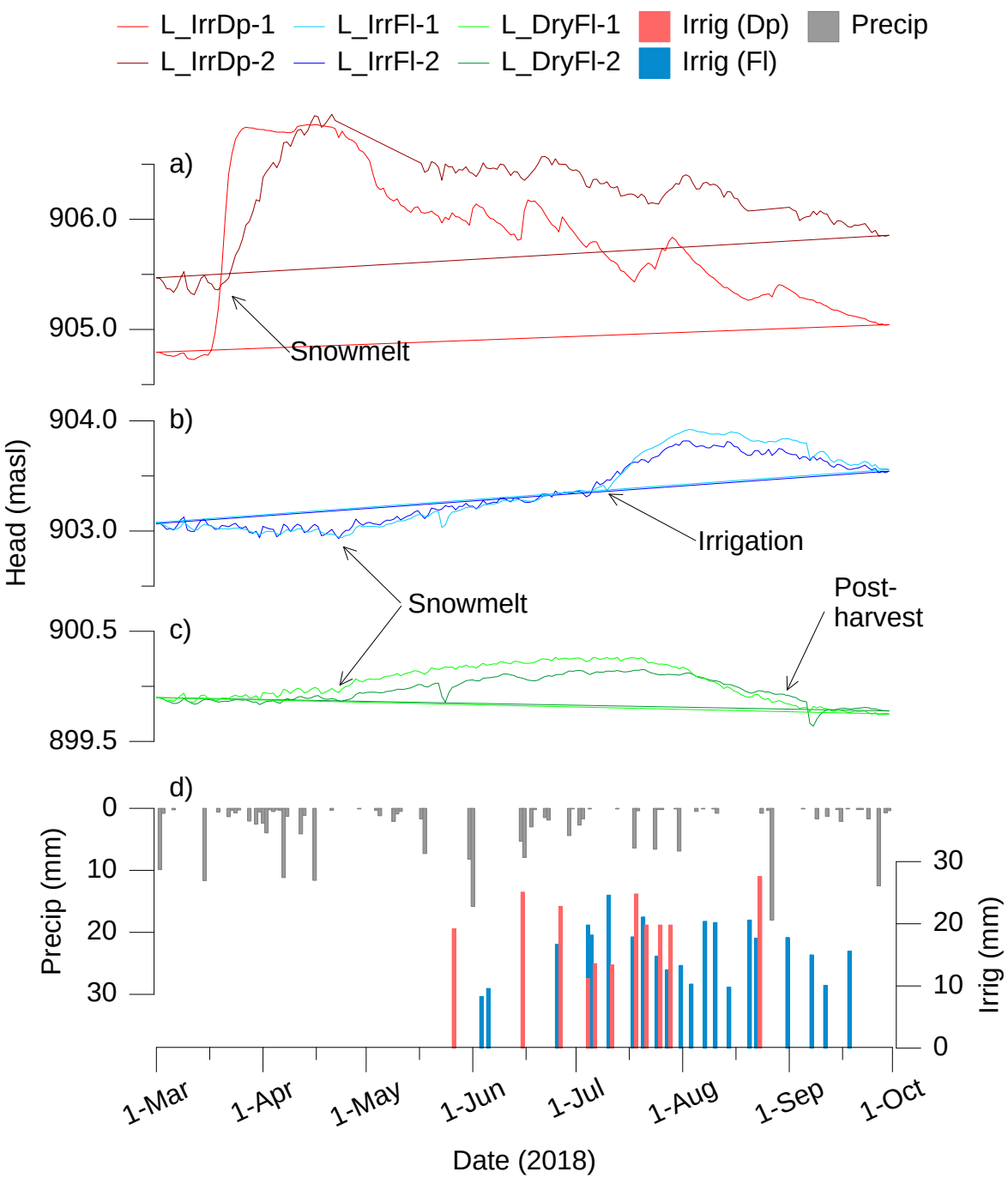

Figure 2.9. Water levels from monitoring wells at LDF from March to September, 2018 at L_IrrDp (a), L_IrrFl (b) and L_DryFl (c). Irrigation applied and precipitation are also shown (d). Arrows indicate what are interpreted to be responses to snowmelt, irrigation and harvest. Note that wells were sampled on May 23 and September 7 resulting in a perceptible decrease in in water level in slow-recovering wells.

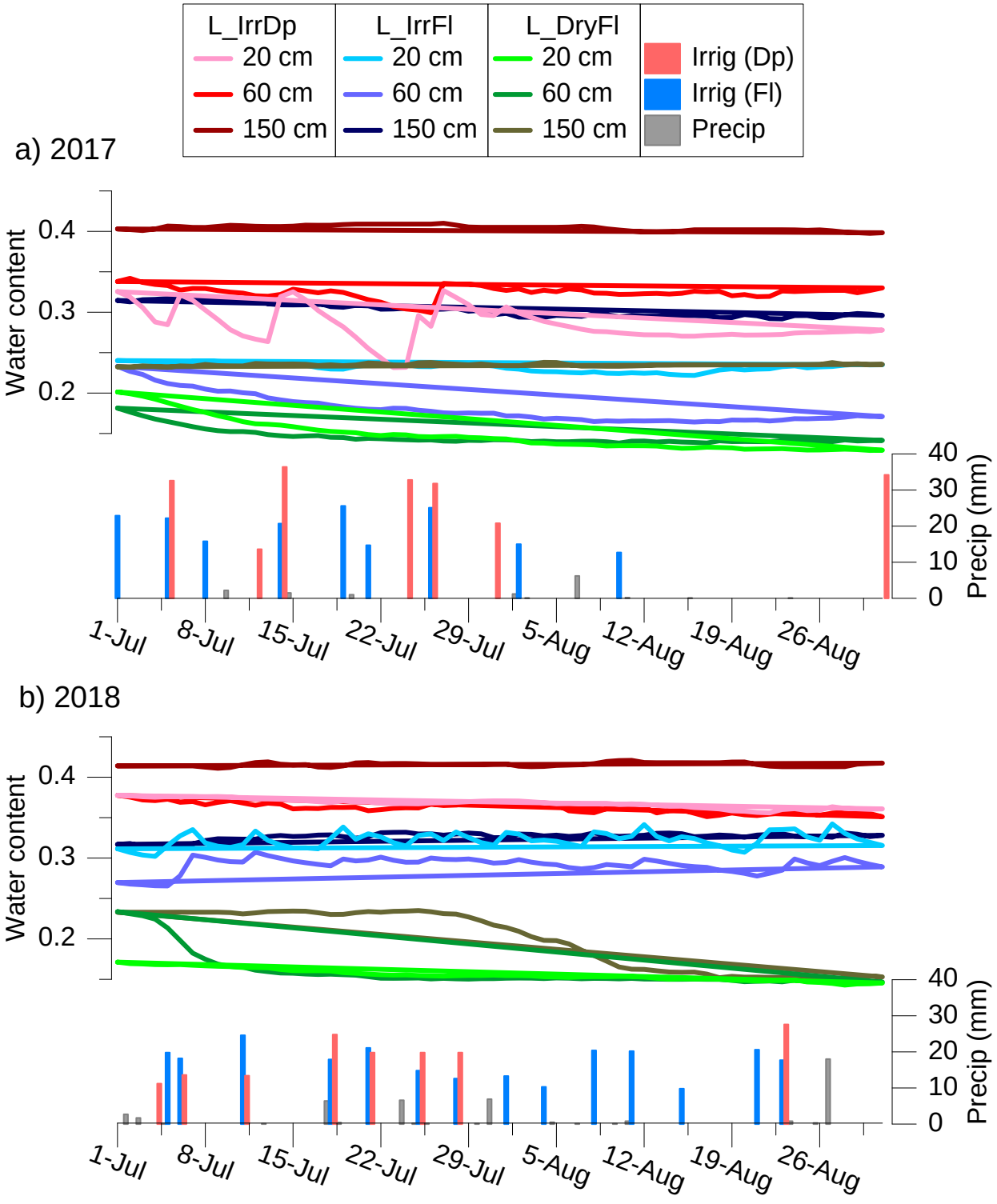

Figure 2.10. Soil moisture data from 20, 60 and 150 cmbgs from all fields at LDF in July-August of 2017 (a) and 2018 (b). Precipitation and irrigation for each year are also indicated.

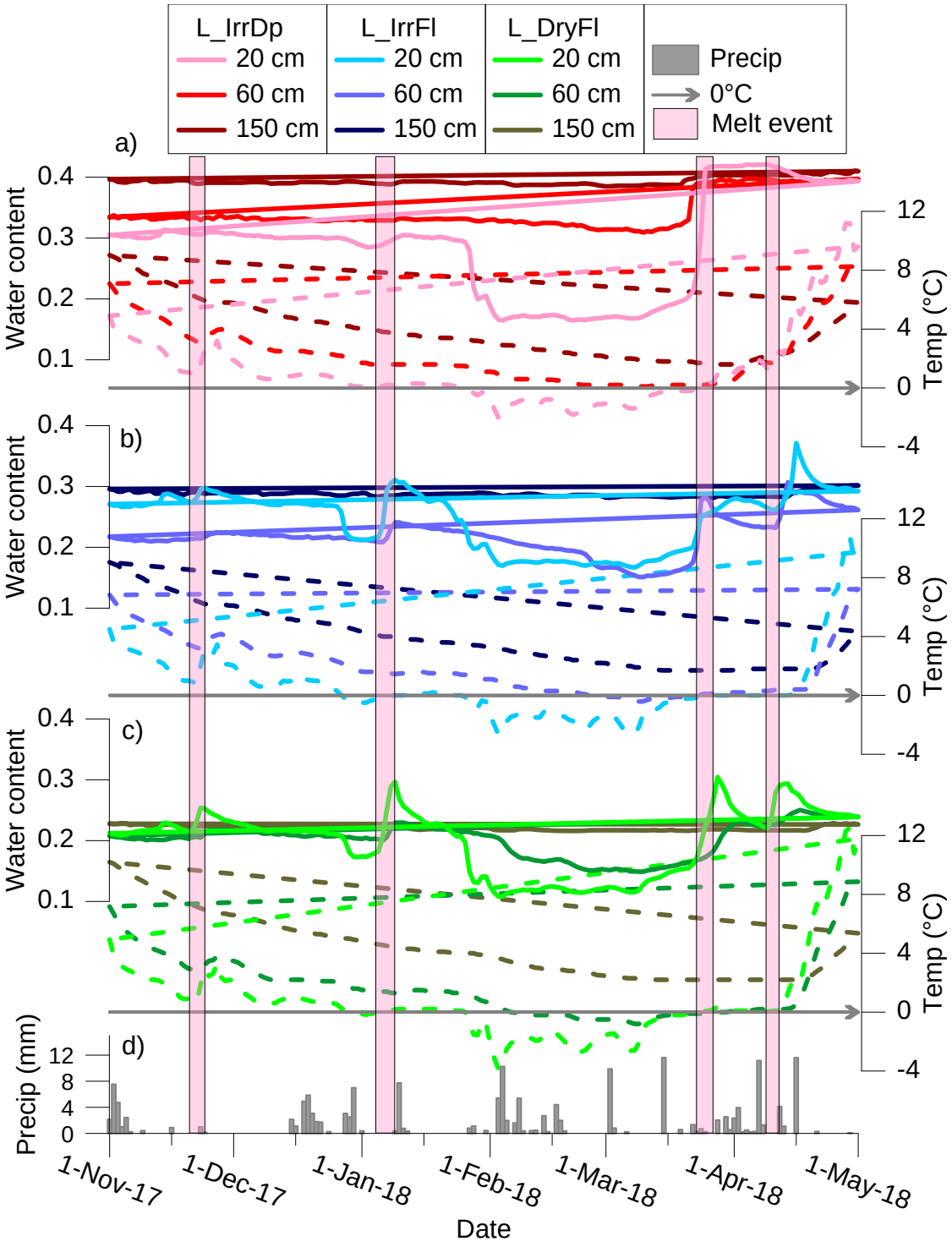

Figure 2.11. Volumetric soil water content (solid lines) and temperature (dashed lines) data from 20, 60 and 150 cmbgs at L_IrrDp (a), L_IrrFl (b) and L_DryFl (c) from November 1, 2017 to April 30, 2018. Precipitation is predominantly snow and was similar for all fields (d). Mid-winter melt periods are indicated by shaded rectangles**.**

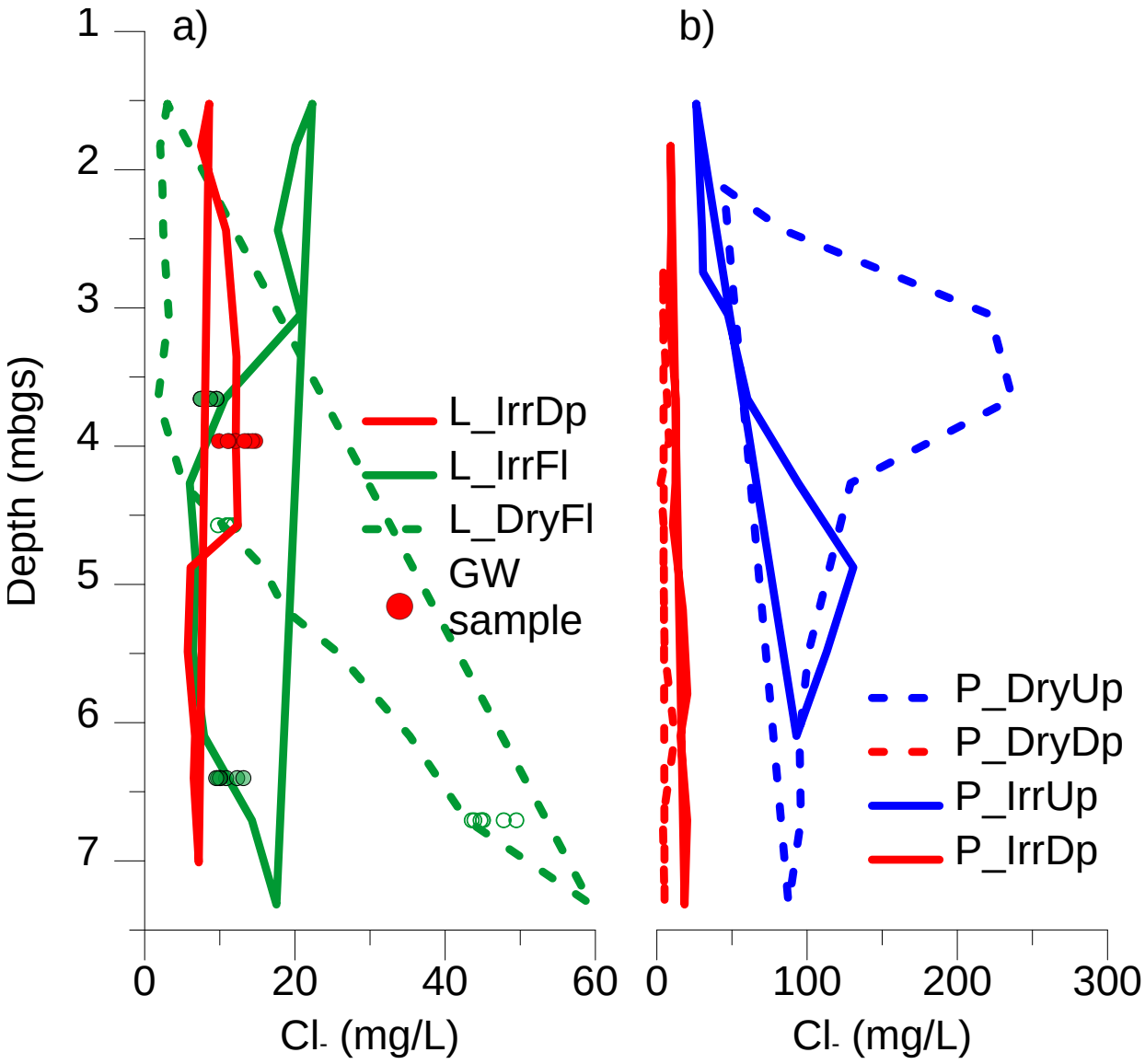

Figure 2.12. Chloride concentration profiles of porewater extracts from borehole samples from LDF (a) and PP (b). Boreholes were sampled approximately every 60 cm. Only samples below the active rootzone (1.5 m) are shown. Groundwater samples from monitoring wells at LDF are also shown. Depressions are red, uplands are blue and flatlands are green. Dryland fields are shown with dashed lines while irrigated fields are shown with solid lines. Note the difference in the x-axis scale between a and b.

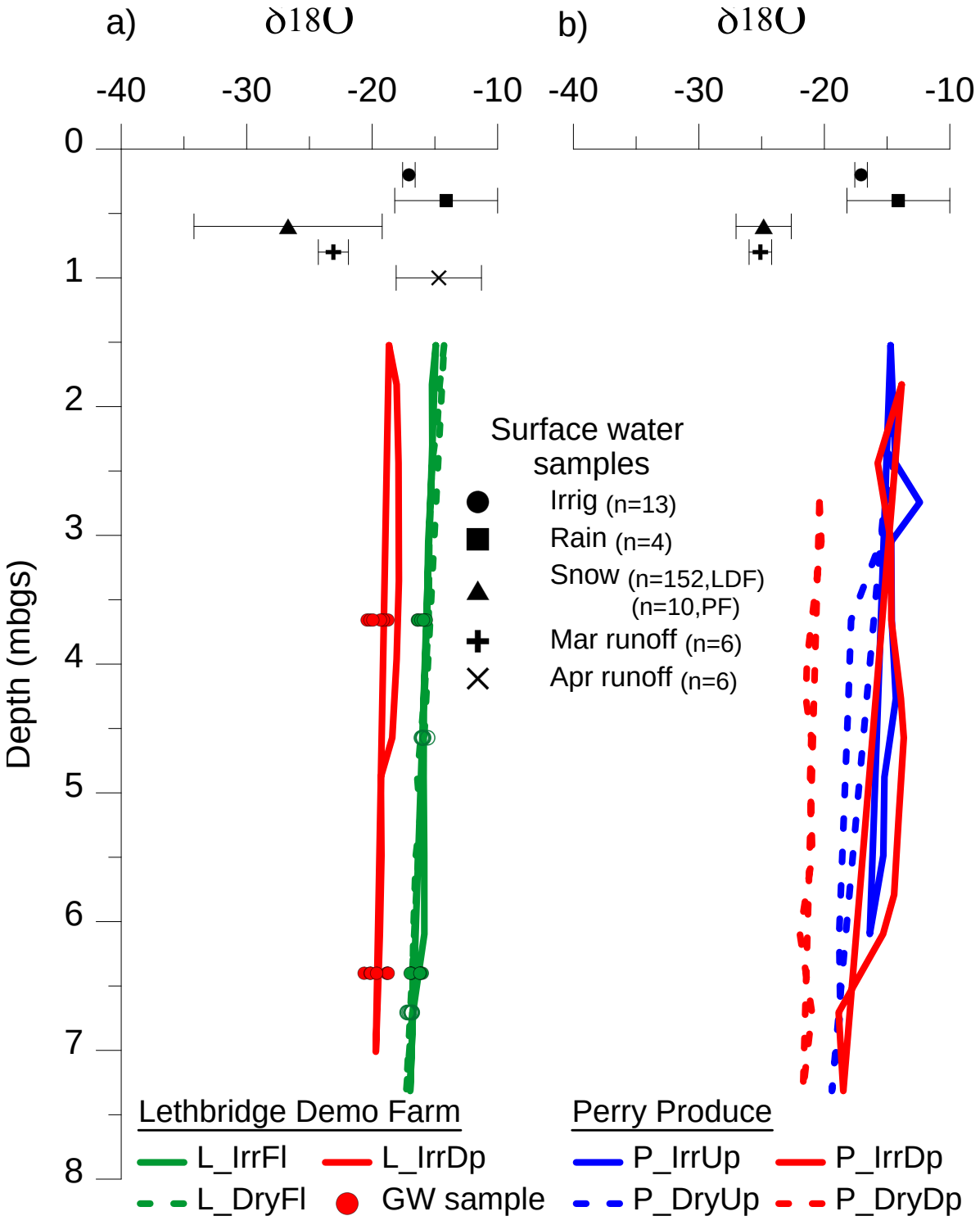

Figure 2.13. Results from stable isotope analyses showing $\delta^{18}O$ for porewater extracts from LDF (a) and PP (b) borehole samples, groundwater samples from LDF, and snow, rain, irrigation water, and runoff samples from both study sites. Number of samples (n) is shown in the legend. Only samples below the active rootzone (1.5m) are shown. Depressions are red, uplands are blue and flatlands are green. Dryland fields are lines while irrigated fields are solid lines.

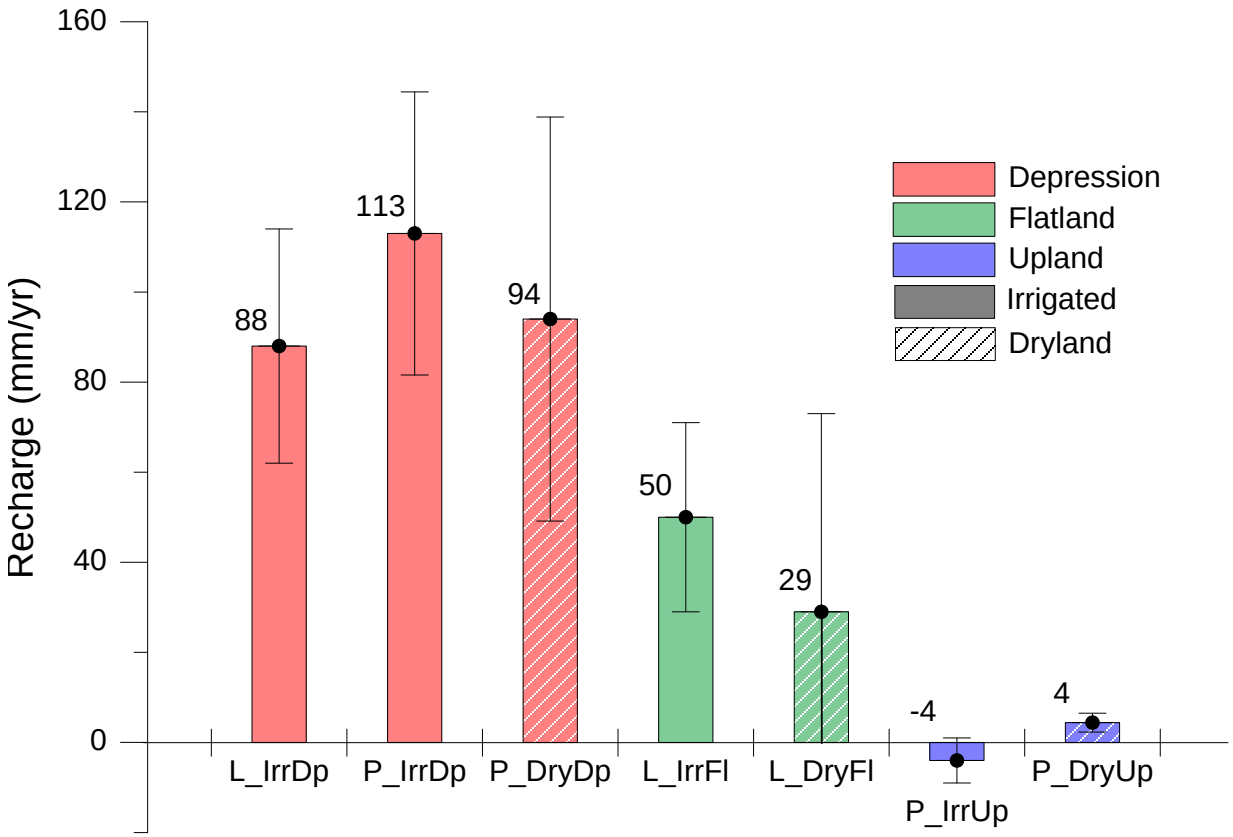

Figure 2.14. Annual recharge rates calculated using the modified CMB method. Error bars represent the uncertainty in recharge estimates.

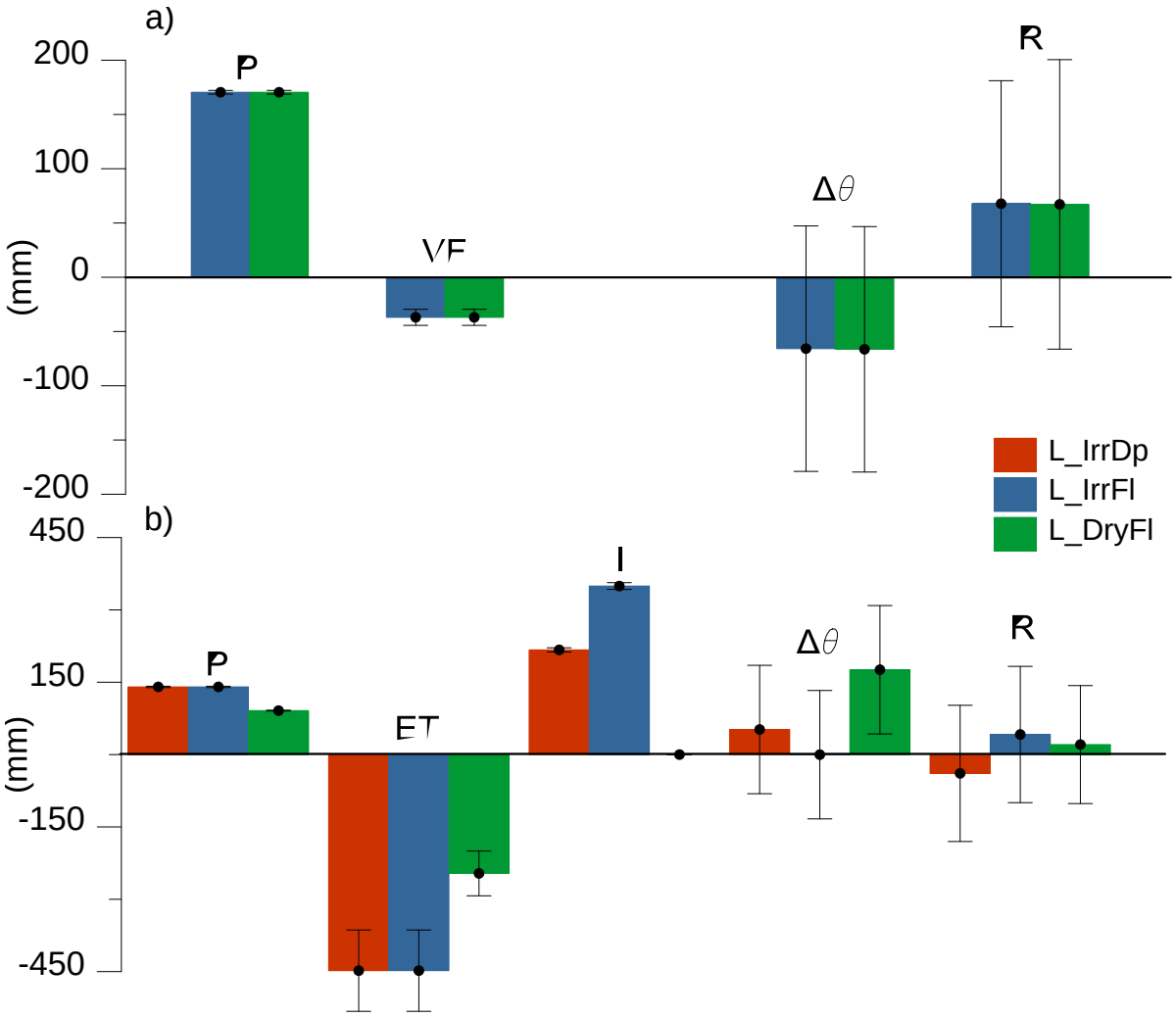

Figure 2.15. Water balance results from a) the overwinter season (November 30, 2017 to April 30, 2018) and b) the growing season (seed date to harvest date) for the instrumented fields at LDF. Note that a negative Δθ in the water balance corresponds to a positive change in water content in the profile. *P* = precipitation; *VF* = vapour flux; *ET* = evapotranspiration; *I* = irrigation; *R* = recharge; *Δθ* = change in soil moisture storage from 0-2 mbgs.

Table 2.5. Values for each parameter used to calculate recharge using the water balance method. The estimated uncertainty for each parameter is also listed. Details on error analysis calculations can be found in Appendix G.

Parameter	Overwinter		Summer	
	Value (mm)	Error (±δ) (mm)	Value (mm)	Error (±δ) (mm)
L_IrrDp:				
P	n/a		140.3	1.4
I			217.1	4.3
ET*			448.0	84.3
Δθ			-51.5	113.1
R			-39.0	141.2
L_IrrFl:				
P	170.5	1.7	140.3	1.4
I	0.0	0.0	349.5	7.0
ET*	36.9	7.4	448.0	84.3
Δθ	65.8	113.1	0.2	113.1
R	67.7	113.4	41.6	141.3
L_DryFl:				
P	170.5	1.7	91.2	0.9
I	0.0	0.0	0.0	0.0
ET*	36.9	7.4	246.3	46.4
Δθ	66.4	113.1	-175.9	113.1
R	67.1	113.4	20.8	122.3

* ET = evapotranspiration for Summer recharge calculations, but represents VF (vapour flux) for overwinter calculations. VF = sublimation + evaporation.

Table 2.6. Recharge estimates obtained for all study locations using different recharge estimation methods. Winter/Spring season is from November 1, 2017 to April 30, 2018. Summer season is from seeding to harvest 2018. WTF = water table fluctuation method; Wat Bal = water balance method; CMB = chloride mass balance method.

Location	Method	Season	Recharge (mm)
L_IrrDp	WTF	Overwinter	170 ± 34
	Wat Bal	Summer	-39 ± 141*
	CMB	Long term annual	88 ± 26
L_IrrFl	WTF	Overwinter	33 ± 7
	Wat Bal	Overwinter	68 ± 113
	WTF	Summer	42 ± 9
	Wat Bal	Summer	42 ± 141
	CMB	Long term annual	50 ± 21
L_DryFl	WTF	Overwinter	33 ± 7
	Wat Bal	Overwinter	67 ± 113
	Wat Bal	Summer	21 ± 122
	CMB	Long term annual	29 ± 44
P_IrrDp	CMB	Long term annual	113 ± 31
P_IrrUp	CMB	Long term annual	-4 ± 5
P_DryDp	CMB	Long term annual	94 ± 45
P_DryUp	CMB	Long term annual	4 ± 2

*L_IrrDp is a discharge depression during the summer months

Table 2.7. Model input parameters used for all model simulations. Bold entries are values determined via inverse modeling during calibration. Non-bold entries were determined from laboratory measurements (θ_s) or literature estimates (θ_r, α, l).

Layer	Macropore Domain						Matrix Domain				
	θ_r	θ_s	α (1/cm)	$\boldsymbol{n}$	$\boldsymbol{K_s}$ **(cm/day)**	l	θ_r	θ_s	$\boldsymbol{\alpha}$ **(1/cm)**	$\boldsymbol{n}$	$\boldsymbol{\omega}$ **(days)**
1	0	0.12	0.01	**5.07**	**7.02**	0.5	0.01	0.31	**0.08**	**1.03**	**1.50**
2	0	0.11	0.01	**1.78**	**4.31**	0.5	0.01	0.38	**0.01**	**2.47**	**0.00**
3	0	0.10	0.01	**1.27**	**7.56**	0.5	0.01	0.31	**0.13**	**1.06**	**0.19**

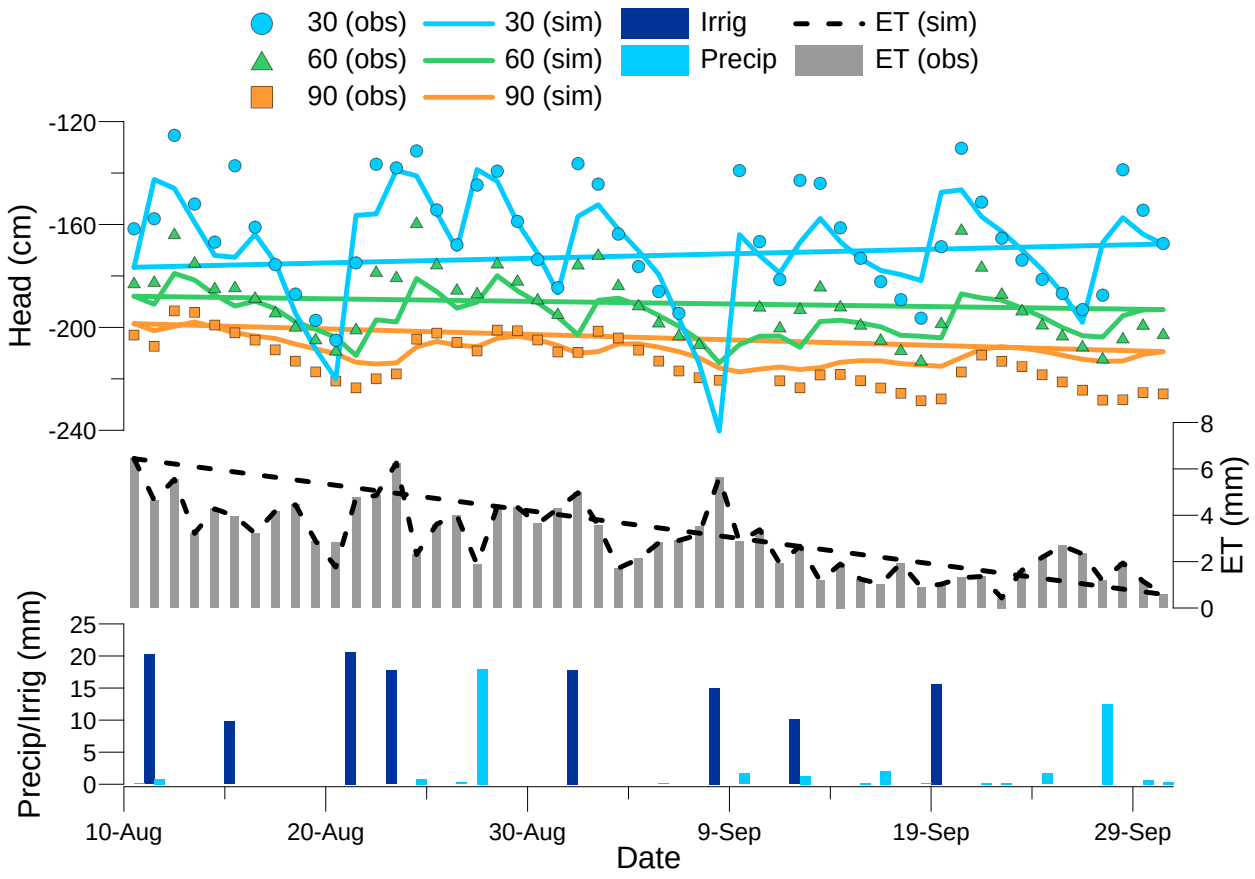

Figure 2.16. Simulated hydraulic head (solid lines) plotted against measured tensiometer data (symbols) from L_IrrFl for the calibration period from August 10 to September 30, 2018. *ET* inputs and model outputs are also shown, as well as irrigation and precipitation amounts.

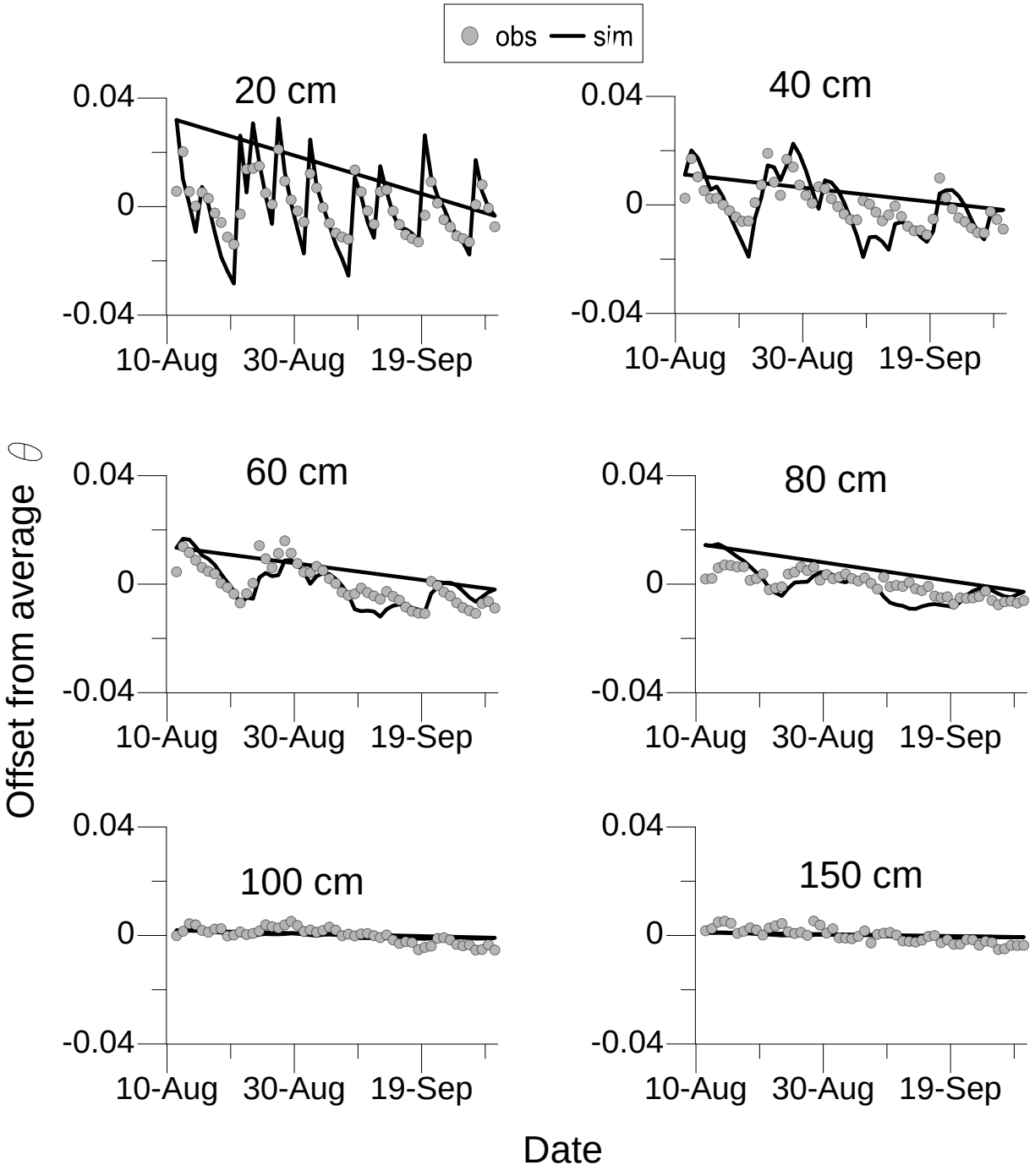

Figure 2.17. Simulated and observed volumetric water content (θ) plotted for each observation depth at L_IrrFl for the calibration period from August 10 to September 30, 2018.Values are plotted as the deviation from the average water content shown in Table 2.8.

Table 2.8. The average simulated and observed volumetric water content (θ) for the calibration period at L_IrrFl for each measurement depth. The Nash-Sutcliffe (NS), root mean square error (RMSE) and mean absolute error (MAE) for each depth are also shown.

Depth (cmbgs)	Mean θ:		NS	RMSE	MAE
	sim	obs			
20	0.32	0.32	0.27	0.01	0.007
40	0.32	0.30	0.73	0.007	0.006
60	0.32	0.28	0.78	0.005	0.004
80	0.33	0.39	0.78	0.005	0.004
100	0.35	0.38	0.96	0.002	0.002
150	0.36	0.33	0.95	0.002	0.002
Average:	0.33	0.33	0.75	0.005	0.004

Table 2.9. Water balance parameters obtained from field-measured data at L_IrrFl compared to calibrated model outputs over the calibration period (August 10-September 30, 2018). Precipitation (*P*) and irrigation (*I*) were based on field-measured values, while evapotranspiration (*ET*), change in water content in the profile (Net $\Delta\theta$) and recharge (*R*) are model outputs.

Parameter (mm)	L_IrrFl	Calib model
P	41.2	41.2
I	126.8	126.8
ET	153.9	152.5
Net Δθ	-15.6	-16.1
R	**29.7**	**31.6**

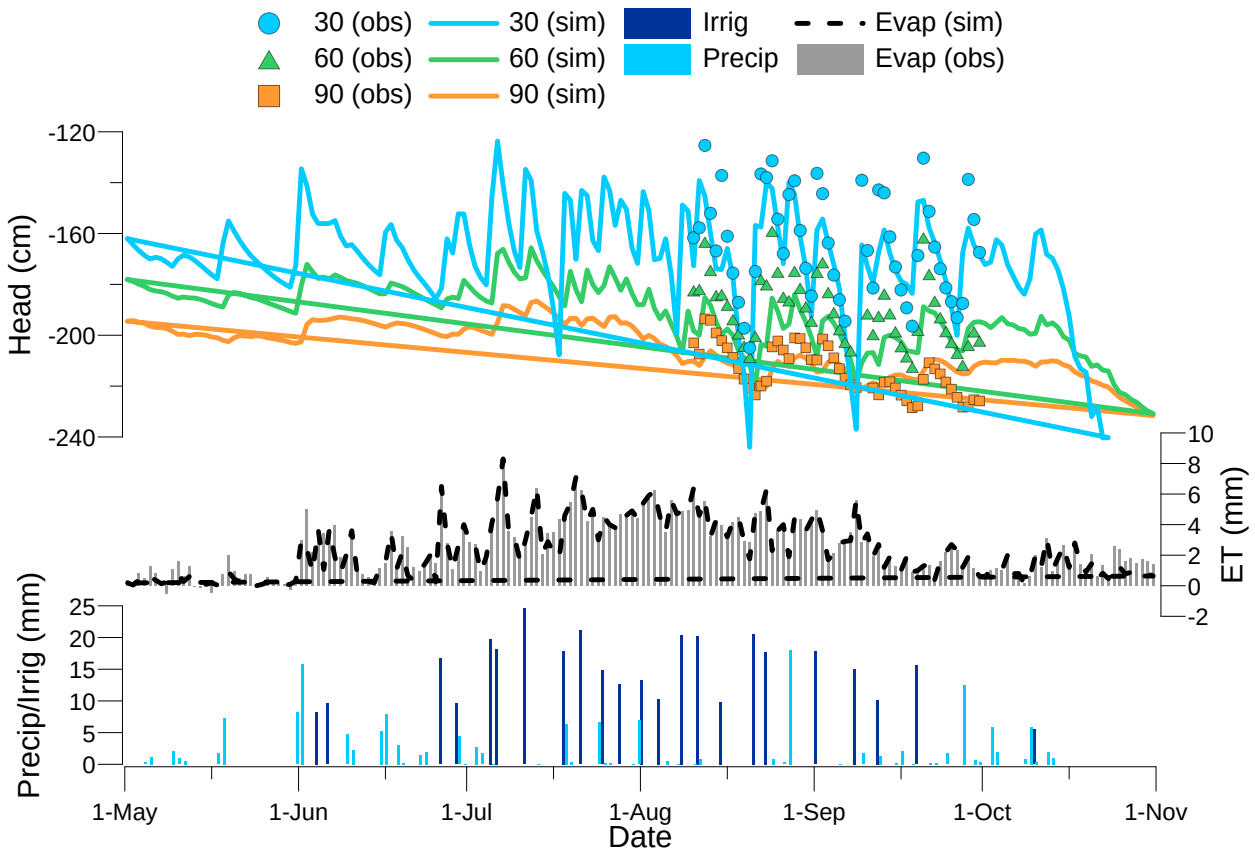

Figure 2.18. Simulated hydraulic head results from the irrigated model (solid lines) plotted alongside field-measured head data (symbols) from L_IrrFl. The modeling period is from May 1 to October 31, but reliable tensiometer data was only collected between August 10 and September 30 (i.e., the calibration period). Seeding was May 24 and harvest was October 30. Measured precipitation, irrigation and evapotranspiration (*ET*) are also shown as well as modeled ET.

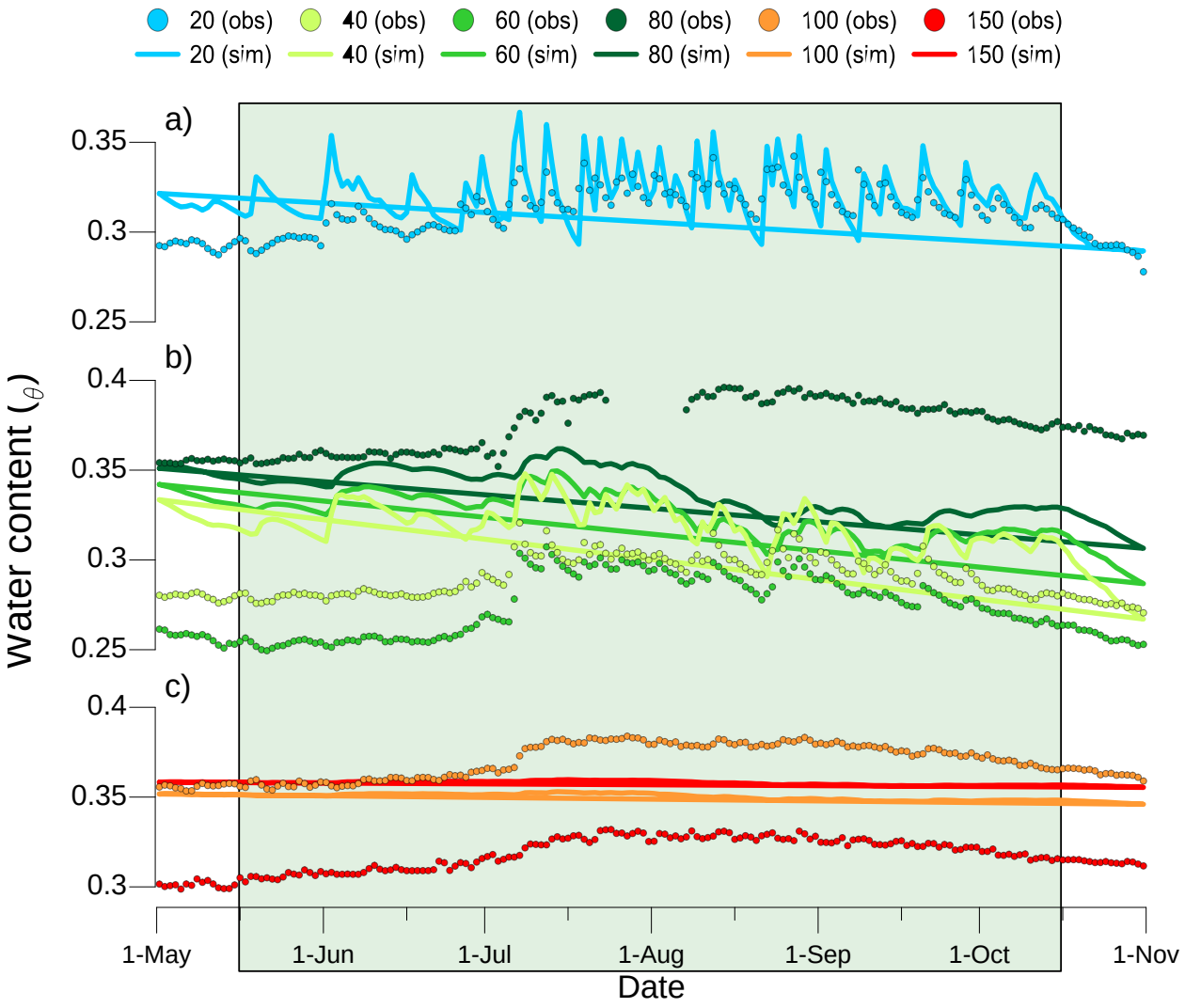

Figure 2.19. Simulated volumetric soil water content results from the irrigated model (solid lines) plotted alongside field-measured water contents (symbols) from L_IrrFl. The model was divided into three layers: Layer 1 (a) from 0 to 35 cm, Layer 2 (b) from 35 to 85 cm and Layer 3 (c) from 85 to 200 cmbgs. The shaded box outlines the time period for the corresponding water balance calculation.

Table 2.10. Results from water balance calculations using field-measured data from L_IrrFl and L_DryFl as well as the irrigated and dry model results. Note that the dryland growing season was shorter than the irrigated growing season, so a post-harvest water balance was also calculated.

	Irrigated		Dryland			
Time interval:	May 15 - Oct 15		May 15 - Aug 15		Aug 16 - Oct 15	
Parameter (mm)	L_IrrFl	Model (irrig)	L_DryFl	Model (dry)	L_DryFl	Model (dry)
Precip	149.3	149.3	91.2	91.2	58.1	58.1
Irrig	349.5	349.5	0.0	0.0	0.0	0.0
ET	427.9	402.5	238.8	152.4	56.9	54.8
Net $\Delta\theta$	24.0	-9.2	-167.1	-95.5	22.6	50.9
Recharge	**46.9**	**105.6**	**19.5**	**34.3**	**-21.4**	**-47.5**

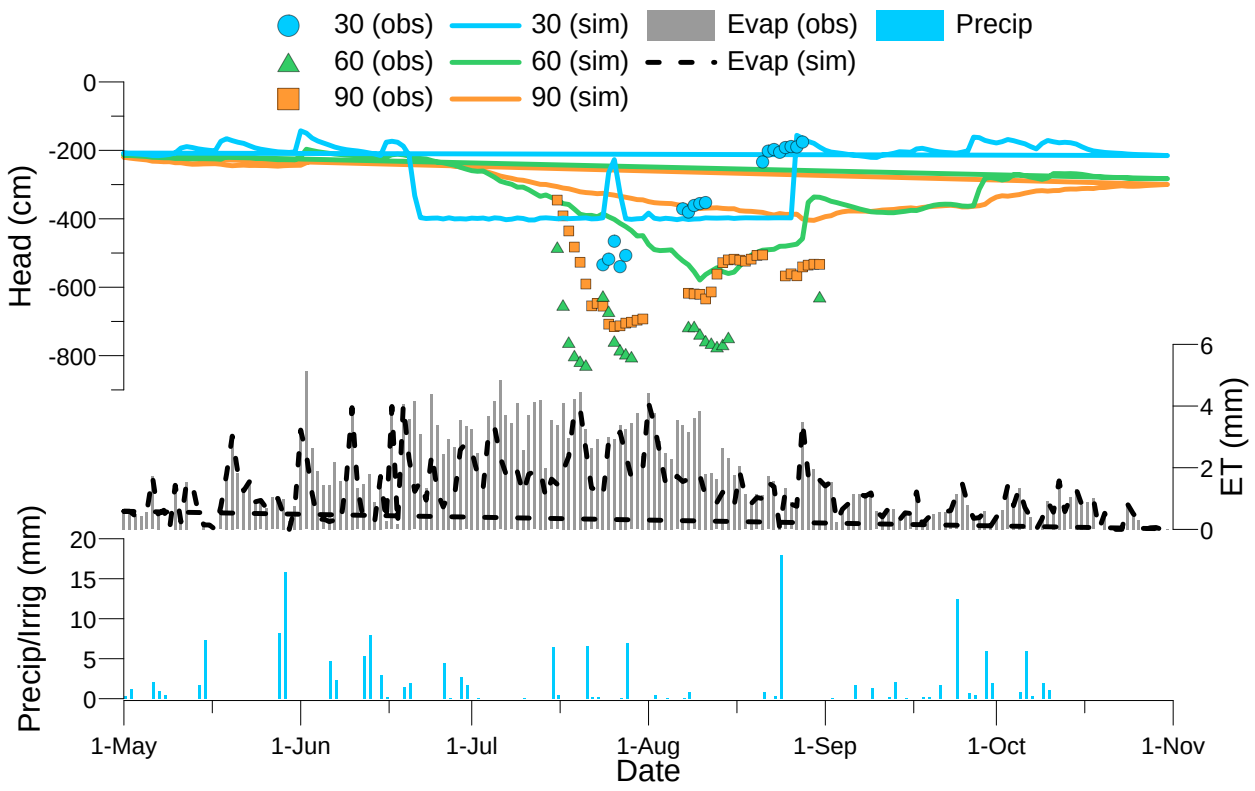

Figure 2.20. Simulated hydraulic head results from the theoretical dryland model (solid lines) plotted alongside field-measured head data (symbols) from L_DryFl.

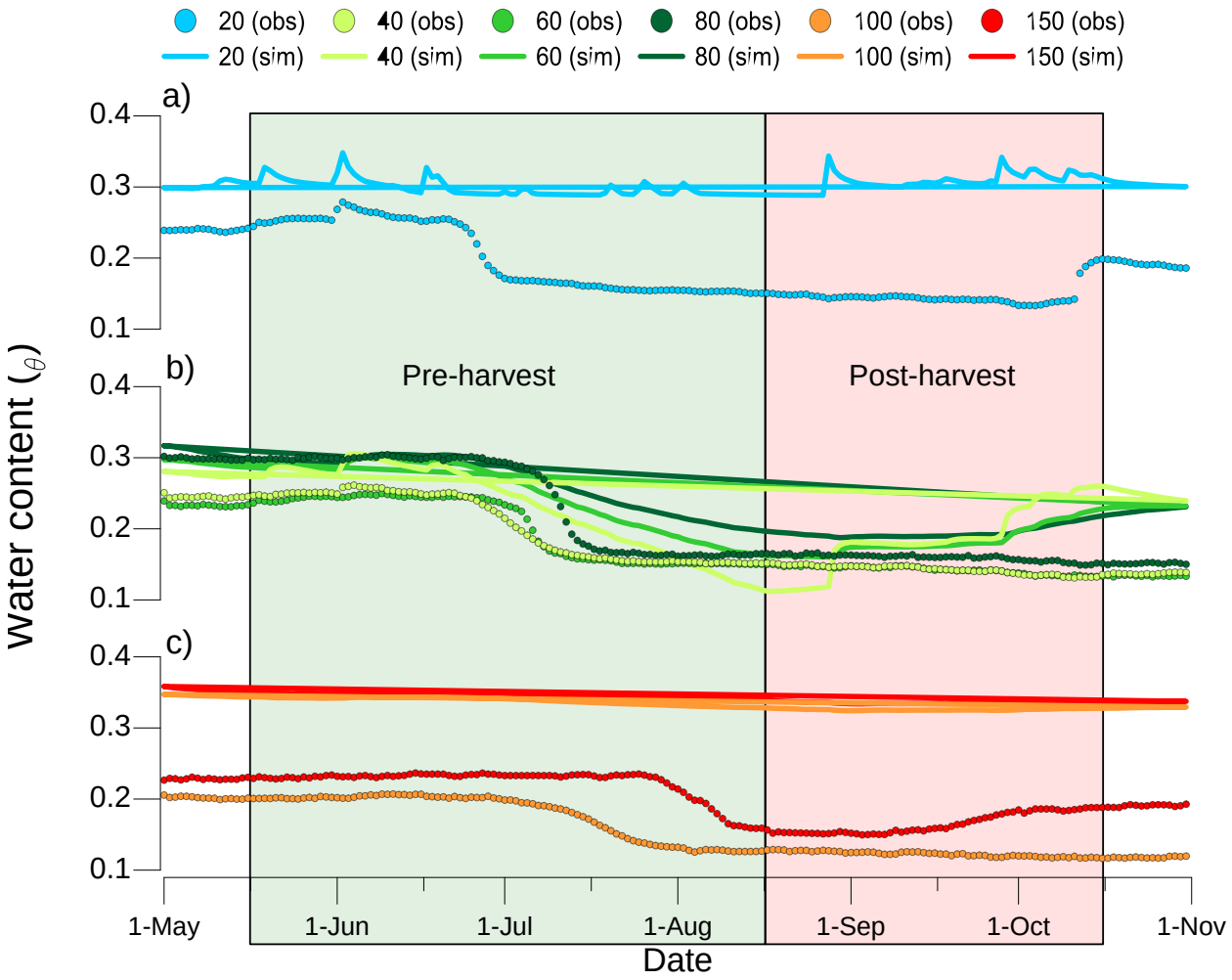

Figure 2.21. Simulated volumetric soil water content results (solid lines) from the theoretical dryland model plotted alongside field-measured water contents (symbols) from L_IrrDl. The model was divided into three layers: Layer 1 (a) from 0 to 35 cm, Layer 2 (b) from 35 to 85 cm and Layer 3 (c) from 85 to 200 cmbgs. The green shaded box outlines the time period for which the "pre-harvest" water balance calculation was done, whereas the red box indicates the "post-harvest" period.

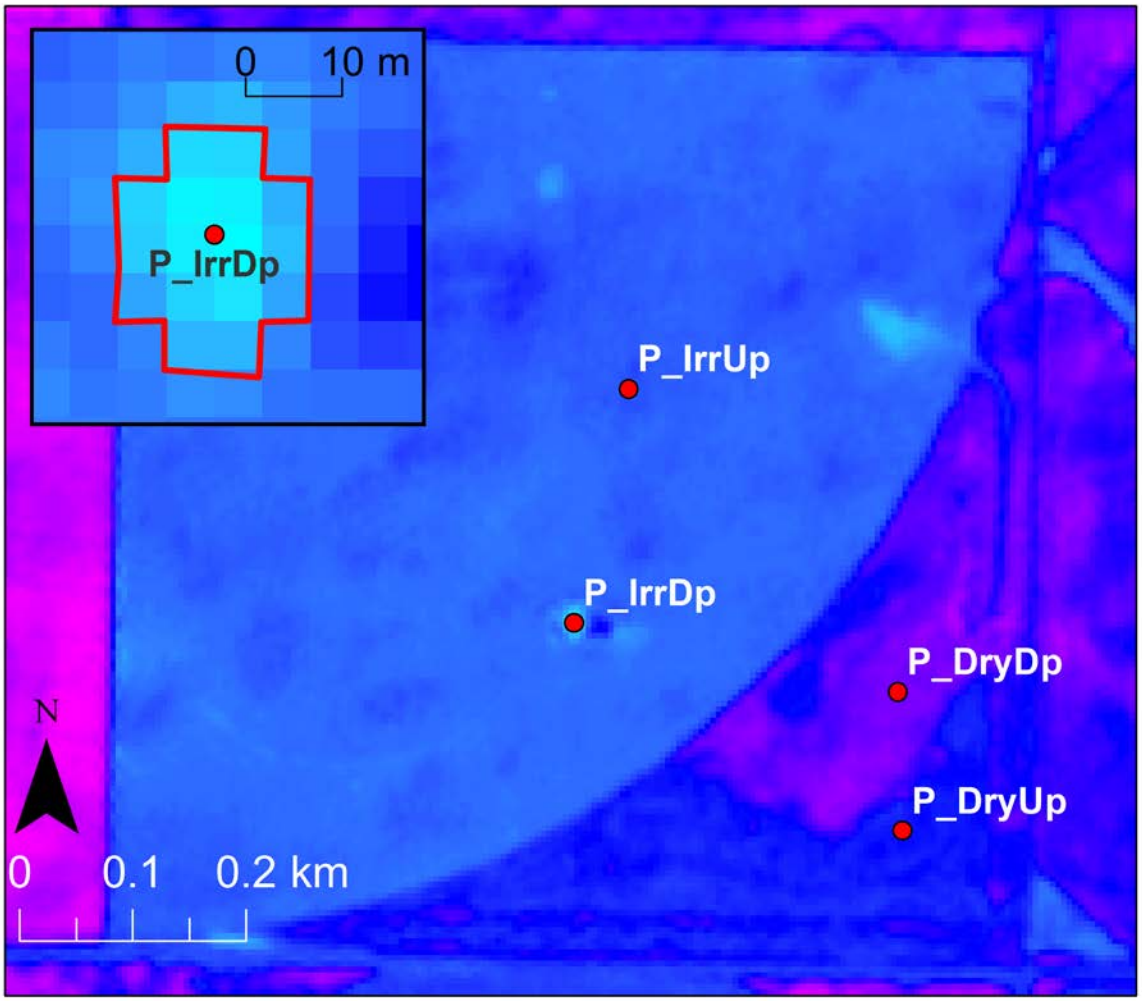

Figure 2.22. Near-infrared satellite imagery of PP from June 28, 2012. The inset shows the area surrounding P_IrrDp where light blue pixels (outlined in red) depict liquid water.

Chapter 3: Summary and future work

3.1 Thesis summary

Previous studies have shown that irrigation can increase recharge rates by up to 6.5 times compared to dryland cultivation (Chiew & McMahon, 1991; Scanlon et al., 2005). This has implications for groundwater resource management, since the rate of replenishment plays a key role in determining sustainable groundwater use policies (Sophocleous, 2000; Zhou, 2009). As such, the goal of this study was to investigate the effects of irrigation on groundwater recharge rates in southern Alberta, where the largest portion of Canada's irrigated lands are situated (Statistics Canada, 2011). Depression-focused recharge rates beneath depressions, and diffuse recharge rates beneath uplands and flatlands, were estimated under both irrigated and dryland conditions at two study sites (LDF and PP) near Lethbridge, Alberta using the chloride mass balance (CMB), the water table fluctuation (WTF) and the water balance methods. The effects of irrigation on the seasonality of recharge events (i.e., overwinter versus summer) were also considered. Additionally, recharge over the growing season was simulated under irrigated and dryland conditions using a numerical model and then compared.

Results from all three recharge estimation methods indicate that, regardless of irrigated or dryland conditions, recharge rates were the highest beneath depressions, moderate beneath flatlands and lowest beneath uplands, which is consistent with previous studies of recharge in the Canadian prairies (van der Kamp & Hayashi, 1998; Berthold et al., 2014). The long-term recharge rates estimated using the CMB method were 88 ± 26 mm/yr and 113 ± 31 mm/yr beneath the irrigated depressions at the LDF and PP sites, respectively, and 94 ± 45 mm/yr beneath the dryland depression at the PP site. Moderate recharge rates were estimated for the irrigated (50 ± 21 mm/yr) and dryland (29 ± 44 mm/yr) flatlands at the LDF site, while estimates

at the PP irrigated (-4 ± 5 mm/yr) and dryland (4 ± 2 mm/yr) uplands were low. The overwinter recharge (snowmelt recharge from November 1, 2017-April 30 2018) at the LDF site was estimated to be 170 ± 34 mm for the irrigated depression, compared to 33 ± 7 mm for both the irrigated and dryland flatlands according the WTF method. Stable isotope (^{2}H and ^{18}O) profiles indicated that snowmelt was likely an important contributor to recharge beneath all depressions, while diffuse recharge beneath uplands and flatlands was more influenced by summer precipitation (rain or irrigation water). However, analysis of satellite imagery and stable isotope profiles at the PP site indicated the possibility of DFR of irrigation runoff beneath the irrigated depression during the summer months.

Like previous studies, this study found that increased fall soil water content prior to soil freezing leads to reduced infiltration of snowmelt during the frozen soil period (Granger et al., 1984; LeBlanc, 2017). This was observed beneath the irrigated depression at the LDF site, which had an average fall soil water content of 0.35 and did not show evidence of mid-winter snowmelt infiltration. However, the average fall soil water content of the irrigated flatland (0.26) was only slightly wetter than the dryland flatland (0.22), and thus did not significantly reduce infiltration of overwinter snowmelt on the irrigated field, as was anticipated. As a result, overwinter recharge was estimated to be the same for both the irrigated and dryland flatlands at the LDF site (33 ± 7 mm using the WTF method and 68 + 113 mm using the water balance method). These results suggest that, in some years, although irrigation increases the fall soil water content, the conditions may not be wet enough to significantly reduce frozen soil infiltrability compared to a dryland field with similar soil characteristics, which can lead to similar amounts of overwinter recharge. Additionally, daily soil moisture and temperature data showed that the majority of overwinter snowmelt infiltration on the flatlands was likely stored within the soil profile due to

freezing of the infiltrating water. As a result, deep drainage of mid-winter snowmelt water did not occur until after the soil had thawed completely, resulting in a single pulse of overwinter recharge in spring for both the irrigated and dryland flatlands.

The amount of recharge estimated over the 2018 growing season (i.e., seeding to harvest) using the water balance method was 42 ± 141 mm for the irrigated flatland at the LDF site, which was twice the amount estimated for the dryland flatland (21 mm). Similarly, the WTF method estimated 42 ± 9 mm of recharge in summer beneath the irrigated flatland, based on a water table response that was most likely related to irrigation events. Numerical modeling resulted in simulated recharge over the growing season period that was 3.1 times higher under irrigated versus dryland conditions. Although summer recharge rates estimated in this study were based only on one growing season, results are consistent with other studies that have reported elevated recharge rates in irrigated areas compared to areas of dryland cultivation (Chiew & McMahon, 1991; Scanlon et al., 2005). However, the extent to which summer recharge is increased on irrigated fields may vary significantly from year to year as a result of factors such as precipitation and crop type.

These results suggest that irrigation can alter the seasonality of recharge on flatland fields. Not only did the irrigated flatland experience increased recharge rates, the majority of annual recharge occurred during the summer months as a result of frequent irrigation. This is in contrast to the dryland flatland, where the major recharge event occurred in spring as a result of snowmelt.

This study has provided important insights into the role of irrigation on the rates, mechanisms and timing of groundwater recharge in southern Alberta. Irrigation-induced recharge has been shown to degrade the quality of shallow groundwater and implies inefficient

irrigation strategies, but may replenish groundwater resources for future use. Understanding the spatiotemporal distribution of groundwater recharge is a key step in quantifying and managing Alberta's groundwater resources.

3.2 Uncertainties and limitations

A significant limitation of this study was the duration of the study period, since only one spring snowmelt event and two growing seasons were fully captured at the LDF site. Additionally, the period over which the water balance calculations and numerical modeling could be performed was further reduced to one growing season due to malfunctioning equipment that prevented estimation of evapotranspiration. Climatic conditions, such as average air temperature and amount of precipitation, vary significantly on both an annual and decadal scale, resulting in similar variability in recharge rates (Hayashi & Farrow, 2014). Furthermore, the amount of irrigation applied and the type of crop planted are rarely the same in consecutive years. As such, it is important to keep in mind that the recharge rates estimated in this study for 2017-2018 may not be representative of the conditions in previous years, nor should they be used to predict conditions in future years, especially in light of a changing global climate. Instead, they should be interpreted as snapshots in time within the larger context of long-term (i.e., decadal or longer) climatic trends.

The CMB method used in this study attempted to account for some of this inter-annual climatic variability by estimating the average annual recharge rate since the time that irrigation began: approximately 40 years (1977-2017) for the LDF site and 15 years (2002-2017) for the PP. This time period is inherently uncertain due to the long history of irrigation in southern Alberta, during which many changes in land-use and land ownership have occurred.

Additionally, while information on historical annual rates was available for some datasets (e.g., precipitation, irrigation, fertilizer inputs), other datasets (e.g., chloride concentration in irrigation water, amount of overland flow) collected during the study period represent only 2 yrs (or less) of inputs. Therefore, the scope and representativeness of each dataset should be kept in mind when interpreting the long-term recharge estimates. Recharge estimates were sensitive to the chloride concentration in the groundwater (C_R), which, for some profiles, varied greatly with depth. A uniform interval (2.5-7.5 mbgs) was chosen over which to average C_R at each sub-site, but it is likely that the actual portion of the subsurface that is representative of the total irrigation period varies significantly at each sub-site. This was not accounted for in the study.

The components of the water balance equation typically have errors that are large compared to the magnitude of recharge, especially in arid climates (Gee & Hillel, 1988). As a result, the magnitude of error in estimated recharge rates can often be of the same order of magnitude as the recharge estimate itself, if not greater (Scanlon et al., 2006). The recharge estimates obtained in this study using the water balance method are subject to large errors (Appendix G), however, the results are still considered useful when comparing relative rates between irrigated and dryland fields, or uplands and depressions. In particular, large errors associated with ET measurements contributed to considerable uncertainty in recharge estimates. Greater accuracy in ET measurements would have improved recharge estimates.

Recharge estimated using the WTF method is also prone to error since the WTF method assumes groundwater level increases are due solely to recharging water arriving at the water table from above. It does not account for other inputs/outputs such as lateral groundwater flow, pumping, connection to surface water bodies, barometric pressure fluctuations, etc. There is a slight horizontal hydraulic head gradient across the LDF site of 0.004 (Rodvang, 2002), however

the impacts of this and other potential causes of water table fluctuation were not considered. Additionally, the value of S_y can vary with the position of the water table, although assuming a constant S_y is considered a reasonable approximation if the depth to the water table is greater than 2 m (Shah & Ross, 2009), which is the case at the LDF flatland sub-sites. The S_y value applied to all calculations could also have been improved by applying the method of Cheng et al. (2015) on re-packed soil rings from borehole samples near the water table.

There are several limitations associated with the modeling exercise that should be addressed. Firstly, even a well-calibrated or "history-matched" model is subject to the issue of non-uniqueness (Tonomi, 2000), and the soil hydraulic parameters obtained during calibration are only one of many possible combinations of parameters that would satisfy the inverse model solution. Uncertainties in simulated recharge rates were likely a result of several compounding factors, the most significant being that the calibration period was likely not sufficiently long to capture enough variability in soil pressure head/moisture conditions. Since model input parameters were optimized during the calibration period when the crop was fully mature, a longer calibration period that includes early crop stages would have potentially improved these parameter estimations. The fact that recharge was consistently over-estimated was likely a combined result of hydraulic parameters that promoted more drainage through the profile than expected, as well as possible overestimation of the macropore domain (since the dual-porosity model prevents flow in the matrix). A dual-permeability model, which allows flow in both the matrix and macropore domains, would likely have improved results.

Additionally, the use of actual ET rather than potential ET results in ET values that are consistently underestimated and introduces uncertainty into model simulations and the resulting water balance calculations. Ideally, potential ET rates should be estimated by other means and

the model should be re-calibrated to allow for the proper calculation of absolute ET within HYDRUS.

The limitations of the model are especially apparent in the dryland scenario where the dual-porosity approach does not lend itself well to extreme dry conditions, especially when calibrated to wet conditions. The dryland model would be significantly improved if enough head data was available for a dryland calibration period, and if a dual-permeability model had been used. Additionally, daily *ET* is significantly underestimated, likely related to the fact that HYDRUS-1D assumes daily *ET* inputs are potential rates, as opposed to actual ET, which was used for this study.

3.3 Recommendations for future work

The findings of this study would have benefitted from a longer study period in order to better capture the inter-annual variability of recharge mechanisms at each site. Therefore, future studies should focus on long-term monitoring (e.g., several years to decades) of water table fluctuations and meteorological and vadose zone fluxes, under both irrigated and dryland conditions. Analysis of any available historical long-term datasets would also be valuable. This would provide better estimates of the average added contribution of irrigation to recharge on an annual basis. Similarly, additional study sites comprising both irrigated and dryland crops throughout the province would provide a better understanding of the spatial variability of recharge within the irrigated region. With datasets spanning several years and multiple study sites, the effects of different irrigated crops on recharge could also be investigated, something this study did not consider. Ideally, future studies would capture a wide variety of crop types over time spans that capture wet and drought years in order to better understand the combined

spatiotemporal variability of groundwater recharge within the irrigated region of Alberta. Furthermore, only a subset of the available recharge estimation methods was described in this study (Section 1.3), and an even smaller subset was actually employed to estimate recharge at the study sites (i.e., CMB, WTF and water balance methods). Recharge rates estimated at the two study sites in this study could be corroborated with estimates using other methods (e.g., lysimetry, Darcy's Law, historical tracers, applied tracers, etc.). Alternatively, the same methods used in this study could be used again at other study sites, to determine repeatability and/or variability of those methods under different conditions.

Additional numerical modeling of recharge under irrigated and dryland conditions in southern Alberta would be beneficial. Models should be calibrated to field data collected under both irrigated and dryland conditions, and, ideally, the calibration period should span an entire growing season. Models could be used to compare the effects of different crop types and soil characteristics on recharge rates under both dryland and irrigated conditions. Additionally, simulations could be used to estimate the effects of a warming climate on recharge in irrigated regions. Future researchers would benefit from applying different modeling approaches (i.e., dual-permeability domain versus dual-porosity domain; bucket models versus models based on the Richards equation) to compare and contrast simulated recharge rates at a given location. Modeling infiltration through frozen, irrigated soils would also be beneficial to determine the level of fall soil moisture required to reduce overwinter recharge compared to dryland fall conditions. Eventually, large scale (regional) modeling of groundwater resources in southern Alberta should strive to include different recharge rates for irrigated and dryland cultivated areas.

This study found evidence of potential DFR of irrigation water in summer as a result of runoff and ponding after irrigation events. Further investigation should be done to determine

whether this is a common occurrence and the extent to which this mechanism can contribute to recharge.

An interesting future study would include investigating the effects of climate change on irrigation as an agricultural practice, and, in turn, how that would affect groundwater recharge. For example, recent climate change projections predict warmer temperatures coupled with increased precipitation and a longer snow-free period in Alberta (Jiang et al., 2017). These changes in climate alone would certainly affect groundwater recharge rates, but the potential changes in land-use will also have an impact on recharge. In particular, it is unclear whether the projected future climate would increase or decrease the need for irrigation in southern Alberta, since crops would receive increased levels of summer precipitation, but also be susceptible to higher ET rates in summer. Longer frost-free periods could promote the production of crop types not typically grown in Alberta (e.g., berries) (Motha & Baier, 2005), which would also alter irrigation regimes. Shorter winters coupled with increased summer precipitation and changes in irrigation regimes would affect both the timing and magnitude of overwinter and summer recharge. The future relationships between climate, irrigation practices and groundwater recharge are largely unknown and research in this field is certainly needed.

This study briefly touched on the impacts of irrigation on groundwater quality. Although some work is already being done to assess the level of groundwater degradation in cultivated regions of Alberta (Miller et al., 1995; Hill et al., 1996; Rodvang et al., 2004), research is needed to determine mitigation strategies to prevent degradation from continuing and/or remediate it.

References

Abdulrazzak, M. J., Sorman, A. U., & Alhames, A. S. (1989). Water balance approach under extreme arid conditions—a case study of Tabalah Basin, Saudi Arabia. *Hydrological Processes*, *3*(2), 107-122.

Alberta Agriculture and Forestry (AAF). (2000). Irrigation in Alberta. (Series of documents). Technology and innovation Branch. Accessed March 2019. URL https://www1.agric.gov.ab.ca/$department/deptdocs.nsf/all/irr7197

Alberta Agriculture and Forestry (AAF). (2003). Agroclimatic Atlas of Alberta. (Series of documents). Accessed January 2019. URL https://www1.agric.gov.ab.ca/$department/deptdocs.nsf/all/sag6278

Alberta Agriculture and Forestry (AAF). (2018) Amount of K fertilizer applied to barley depending on soil type. Accessed August 2018. URL http://www1.agric.gov.ab.ca/$department/deptdocs.nsf/all/agdex12433

Alberta Agriculture and Forestry (AAF). (2018) Amount of K fertilizer applied to pasture in Alberta. Accessed August 2018. URL https://www1.agric.gov.ab.ca/$department/deptdocs.nsf/all/agdex10473

Alberta Environment. (2005). Background Information for Public Consultation on the South Saskatchewan River Basin's Draft Water Management. Alberta Environment, Edmonton, Alberta.

Alberta Water Council. (2008). Water for life: A renewal. URL https://open.alberta.ca/publications/9780778576709#summary

Alberta Water Portal (2018). Agriculture and Irrigation in Alberta. Accessed May 2019. URL https://albertawater.com/what-is-water-used-for-in-alberta/agriculture-in-alberta

Ali, M. K., & Klein, K. K. (2014). Water use efficiency and productivity of the irrigation districts in Southern Alberta. *Water Resources Management*, *28*(10), 2751-2766.

Allen, R. G., Howell, T. A., Pruitt, W.O. (1991). Lysimeters for evapotranspiration and environmental measurements. In: Proceedings International Symposium on Lysimetry, Walter IA, Jensen ME (eds) American Society of Civil Engineers, New York, 444 pp

Allen, R. G., Pereira, L. S., Raes, D., & Smith, M. (1998). Crop evapotranspiration-Guidelines for computing crop water requirements-FAO Irrigation and drainage paper 56. *Fao, Rome*, *300*(9), D05109.

Allison, G. B., Barnes, C. J., Hughes, M. W., & Leaney, F. W. J. (1984). Effect of climate and vegetation on oxygen-18 and deuterium profiles in soils. *Isotopes Hydrology, IAEA, Vienna*, 105-122.

Allison, G. B., Gee, G. W., & Tyler, S. W. (1994). Vadose-zone techniques for estimating groundwater recharge in arid and semiarid regions. *Soil Science Society of America Journal*, *58*(1), 6-14.

Allison, G. B., & Hughes, M. W. (1978). The use of environmental chloride and tritium to estimate total recharge to an unconfined aquifer. *Soil Research*, *16*(2), 181-195.

Allison, G. B., & Hughes, M. W. (1983). The use of natural tracers as indicators of soil-water movement in a temperate semi-arid region. *Journal of Hydrology*, *60*(1-4), 157-173.

American Society for Testing and Materials (ASTM). (2013). Standard guide for sampling ground-water monitoring wells. D4448-01. Book of Standards, vol. 11.04. ASTM International. West Conshohocken, PA, United States.

Barr, A. G., Van der Kamp, G., Black, T. A., McCaughey, J. H., & Nesic, Z. (2012). Energy balance closure at the BERMS flux towers in relation to the water balance of the White Gull Creek watershed 1999–2009. *Agricultural and Forest Meteorology*, *153*, 3-13.

Beaulieu, M. S., Bédard, F., Lanciault, P. (2001). Distribution and Concentration of Canadian Livestock. Agricultural and Rural Working Paper Series; Working Paper No. 47. Statistics Canada, Agricultural Division. Ottawa, Ontario.

Bellingham, K. (2007). The Stevens Hydra Probe Inorganic Soil Calibrations. Stevens Water Monitoring Systems Inc. Portland, Oregon, United States.

Bellingham, K. (2015). Comprehensive Stevens HydraProbe Uses Manual. Stevens Water Monitoring Systems Inc. Portland, Oregon, United States.

Bellot, J., Bonet, A., Sanchez, J. R., & Chirino, E. (2001). Likely effects of land use changes on the runoff and aquifer recharge in a semiarid landscape using a hydrological model. *Landscape and Urban Planning*, *55*(1), 41-53.

Berthold, S., Bentley, L. R., & Hayashi, M. (2004). Integrated hydrogeological and geophysical study of depression-focused groundwater recharge in the Canadian prairies. *Water Resources Research*, *40*(6).

Bishop, J. M., Callaghan, M. V., Cey, E. E., & Bentley, L. R. (2015). Measurement and simulation of subsurface tracer migration to tile drains in low permeability, macroporous soil. *Water Resources Research*, *51*(6), 3956-3981.

Bjornlund, H., Nicol, L., & Klein, K. K. (2009). The adoption of improved irrigation technology and management practices—A study of two irrigation districts in Alberta, Canada. *Agricultural water management*, *96*(1), 121-131.

Bjornlund, H., Xu, W., & Wheeler, S. (2014). An overview of water sharing and participation issues for irrigators and their communities in Alberta: Implications for water policy. *Agricultural Water Management, 145*, 171-180.

Böhlke, J. K. (2002). Groundwater recharge and agricultural contamination. *Hydrogeology Journal*, *10*(1), 153-179.

Bouwer, H., & Rice, R. C. (1976). A slug test for determining hydraulic conductivity of unconfined aquifers with completely or partially penetrating wells. *Water Resources Research*, *12*(3), 423-428.

Canola Council of Canada (CCC). (2017). Canola Encyclopedia, Crop Development, Growth Stages. Online document access January 2019. URL https://www.canolacouncil.org/canola-encyclopedia/crop-development/growth-stages/#roots

Chang, C., & Entz, T. (1996). Nitrate leaching losses under repeated cattle feedlot manure applications in southern Alberta. *Journal of Environmental Quality*, *25*(1), 145-153.

Charuchittipan, D., Babel, W., Mauder, M., Leps, J. P., & Foken, T. (2014). Extension of the averaging time in eddy-covariance measurements and its effect on the energy balance closure. *Boundary-layer Meteorology*, *152*(3), 303-327.

Cheng, D., Wang, Y., Duan, J., Chen, X., and S. Yang. (2015). A new analytical expression for ultimate specific yield and shallow groundwater drainage. *Hydrological Processes. 29.* 1905-1911.

Chiew, F. H. S., & McMahon, T. A. (1991). Groundwater recharge from rainfall and irrigation in the Campaspe River Basin. *Soil Research*, *29*(5), 651-670.

Canadian Climate Normals 1981-2010 Station Data. Accessed January 2019. URL http://climate.weather.gc.ca/climate_normals/index_e.html

Cook, P. G., Jolly, I. D., Leaney, F. W., Walker, G. R., Allan, G. L., Fifield, L. K., & Allison, G. B. (1994). Unsaturated zone tritium and chlorine 36 profiles from southern Australia: Their use as tracers of soil water movement. *Water Resources Research*, *30*(6), 1709-1719.

Cook, P. G., Walker, G. R., & Jolly, I. D. (1989). Spatial variability of groundwater recharge in a semiarid region. *Journal of Hydrology*, *111*(1-4), 195-212.

Davisson, M. L., & Criss, R. E. (1995). Stable isotope and groundwater flow dynamics of agricultural irrigation recharge into groundwater resources of the Central Valley, California. International Symposium on Isotopes in Water Resources Management. Lawrence Livermore National Lab., CA (United States).

Duffield, G. M. (2007). *AQTESOLV for Windows Version 4.5 User's Guide*, HydroSOLVE, Inc., Reston, VA.

Eisenlohr Jr, W. S. (1972). Hydrologic investigations of prairie potholes in North Dakota, 1959-68. Geological Survey Professional Paper No. 585-A. United States Government Printing Office, Washington, USA.

Enfield, C. G., Hsieh, J. J. C., & Warrick, A. W. (1973). Evaluation of Water Flux Above A Deep Water Table Using Thermocouple Psychrometers 1. *Soil Science Society of America Journal*, *37*(6), 968-970.

Exner, M. E., Hirsh, A. J., & Spalding, R. F. (2014). Nebraska's groundwater legacy: Nitrate contamination beneath irrigated cropland. *Water Resources Research*, *50*(5), 4474-4489.

Feddes, R. A., Kowalik, P. J., & Zaradny, H. (1978). *Simulation of Field Water Use and Crop Yield.* John Wiley & Sons, New York, NY.

Fenton, M., Schreiner, B., Nielson, E., & Pawlowicz, J. (1994). Quaternary Geology of the Western Plains. In G.D. Mossop and I. Shetsen (comp). Geological Atlas of the Western Canada Sedimentary Basin. Canadian Society of Petroleum Geologists and Alberta Research Council. URL https://ags.aer.ca/publications/chapter-26-quaternary-geology-of-the-western-plains

Fenton, M. M., Waters, E.J., Pawley, S.M., Atkinson, N., Utting, D.J. & Mckay, K. (2013). Surficial geology of Alberta. Alberta Energy Regulator, AER/AGS Map 601.URL https://ags.aer.ca/document/MAP/MAP_601.pdf

Fitters, T. F., Mooney, S. J., & Sparkes, D. L. (2018). Sugar beet root growth under different watering regimes: A minirhizotron study. *Environmental and Experimental Botany*, *155*, 79-86.

Flury, M., Flühler, H., Jury, W. A., & Leuenberger, J. (1994). Susceptibility of soils to preferential flow of water: A field study. *Water Resources Research*, *30*(7), 1945-1954.

Foken, T. (2008). The energy balance closure problem: an overview. *Ecological Applications*, *18*(6), 1351-1367.

Foster, S. S. D., Morris, B. L., & Lawrence, A. R. (1994). Effects of urbanization on groundwater recharge. In *Groundwater problems in urban areas: Proceedings of the International Conference organized by the Institution of Civil Engineers and held in London, 2–3 June 1993* (pp. 43-63). Thomas Telford Publishing.

Freeze, R. A., & Banner, J. (1970). The mechanism of natural ground-water recharge and discharge: 2. Laboratory column experiments and field measurements. *Water Resources Research*, *6*(1), 138-155.

Gaye, C. B., & Edmunds, W. M. (1996). Groundwater recharge estimation using chloride, stable isotopes and tritium profiles in the sands of northwestern Senegal. *Environmental Geology*, *27*(3), 246-251.

Gee, G. W., & Hillel, D. (1988). Groundwater recharge in arid regions: review and critique of estimation methods. *Hydrological Processes*, *2*(3), 255-266.

Gee, G. W., Wierenga, P. J., Andraski, B. J., Young, M. H., Fayer, M. J., & Rockhold, M. L. (1994). Variations in water balance and recharge potential at three western desert sites. *Soil Science Society of America Journal*, *58*(1), 63-72.

Gerke, H. H., & Genuchten, M. V. (1993). A dual-porosity model for simulating the preferential movement of water and solutes in structured porous media. *Water Resources Research*, *29*(2), 305-319.

Government of Alberta. (2018). Population Projection, Alberta and Census Divisions, 2018-2046. Treasury Board and Finance, Office of Statistics and Information – Demography.

Government of Canada. (2017). Adjusted and homogenized Canadian climate data. Accessed September 2018. URL https://www.canada.ca/en/environment-climate-change/services/climate-change/science-research-data/climate-trends-variability/adjusted-homogenized-canadian-data.html

Government of Canada. (2018). Monitoring of Atmospheric Precipitation Chemistry, Major Ions. Environment and Climate Change Canada Data. Accessed September 2018. URL http://data.ec.gc.ca/data/air/monitor/monitoring-of-atmospheric-precipitation-chemistry/major-ions/?lang=en

Granger, R. J., Gray, D. M., & Dyck, G. E. (1984). Snowmelt infiltration to frozen prairie soils. *Canadian Journal of Earth Sciences*, *21*(6), 669-677.

Hayashi, M., & Farrow, C. R. (2014). Watershed-scale response of groundwater recharge to inter-annual and inter-decadal variability in precipitation (Alberta, Canada). *Hydrogeology Journal*, *22*(8), 1825-1839.

Hayashi, M., Jackson, J. F., & Xu, L. (2010). Application of the Versatile Soil Moisture Budget model to estimate evaporation from prairie grassland. *Canadian Water Resources Journal*, *35*(2), 187-208.

Hayashi, M., Mohammed, G. A., Harrer, K., & Farrow, C. R. (2012). Performance evaluation and improvement of the Versatile Soil Moisture Budget (VSMB) model. *University of Calgary, Calgary, AB*.

Hayashi, M., & van der Kamp, G. (2000). Simple equations to represent the volume–area–depth relations of shallow wetlands in small topographic depressions. *Journal of Hydrology*, *237*(1-2), 74-85.

Hayashi, M., van der Kamp, G., & Rosenberry, D. O. (2016). Hydrology of prairie wetlands: understanding the integrated surface-water and groundwater processes. *Wetlands*, *36*(2), 237-254.

Hayashi, M., van der Kamp, G., & Schmidt, R. (2003). Focused infiltration of snowmelt water in partially frozen soil under small depressions. *Journal of Hydrology*, *270*(3-4), 214-229.

Healy, R. W., & Cook, P. G. (2002). Using groundwater levels to estimate recharge. *Hydrogeology journal*, *10*(1), 91-109.

Hendry, M. J. (1982). Hydraulic Conductivity of a Glacial Till in Alberta a. *Groundwater*, *20*(2), 162-169.

Hendry, M. J., Cherry, J. A., & Wallick, E. I. (1986). Origin and distribution of sulfate in a fractured till in southern Alberta, Canada. *Water Resources Research*, *22*(1), 45-61.

Hibbs, B. J., & Sharp Jr, J. M. (2012). Hydrogeological impacts of urbanization. *Environmental & Engineering Geoscience*, *18*(1), 3-24.

Hobbs, E. H., & Krogman, K. K. (1971). Overwinter precipitation storage in irrigated and non-irrigated Chin loam soil. *Canadian Journal of Soil Science*, *51*(1), 13-18.

Huang, T., & Pang, Z. (2011). Estimating groundwater recharge following land-use change using chloride mass balance of soil profiles: a case study at Guyuan and Xifeng in the Loess Plateau of China. *Hydrogeology Journal*, *19*(1), 177-186.

International Panel on Climate Change (IPCC). (2014). *Climate Change 2014: Synthesis Report. Contribution of Working Groups I, II and III to the Fifth Assessment Report of the Intergovernmental Panel on Climate Change* [Core Writing Team, R.K. Pachauri and L.A. Meyer (eds.)]. IPCC, Geneva, Switzerland, 151 pp.

Jasechko, S., Birks, S. J., Gleeson, T., Wada, Y., Fawcett, P. J., Sharp, Z. D., ... & Welker, J. M. (2014). The pronounced seasonality of global groundwater recharge. *Water Resources Research*, *50*(11), 8845-8867.

Jiang, R., Gan, T. Y., Xie, J., Wang, N., & Kuo, C. C. (2017). Historical and potential changes of precipitation and temperature of Alberta subjected to climate change impact: 1900–2100. *Theoretical and applied climatology*, *127*(3-4), 725-739.

Jiang, S., Pang, L., Buchan, G. D., Šimůnek, J., Noonan, M. J., & Close, M. E. (2010). Modeling water flow and bacterial transport in undisturbed lysimeters under irrigations of dairy shed effluent and water using HYDRUS-1D. *Water Research*, *44*(4), 1050-1061.

Jiménez-Martínez, J., Skaggs, T. H., Van Genuchten, M. T., & Candela, L. (2009). A root zone modelling approach to estimating groundwater recharge from irrigated areas. *Journal of Hydrology*, *367*(1-2), 138-149.

Johnson, A. I. (1967). Specific yield: compilation of specific yields for various materials.US Geological Survey Water-Supply Paper 1662-D, 74 pp.

Jones, T. L., & Skaggs, R. L. (1987). Influence of hydrologic factors on leaching of solidified low-level waste forms at an arid site field-scale lysimeter facility, PNL-SA- 14908, *Proceedings* of *the 4fh International Hazardous Waste Symposium on Environmental Aspects of Stabilization/Solidification* of *Hazardous and Radioactive Wastes,* American Society of Testing Materials, Philadelphia, Pennsylvania

Kendy, E., Gérard-Marchant, P., Todd Walter, M., Zhang, Y., Liu, C., & Steenhuis, T. S. (2003). A soil-water-balance approach to quantify groundwater recharge from irrigated cropland in the north China plain. *Hydrological Processes*, *17*(10), 2011-2031.

Kengni, L., Vachaud, G., Thony, J. L., Laty, R., Garino, B., Casabianca, H., ... & Viscogliosi, R. (1994). Field measurements of water and nitrogen losses under irrigated maize. *Journal of Hydrology*, *162*(1-2), 23-46.

Kitching, R., Shearer, T.R. (1982). Construction and operation of a large undisturbed lysimeter to measure recharge to the chalk aquifer, England. *Journal of Hydrology*, 56:267–277

Kitching, R., Shearer, T,R., Shedlock, S.L., (1977). Recharge to Bunter Sandstone determined from lysimeters. *Journal of Hydrology*, 33:217–232

Klute, A. (1986). Water retention: laboratory methods. In. A. Klute (Ed.), *Methods of soil analysis: part 1—physical and mineralogical methods* (pp. 635-662).Madison, Wisconsin, USA: Soil Science Society of America, Inc.

Kocaoglu, S.S., & Pettapiece, W.W. (1980). Soils of the Lethbridge area (82 H NE). Alberta Institute of Pedology Map No. M-80-3. Agriculture Canada.

Kochendorfer, J., Rasmussen, R., Wolff, M., Baker, B., Hall, M. E., Meyers, T., ... & Leeper, R. (2017). The quantification and correction of wind-induced precipitation measurement errors. *Hydrology and Earth System Sciences*, *21*(4), 1973-1989.

Koehler, G., Wassenaar, L. I., & Hendry, M. J. (2000). An automated technique for measuring δD and δ18O values of porewater by direct CO2 and H2 equilibration. *Analytical Chemistry*, *72*(22), 5659-5664.

Koeniger, P., Gaj, M., Beyer, M., & Himmelsbach, T. (2016). Review on soil water isotope-based groundwater recharge estimations. *Hydrological Processes*, *30*(16), 2817-2834.

Kyte, E. (2018). *Evaluation of nitrate in groundwater under long-term manure application* (Master's thesis, Science). Department of Geoscience, University of Calgary.

LeBlanc, F. (2017). *Laboratory Investigation of Infiltration Processes in Frozen Soil and the Influence of Antecedent Moisture Content and Macroporosity*. (Master's thesis, Science). Department of Geoscience, University of Calgary.

Lemay, T. G. & Guha, S. (2009): Compilation of Alberta groundwater information from existing maps and data sources; Energy Resources Conservation Board, ERCB/AGS Open File Report 2009-02, 43 p.

Lerner, D. N. (1990). Groundwater recharge in urban areas. *Atmospheric Environment. Part B. Urban Atmosphere*, *24*(1), 29-33.

Lerner, D. N., & Harris, B. (2009). The relationship between land use and groundwater resources and quality. *Land Use Policy*, *26*, S265-S273.

Li, Y., Šimůnek, J., Jing, L., Zhang, Z., & Ni, L. (2014). Evaluation of water movement and water losses in a direct-seeded-rice field experiment using Hydrus-1D. *Agricultural Water Management*, *142*, 38-46.

Lissey, A. (1968). Surficial mapping of groundwater flow systems with the application to the Oak River Basin, Manitoba. (Doctoral dissertation, University of Saskatchewan).

Lissey, A. (1971). Depression-focused transient groundwater flow patterns in Manitoba. *Geological Association of Canada Special Paper*, *9*, 333-341.

Lu, X., Jin, M., van Genuchten, M.T., & Wang, B. (2011). Groundwater recharge at five representative sites in the Hebei Plain, China. *Groundwater*, *49*(2), 286-294.

MacCormack, K. E., Atkinson, N., Lyster, S. (2015). Sediment thickness of Alberta. Alberta Energy Regulator, AER/AGS Map 603. URL https://ags.aer.ca/document/MAP/MAP_603.pdf

MacDonald, G. M. (1989). Postglacial palaeoecology of the subalpine forest—grassland ecotone of southwestern Alberta: New insights on vegetation and climate change in the Canadian Rocky Mountains and adjacent foothills. *Palaeogeography, Palaeoclimatology, Palaeoecology*, *73*(3-4), 155-173.

MacMillan, R. A. & Pettapiece, W. W. (2000). Alberta Landforms: Quantitative morphometric descriptions and classification of typical Alberta landforms. Technical Bulletin No. 2000-2E. Research Branch, Agriculture and Agri-Food Canada, Semiarid Prairie Agricultural Research Centre, Swift Current, SK. 118 pp.

Maréchal, J. C., Dewandel, B., Ahmed, S., Galeazzi, L., & Zaidi, F. K. (2006). Combined estimation of specific yield and natural recharge in a semi-arid groundwater basin with irrigated agriculture. *Journal of Hydrology*, *329*(1-2), 281-293.

McMahon, P. B., Dennehy, K. F., Michel, R. L., Sophocleous, M. A., Ellett, K. M., & Hurlbut, D. B. (2003). Water Movement Through Thick Unsaturated Zones Overlying the Central High Plains Aquifer, Southwestern Kansas. Water-Resources Investigations Report No. 3-4171. US Dept. of the Interior, US Geological Survey

Maulé, C. P., Chanasyk, D. S., & Muehlenbachs, K. (1994). Isotopic determination of snow-water contribution to soil water and groundwater. *Journal of Hydrology*, *155*(1-2), 73-91.

Miller, J. J., Foroud, N., Hill, B. D., & Lindwall, C. W. (1995). Herbicides in surface runoff and groundwater under surface irrigation in southern Alberta. *Canadian Journal of Soil Science*, *75*(1), 145-148.

Mitchell, P., & Prepas, E. E. (Eds.). (1990). Atlas of Alberta lakes. University of Alberta. Accessed online at http://albertalakes.ualberta.ca/?page=lake&region=4&lake=122 on March 22, 2019.

Mohammed, A. A., Pavlovskii, I., Cey, E. E., & Hayashi, M. (2019). Effects of preferential flow on snowmelt partitioning and groundwater recharge in frozen soils. *Hydrology and Earth System Science.* Discussion., https://doi.org/10.5194/hess-2019-169, in review.

Motha, R. P., & Baier, W. (2005). Impacts of present and future climate change and climate variability on agriculture in the temperate regions: North America. *Climatic Change*, *70*(1-2), 137-164.

Mualem, Y. (1976). A new model for predicting the hydraulic conductivity of unsaturated porous media. *Water Resources Research*, *12*(3), 513-522.

Muenchrath, A. (2018). Laboratory investigation on the performance of three soil moisture sensors in six soils. Unpublished manuscript, Department of Geoscience, University of Calgary, Calgary, Canada.

Musick, J. T. (1970). Effect of antecedent soil water on pre-season rainfall storage in a slowly permeable irrigated soil. *Journal of Soil and Water Conservation*, *25*, 99-101.

Nash, J. E., & Sutcliffe, J. V. (1970). River flow forecasting through conceptual models part I—A discussion of principles. *Journal of Hydrology*, *10*(3), 282-290.

Nkemdirim, L. C. (1996). Canada's chinook belt. *International Journal of Climatology*, *16*(4), 441-462.

Noorduijn, S. L., Hayashi, M., Mohammed, G. A., & Mohammed, A. A. (2018). A Coupled Soil Water Balance Model for Simulating Depression-Focused Groundwater Recharge. *Vadose Zone Journal*, *17*(1).

Oncley, S. P., Foken, T., Vogt, R., Kohsiek, W., DeBruin, H. A. R., Bernhofer, C., ... & Lehner, I. (2007). The energy balance experiment EBEX-2000. Part I: overview and energy balance. *Boundary-Layer Meteorology*, *123*(1), 1-28.

Pavlovskii I., Hayashi, M., & Cey, E. (2019). Estimation of depression-focussed groundwater recharge using chloride mass balance: problems and solutions across scales. *Hydrogeology Journal* - In Press

Pavlovskii, I., Hayashi, M., & Itenfisu, D. (2019). Midwinter melts in the Canadian prairies: energy balance and hydrological effects. *Hydrology and Earth System Sciences*, *23*(4), 1867-1883.

Pavlovskii, I., Hayashi, M., & Lennon, M. R. (2018). Transformation of snow isotopic signature along groundwater recharge pathways in the Canadian Prairies. *Journal of Hydrology*, *563*, 1147-1160.

Planet Team (2017). Planet Application Program Interface: In Space for Life on Earth. San Francisco, CA. https://api.planet.com.

Powell, R. M., & Puls, R. W. (1993). Passive sampling of groundwater monitoring wells without purging: multilevel well chemistry and tracer disappearance. *Journal of Contaminant Hydrology*, *12*(1-2), 51-77.

Prior, G. J., Hathway, B., Glombick, P.M., Pana, D.I., Banks, C.J., Hay, D.C., Schneider, C.L., Grobe, M., Elgr, R. and Weiss, J.A. (2013). Bedrock geology of Alberta. Alberta Energy Regulator, AER/AGS Map 600. URL https://ags.aer.ca/document/MAP/MAP_600.pdf

Qin, D., Qian, Y., Han, L., Wang, Z., Li, C., & Zhao, Z. (2011). Assessing impact of irrigation water on groundwater recharge and quality in arid environment using CFCs, tritium and stable isotopes, in the Zhangye Basin, Northwest China. *Journal of Hydrology*, *405*(1-2), 194-208.

Rehm, B. W., Moran, S. R., & Groenewold, G. H. (1982). Natural groundwater recharge in an upland area of central North Dakota, USA. *Journal of Hydrology*, 59(3-4), 293-314.

Rhoades JD. (1982). Soluble salts. In. A. Klute (Ed.), *Methods of soil analysis: part 2.* (pp. 167-179). Madison, Wisconsin, USA: Soil Science Society of America, Inc.

Rodvang, J. (2002*).* Groundwater at the CACDI Demonstration Farm. Irrigation Branch, Alberta Agriculture, Food and Rural Development. Lethbridge, Alberta.

Rodvang, S. J., Mikalson, D. M., & Ryan, M. C. (2004). Changes in ground water quality in an irrigated area of southern Alberta. *Journal of Environmental Quality*, *33*(2), 476-487.

Rushton, K. R., & Ward, C. (1979). The estimation of groundwater recharge. *Journal of Hydrology*, *41*(3-4), 345-361.

Sauchyn, D. J., St-Jacques, J. M., Barrow, E., Nemeth, M. W., MacDonald, R. J., Sheer, A. M. S., & Sheer, D. P. (2016). Adaptive water resource planning in the South Saskatchewan River Basin: use of scenarios of hydroclimatic variability and extremes. *JAWRA Journal of the American Water Resources Association*, *52*(1), 222-240.

Sauder, P. M. (1949, November). The St. Mary and Milk Rivers Irrigation Development. *Canadian Cattleman*, URL https://www.canadiancattlemen.ca/2015/10/15/history-the-st-mary-and-milk-rivers-irrigation-development/

Scanlon, B. R. (1991). Evaluation of moisture flux from chloride data in desert soils. *Journal of Hydrology*, *128*(1-4), 137-156.

Scanlon, B. R. (2000). Uncertainties in estimating water fluxes and residence times using environmental tracers in an arid unsaturated zone. *Water Resources Research*, *36*(2), 395-409.

Scanlon, B. R., & Goldsmith, R. S. (1997). Field study of spatial variability in unsaturated flow beneath and adjacent to playas. *Water Resources Research*, *33*(10), 2239-2252.

Scanlon, B. R., Healy, R. W., & Cook, P. G. (2002). Choosing appropriate techniques for quantifying groundwater recharge. *Hydrogeology Journal*, *10*(1), 18-39.

Scanlon, B. R., Keese, K. E., Flint, A. L., Flint, L. E., Gaye, C. B., Edmunds, W. M., & Simmers, I. (2006). Global synthesis of groundwater recharge in semiarid and arid regions. *Hydrological Processes: An International Journal*, *20*(15), 3335-3370.

Scanlon, B. R., Reedy, R. C., Stonestrom, D. A., Prudic, D. E., & Dennehy, K. F. (2005). Impact of land use and land cover change on groundwater recharge and quality in the southwestern US. *Global Change Biology*, *11*(10), 1577-1593.

Seyfried, M. S., Grant, L. E., Du, E., & Humes, K. (2005). Dielectric loss and calibration of the Hydra Probe soil water sensor. *Vadose Zone Journal*, *4*(4), 1070-1079.

Shah, N., & Ross, M. (2009). Variability in specific yield under shallow water table conditions. *Journal of Hydrologic Engineering*, *14*(12), 1290-1298.

Sharp, J. M. (2010). The impacts of urbanization on groundwater systems and recharge. *Aqua Mundi*, *1*(3).

Shetsen, I. (1987). Quaternary geology, southern Alberta. Alberta Research Council, ARC/AGS Map 207. URL https://ags.aer.ca/document/MAP/Map_207.pdf

Shetsen, I. (2005). Surficial geology of Lethbridge, Alberta, NTS 82H and NTS 82I. Alberta Energy Regulator, AER/AGS Map 206. URL https://ags.aer.ca/document/MAP/Map_206.pdf

Shjeflo, J. B. (1968). Evapotranspiration and the water budget of prairie potholes in North Dakota. U.S. Geological Survey, Professional Paper. 585-B, 49 pp.

Šimůnek, J., Huang, K., & Van Genuchten, M. T. (1998). The HYDRUS code for simulating the one-dimensional movement of water, heat, and multiple solutes in variably-saturated media. *US Salinity Laboratory Research Report*, *144*.

Šimůnek, J., Jarvis, N. J., Van Genuchten, M. T., & Gärdenäs, A. (2003). Review and comparison of models for describing non-equilibrium and preferential flow and transport in the vadose zone. *Journal of Hydrology*, *272*(1-4), 14-35.

Šimůnek, J., Šejna, M., Saito, H., Sakai, M., & van Genuchten, M. T. (2013). The HYDRUS-1D Software Package for Simulating the Movement of Water, Heat, and Multiple Solutes in Variably Saturated Media, Version 4.17, *HYDRUS Software Series 3*, Department of Environmental Sciences, University of California Riverside, Riverside, California, USA, pp. 343.

Soil Classification Working Group. (1998). *The Canadian System of Soil Classification*, 3rd ed. Agriculture and Agri-Food Canada Publication 1646, 187 pp.

Sophocleous, M. (2000). The origin and evolution of safe-yield policies in the Kansas Groundwater Management Districts. *Natural Resources Research*, *9*(2), 99-110.

St. Mary's Irrigation District (SMID). Annual irrigation reports. Accessed September 2018. URL https://www.smrid.com/information/#1479789524501-8a61dc52-acf3

Statistics Canada. (2011). Environment Accounts and Statistics Division, Agricultural Water Survey (survey number 5145). Accessed May 2019. URL https://www150.statcan.gc.ca/n1/pub/16-402-x/2011001/ct002-eng.htm

Statistics Canada. Table 32-10-0038-01. Fertilizer shipments to Canada agriculture and export markets, by product type and fertilizer year, cumulative data (x 1000). Accessed September 2018. URL https://www150.statcan.gc.ca/t1/tbl1/en/tv.action?pid=3210003801&pickMembers%5B0%5D=1.9

Statistics Canada. Table 32-10-0406-01. Land use. Accessed September 2018. URL https://www150.statcan.gc.ca/t1/tbl1/en/tv.action?pid=3210040601

Statistics Canada. Table 38-10-0241-01. Total area that received irrigation by crop type. Accessed August 2018. URL https://www150.statcan.gc.ca/t1/tbl1/en/tv.action?pid=3810024101

Stephens, D. B., & Knowlton Jr, R. (1986). Soil water movement and recharge through sand at a semiarid site in New Mexico. *Water Resources Research*, *22*(6), 881-889.

Summers, P. W., & Hitchon, B. (1973). Source and budget of sulfate in precipitation from central Alberta, Canada. *Journal of the Air Pollution Control Association*, *23*(3), 194-199.

Tomomi, Y. (2000). Non-uniqueness of history matching. In *SPE Asia Pacific Conference on Integrated Modelling for Asset Management*. Society of Petroleum Engineers.

Topp, G. C., Davis, J. L., & Annan, A. P. (1980). Electromagnetic determination of soil water content: Measurements in coaxial transmission lines. *Water Resources Research*, *16*(3), 574-582.

Twine, T. E., Kustas, W. P., Norman, J. M., Cook, D. R., Houser, P., Meyers, T. P., ... & Wesely, M. L. (2000). Correcting eddy-covariance flux underestimates over a grassland. *Agricultural and Forest Meteorology*, *103*(3), 279-300.

van der Kamp, G., & Hayashi, M. (1998). The groundwater recharge function of small wetlands in the semi-arid northern prairies. Great Plains Research, 39-56.

van der Valk, A. G. (2005). The prairie potholes of North America. In L. Fraser & P. Keddy (Eds). The World's Largest Wetlands: Ecology and Conservation (pp.393-423). Cambridge University, United Kingdom. Cambridge University Press.

van Dijk, T. (2005). Depression-focused recharge and the impacts of land use on the hydrology of small depressions in Calgary, Alberta, MSc Thesis, University of Calgary, AB, Canada, 158 pp

van Genuchten, M.T. (1980). A closed-form equation for predicting the hydraulic conductivity of unsaturated soils 1. *Soil Science Society of America Journal*, *44*(5), 892-898.

Varni, M., Comas, R., Weinzettel, P., & Dietrich, S. (2013). Application of the water table fluctuation method to characterize groundwater recharge in the Pampa plain, Argentina. *Hydrological Sciences Journal*, *58*(7), 1445-1455.

Wang, B., Jin, M., Nimmo, J. R., Yang, L., & Wang, W. (2008). Estimating groundwater recharge in Hebei Plain, China under varying land use practices using tritium and bromide tracers. *Journal of Hydrology*, *356*(1-2), 209-222.

Watanabe, K., & Kugisaki, Y. (2017). Effect of macropores on soil freezing and thawing with infiltration. *Hydrological Processes*, *31*(2), 270-278.

Webb, E. K., Pearman, G. I., & Leuning, R. (1980). Correction of flux measurements for density effects due to heat and water vapour transfer. *Quarterly Journal of the Royal Meteorological Society*, *106*(447), 85-100.

Wentworth, C. K. (1922). A scale of grade and class terms for clastic sediments. *The Journal of Geology*, *30*(5), 377-392.

Wight, J. R., & Black, A. L. (1978). Soil water use and recharge in a fertilized mixed prairie plant community. *Journal of Range Management*, 280-282.

Wilczak, J. M., Oncley, S. P., & Stage, S. A. (2001). Sonic anemometer tilt correction algorithms. *Boundary-Layer Meteorology*, *99*(1), 127-150.

Willis, T. M., & Black, A. S. (1996). Irrigation increases groundwater recharge in the Macquarie Valley. *Soil Research*, *34*(6), 837-847.

Wilson, K., Goldstein, A., Falge, E., Aubinet, M., Baldocchi, D., Berbigier, P., ... & Grelle, A. (2002). Energy balance closure at FLUXNET sites. *Agricultural and Forest Meteorology*, *113*(1-4), 223-243.

Winter, T. C. (1989). Hydrologic studies of wetlands in the northern prairies. In: van der Valk A (ed) Northern prairie wetlands. Iowa State University Press, Iowa City, IA, pp 17–54

Young, M. H., Wierenga, P. J., & Mancino, C. F. (1996). Large weighing lysimeters for water use and deep percolation studies. *Soil Science*, *161*(8), 491-501.

Zebarth, B. J., De Jong, E., & Henry, J. L. (1989a). Water flow in a hummocky landscape in central Saskatchewan, Canada, II. Saturated flow and groundwater recharge. *Journal of Hydrology*, *110*(1-2), 181-198.

Zebarth, B. J., & De Jong, E. (1989). Water flow in a hummocky landscape in central Saskatchewan, Canada, III. Unsaturated flow in relation to topography and land use. *Journal of Hydrology*, *110*(1-2), 199-218.

Zhou, Y. (2009). A critical review of groundwater budget myth, safe yield and sustainability. *Journal of Hydrology*, *370*(1-4), 207-213.

APPENDIX A: IRRIGATION WATER SAMPLING RESULTS

Water samples were taken from open irrigation canals at several locations between the PP and LDF sites on June 13, 2018. The irrigation water sample taken at the LDF site was from a pipe source rather than an open canal. Sampling locations are shown in Figure A-1a. The stable isotope (^{2}H and ^{18}O) and chloride concentration results of each sample are shown in Figure A-1b and c. Results indicate a trend towards a more positive isotope signature moving from the LDF to the PP site, with a shift of +1.0 ‰ for $\delta^{18}O$ and +4.6 ‰ for $\delta^{2}H$. This shift is likely related to the residence time of water within the open canals in the distribution system. The entire network of canals and pipelines shown in Figure A-1a are all sourced from the Milk River Ridge Reservoir, located approximately 35 km to the south west of Lethbridge. Water flowing through the canals and stored in subsequent reservoirs is subject to evaporation, which will result in a more positive isotope signature for water with longer residence times. The spatial variability in isotopic composition throughout the SMRID was not thoroughly investigated in this study primarily because the shift in values between the LDF and PP sites were small compared to seasonal shifts in isotopic composition of precipitation.

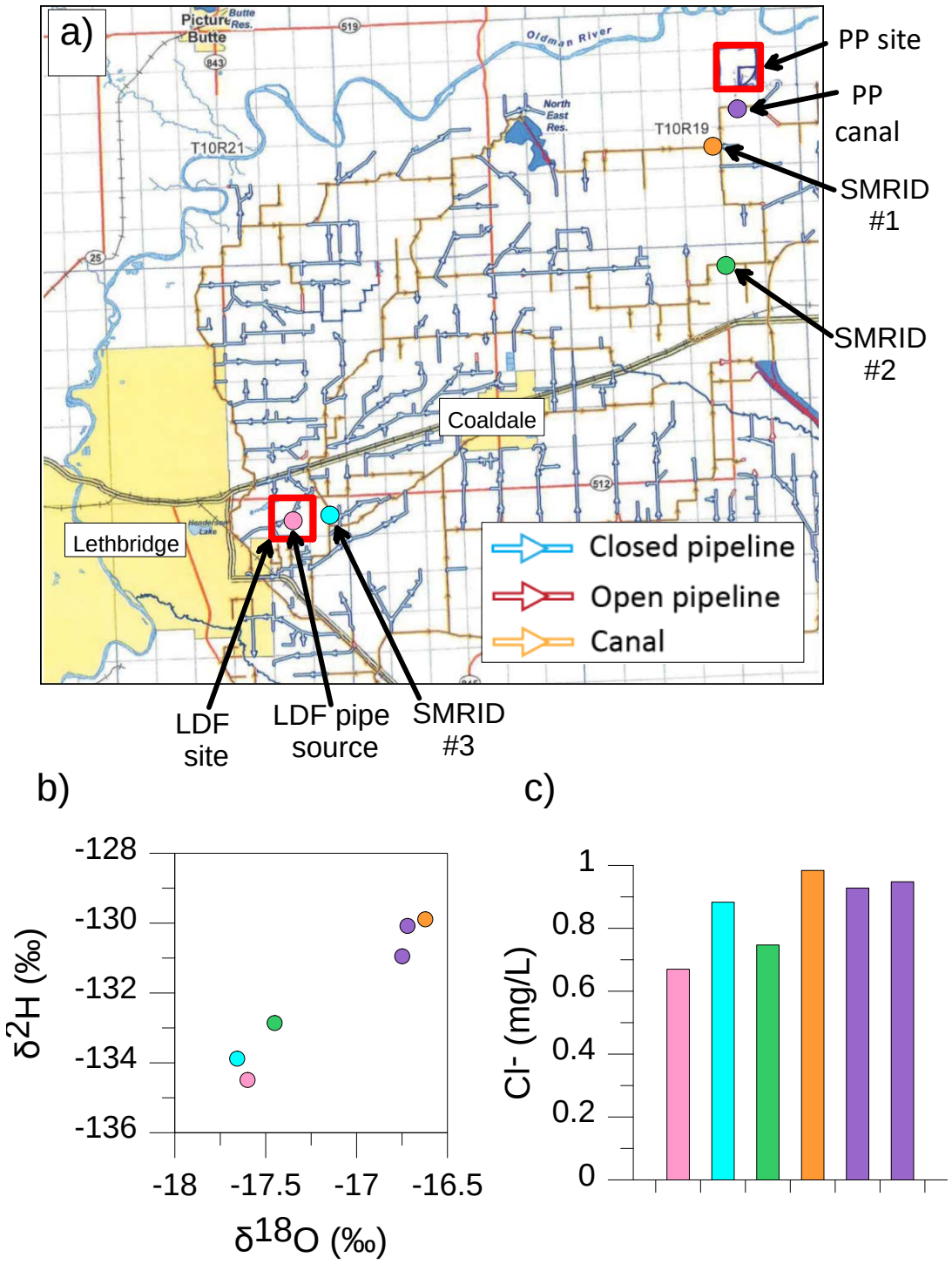

Figure A-1. Irrigation water sample locations (a) collected on June 13, 2018. Stable isotope analysis (b) and chloride concentration (c) are also shown. Colour of sampling point in (a) corresponds to measurements in (b) and (c).

APPENDIX B: BOREHOLE LITHOLOGS

Eight boreholes were drilled at the LDF site in May 2017. Each borehole/well is named after the sub-site where it was drilled and designated as 1, 2 or 3 from shallowest to deepest, respectively. The three deepest boreholes (L_IrrDp-2, L_IrrFl-3 and L_DryFl-3) were drilled using a truck-mounted hollow-stem auger system, sampled at discrete locations and logged. The remaining five wells (L_IrrDp-1, L_IrrFl-1, L_IrrFl-2, L_DryFl-1, L_DryFl-2) were drilled using a truck-mounted solid stem auger system and were not sampled or logged due to proximity (i.e., less than 1 m) to the deep, logged borehole at the given sub-site. Figure B-1 shows the lithologs for each of the three sampled boreholes as well as the screened intervals and depths of each well completed at the LDF site. The deep boreholes were sampled every 0.30 m (1 ft) for the first 1.52 m (5 ft), and then every 0.61 m (2 ft) below that.

Four boreholes were drilled and sampled at the PP site in October 2017 using a truck mounted hollow-stem auger system. Cores were sampled using the same depth intervals as for the LDF boreholes described above. Lithologs are shown in Figure B-2.

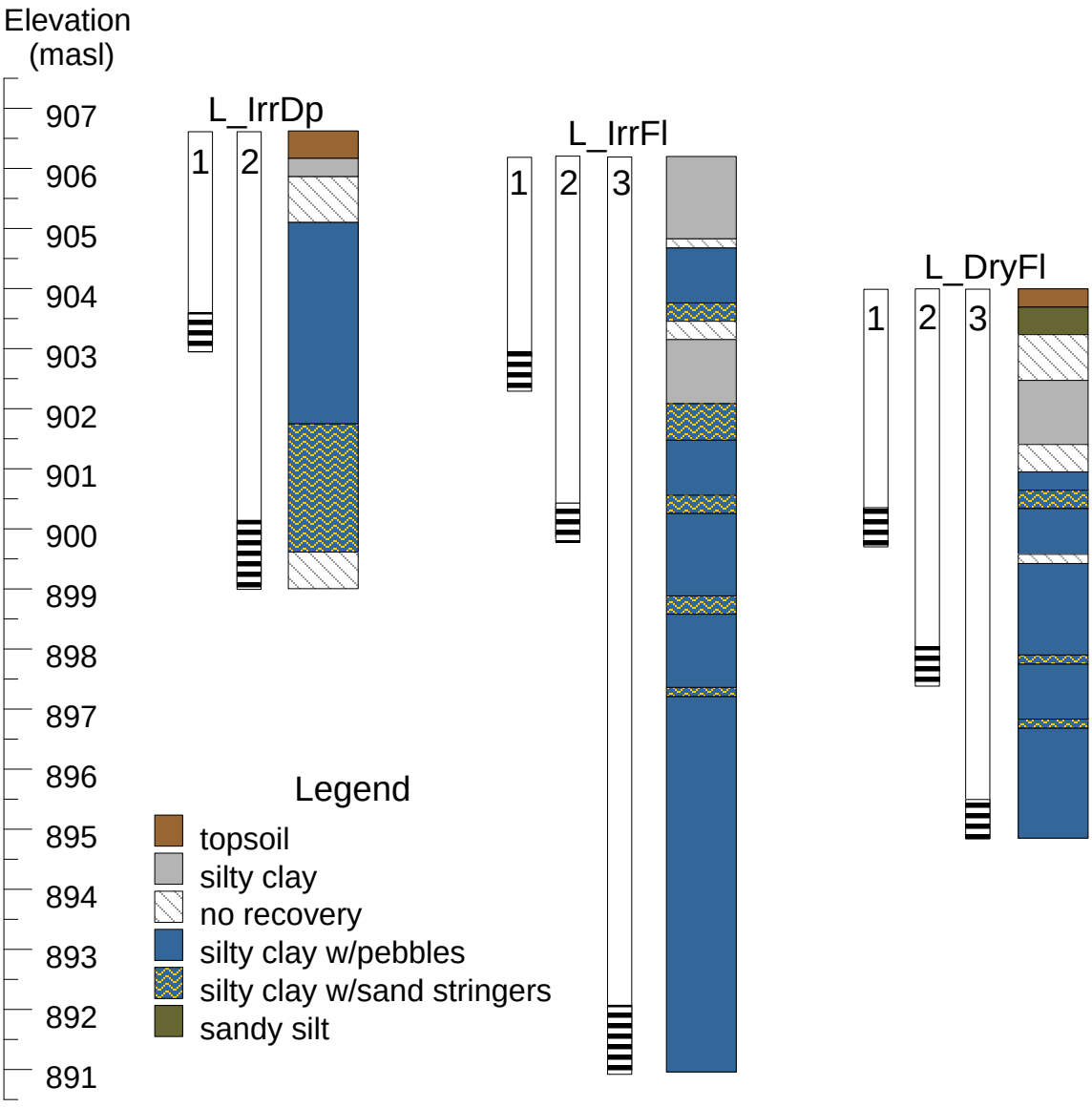

Figure B-1. Schematic of the lithology and well completion details at the LDF site. Horizontal distance between boreholes/wells is not to scale.

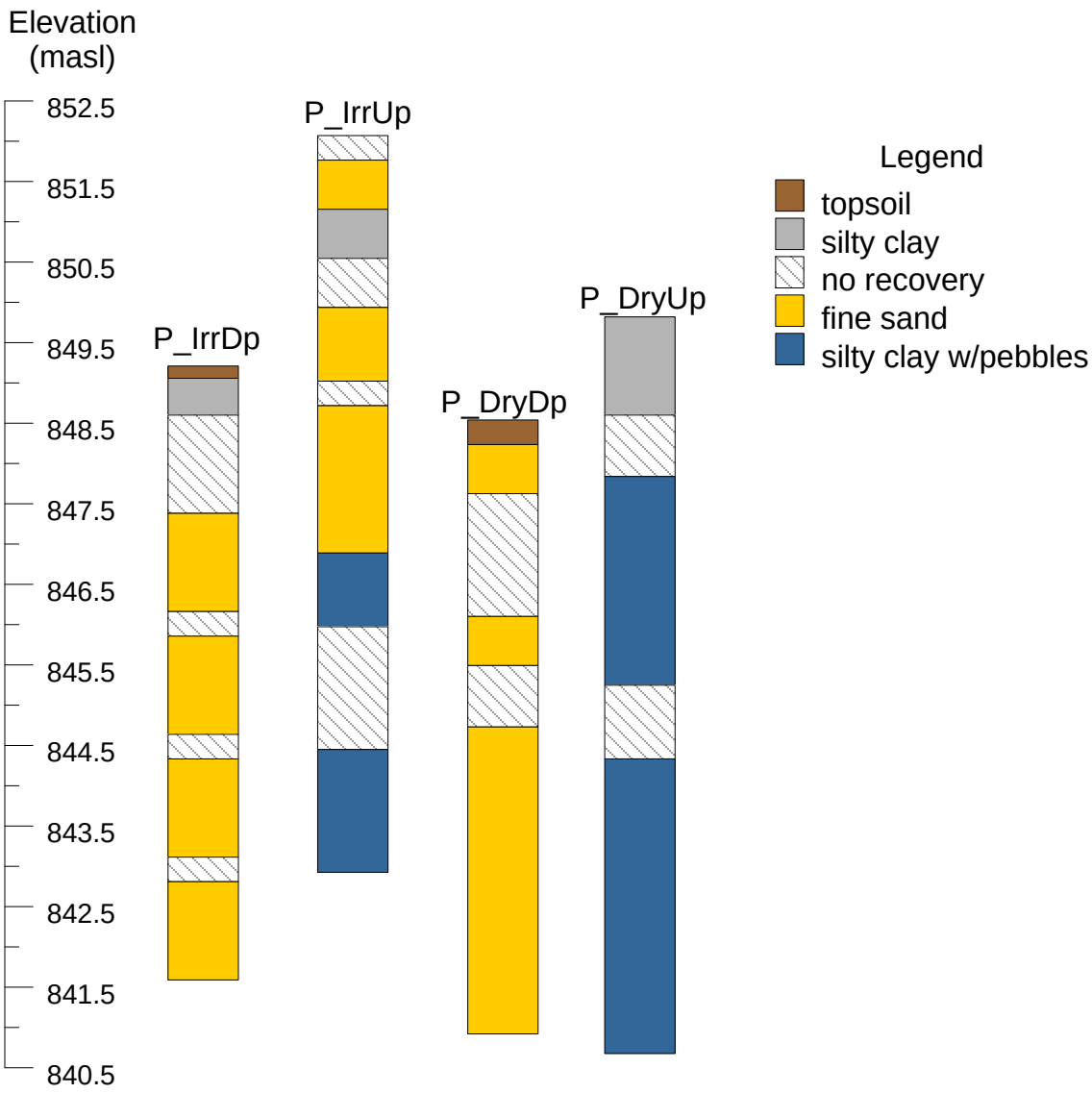

Figure B-2. Schematic of the lithology for boreholes drilled at the PP site. Horizontal distance between boreholes/wells is not to scale.

APPENDIX C: SOIL WATER RETENTION CURVES

Intact soil ring samples were collected from 20, 40, 60, 80, 100 and 150 cmbgs at each of the three LDF sub-sites (L_IrrDp, L_IrrFl and L_DryFl). Soil water retention curves were determined for each intact soil ring sample. The pressure plate extractor method (Klute, 1986) was used over a range of matric potential of approximately -0.01 m to -50 m. Additional measurements were made using the dewpoint potentiometer (Decagon, WP4C) method described by Hayashi et al. (2012) to a minimum matric head of approximately -1000 m. Resultant soil water retention data was fitted to the van Genuchten (1980) model to determine soil water retention parameters. Data points and fitted curves are shown in Figures C-1, C-2 and C-3. Note that the 80 cm sample from L_DryFl was destroyed during sample preparation and data could not be collected.

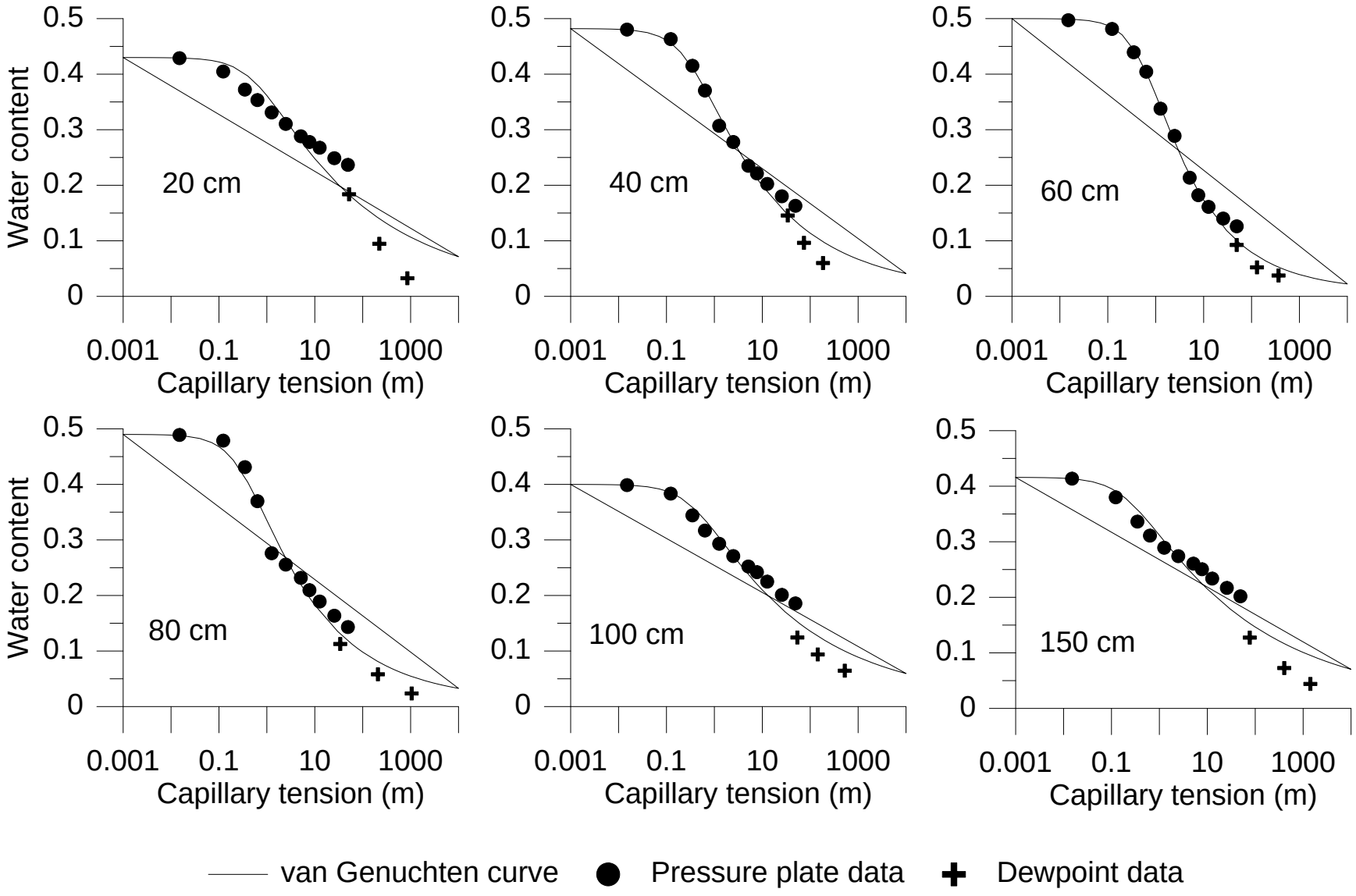

Figure C-1. Soil water retention curves for soil ring samples from L_IrrFl.

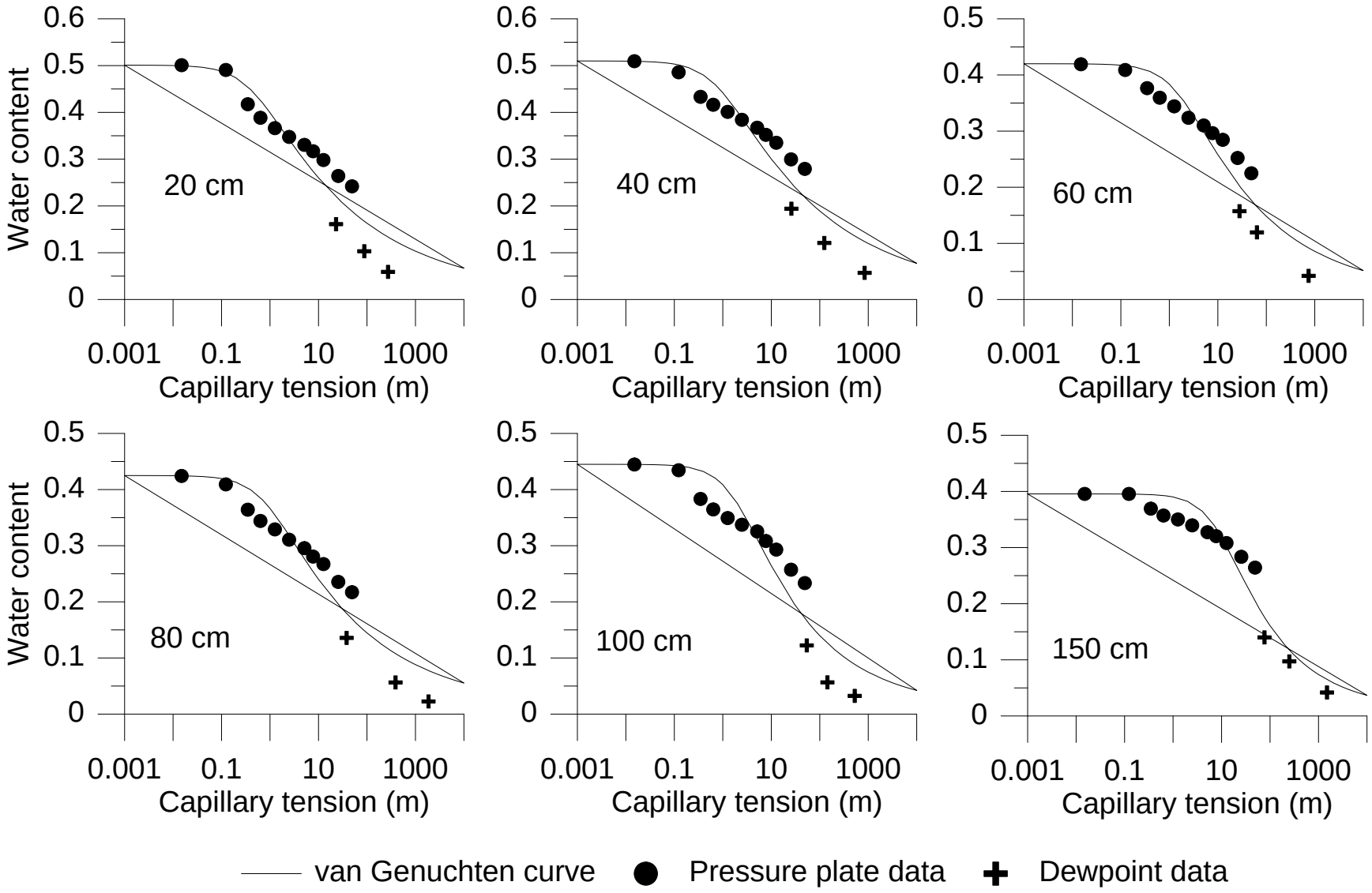

Figure C-2. Soil water retention curves for soil ring samples from L_IrrDp.

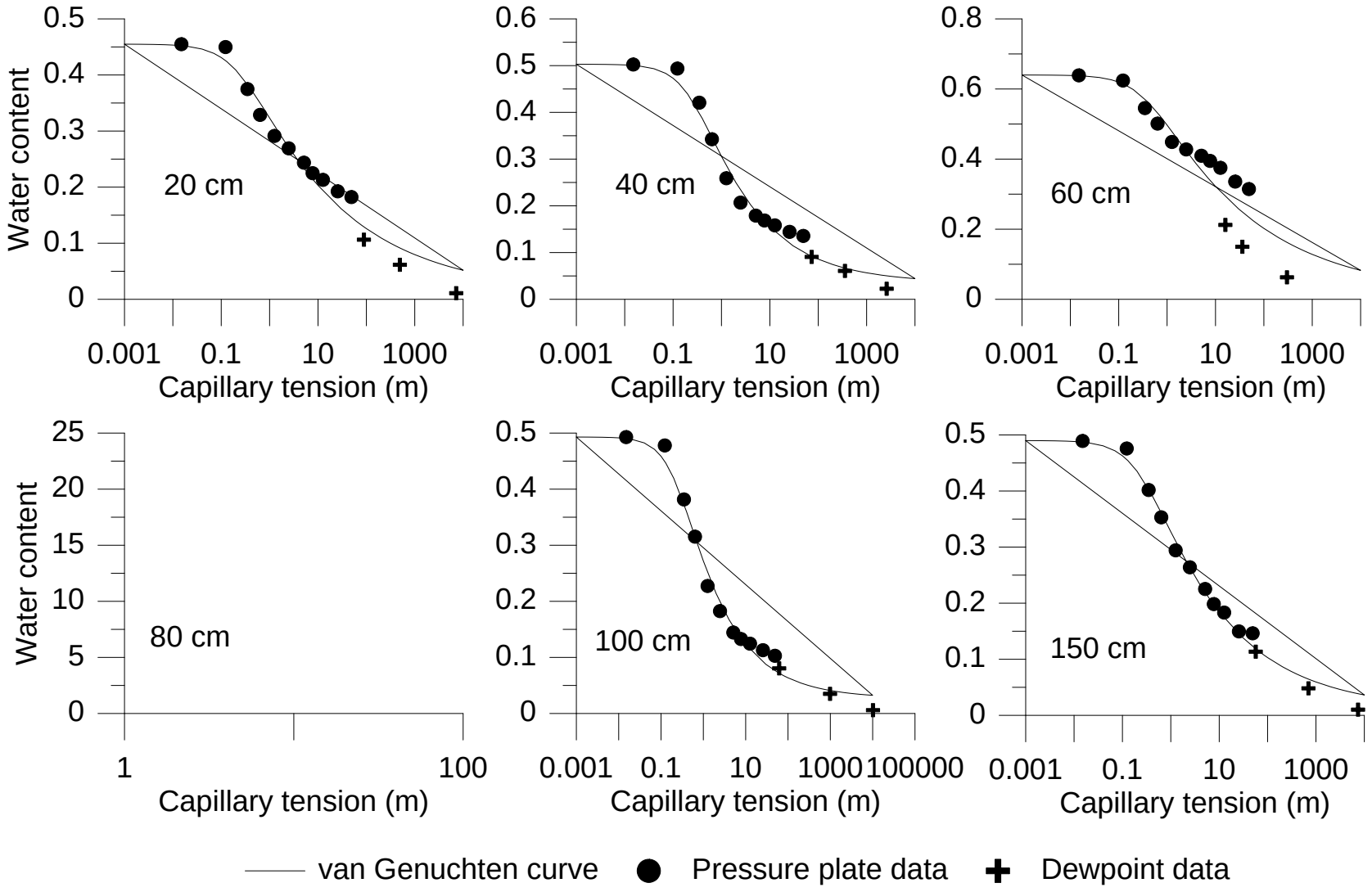

Figure C-3. Soil water retention curves for soil ring samples from L_DryFl.

APPENDIX D: WATER LEVELS

Hydraulic head for the eight monitoring wells at the LDF sites are shown in Figure D-1 from May-24, 2017 (installation of pressure transducers) to November 30, 2018. Wells were sampled on July 27 and October 26, 2017 and May 23 and September 7 2018, lowering the measured water level in some of the slower-recovering wells. The two deepest wells (L_IrrFl-3 and L_DryFl-3) recovered particularly slowly, on the order of weeks to months. As such, water levels below 902 and 998.5 masl were not shown for L-IrrFl-3 and L_DryFl-3, respectively, in order to allow for sufficient details to be shown for the water levels in shallower wells. Several data gaps occurred due to malfunctioning pressure transducers.

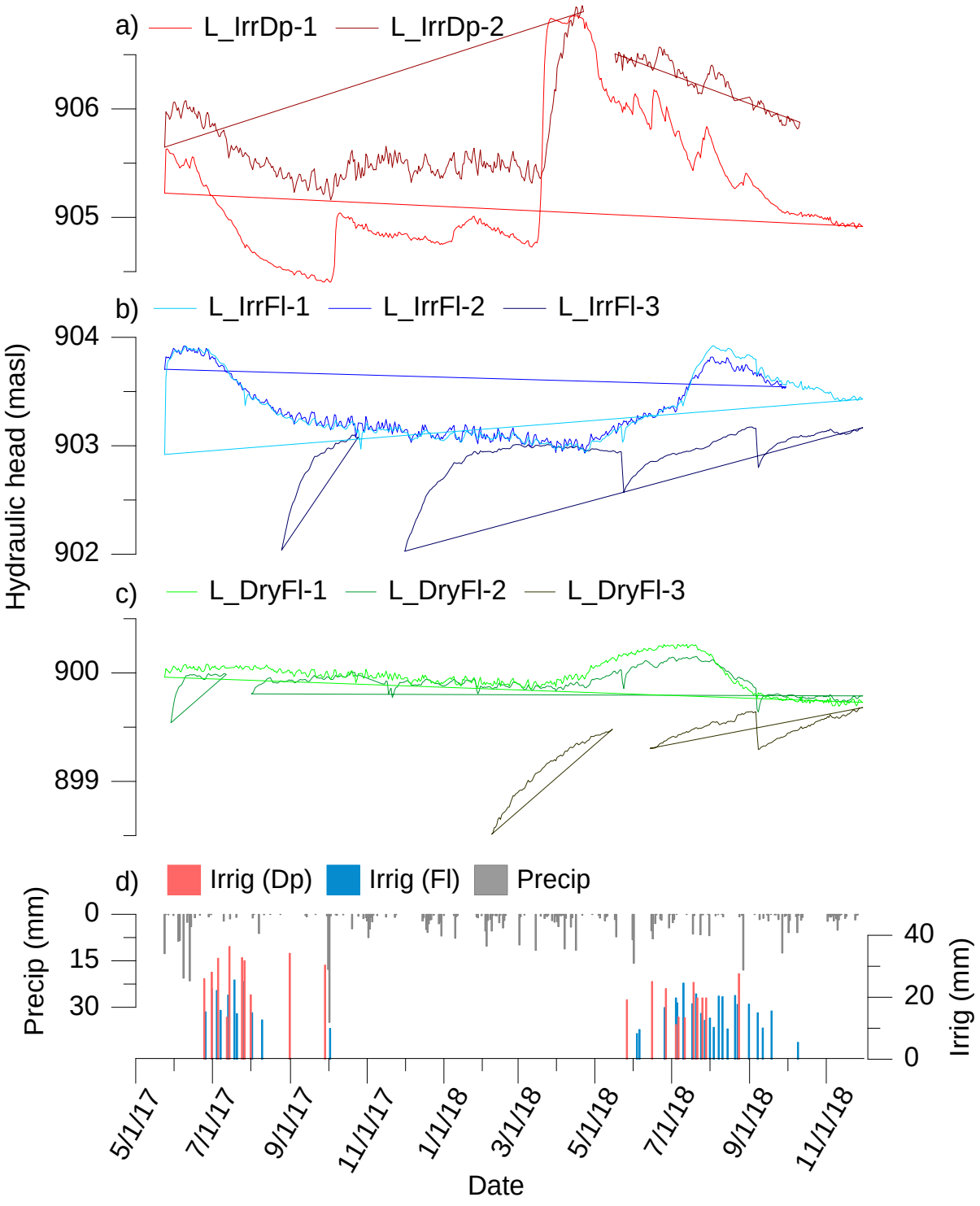

Figure D-1. Hydraulic head in monitoring wells at the LDF site for the duration of the study period.

APPENDIX E: DAILY SOIL MOISTURE DATA

Daily soil moisture data was measured at 20, 40, 60, 80, 100 and 150 cmbgs at the three sub-sites at LDF (L_IrrDp, L_IrrFl and L_DryFl) using HydraProbe sensors. Results from all depths are shown in Figure E-1 from June 1, 2017-November 30, 2018. Although soil moisture sensors were installed on May 8-9, 2017 at each sub-site, readings did not being until June 1, 2017 at L_IrrDp and June 9, 2017 at L_IrrFl due to technical difficulties with the data logging equipment. Some soil moisture sensor cables were destroyed at L_DryFl upon seeding, thus data recordings did not begin until after repairs were complete on June 22, 2017. The approximate length of the frozen period is indicated in Figure E-1, however, the exact length and depth of freezing was slightly different at each profile.

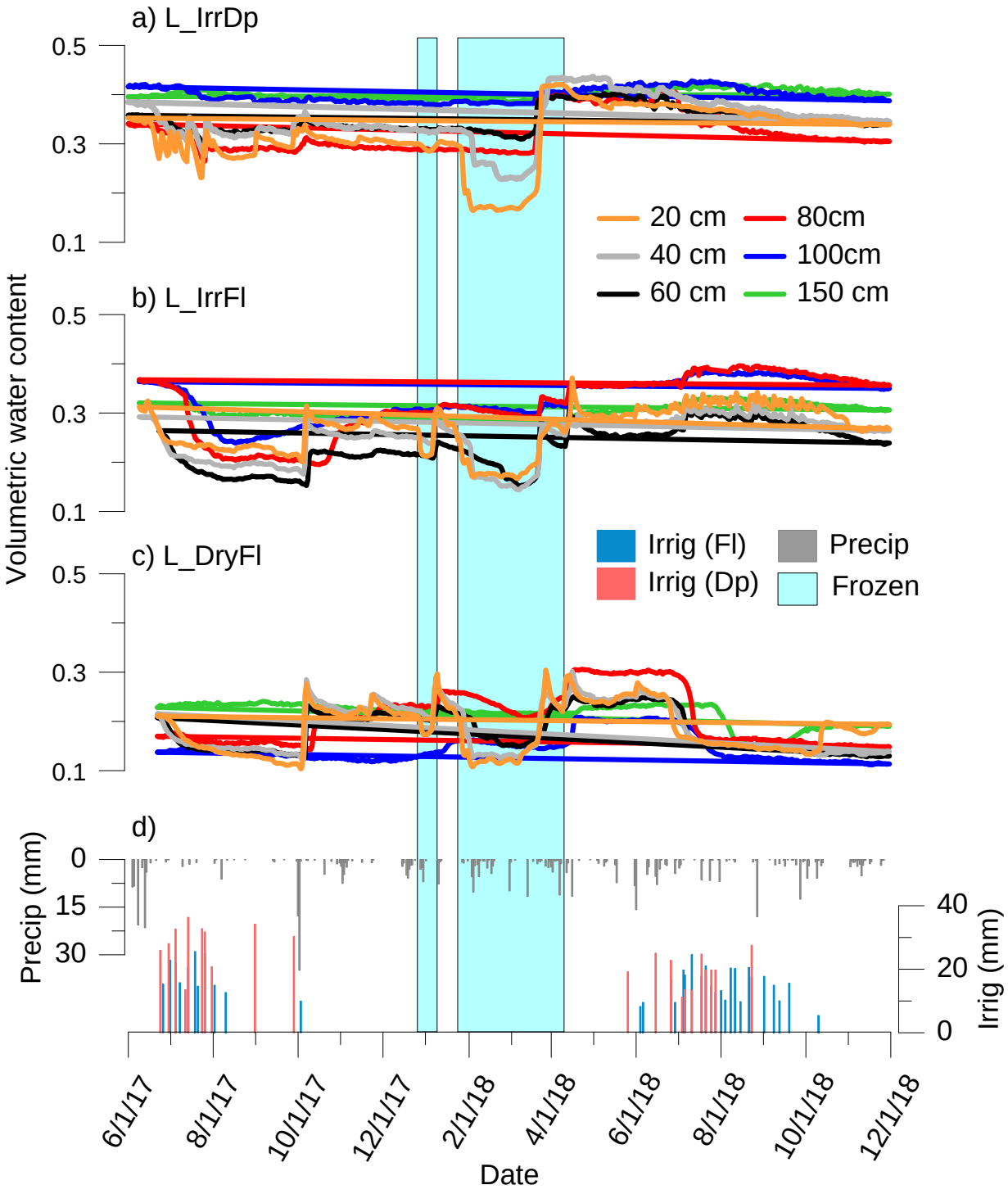

Figure E-1. Volumetric water content of soil profiles at the LDF site for the study period. The approximate length of the frozen period is indicated, but differed slightly for each profile.

APPENDIX F: ^{2}H PROFILES

The $\delta^{2}H$ profiles from stable isotope analysis are shown in Figure F-1, including results from surface water and groundwater samples. Spatial trends and relative isotopic ratios are similar to $\delta^{18}O$ profiles shown in thesis results (Figure 2.1.3).

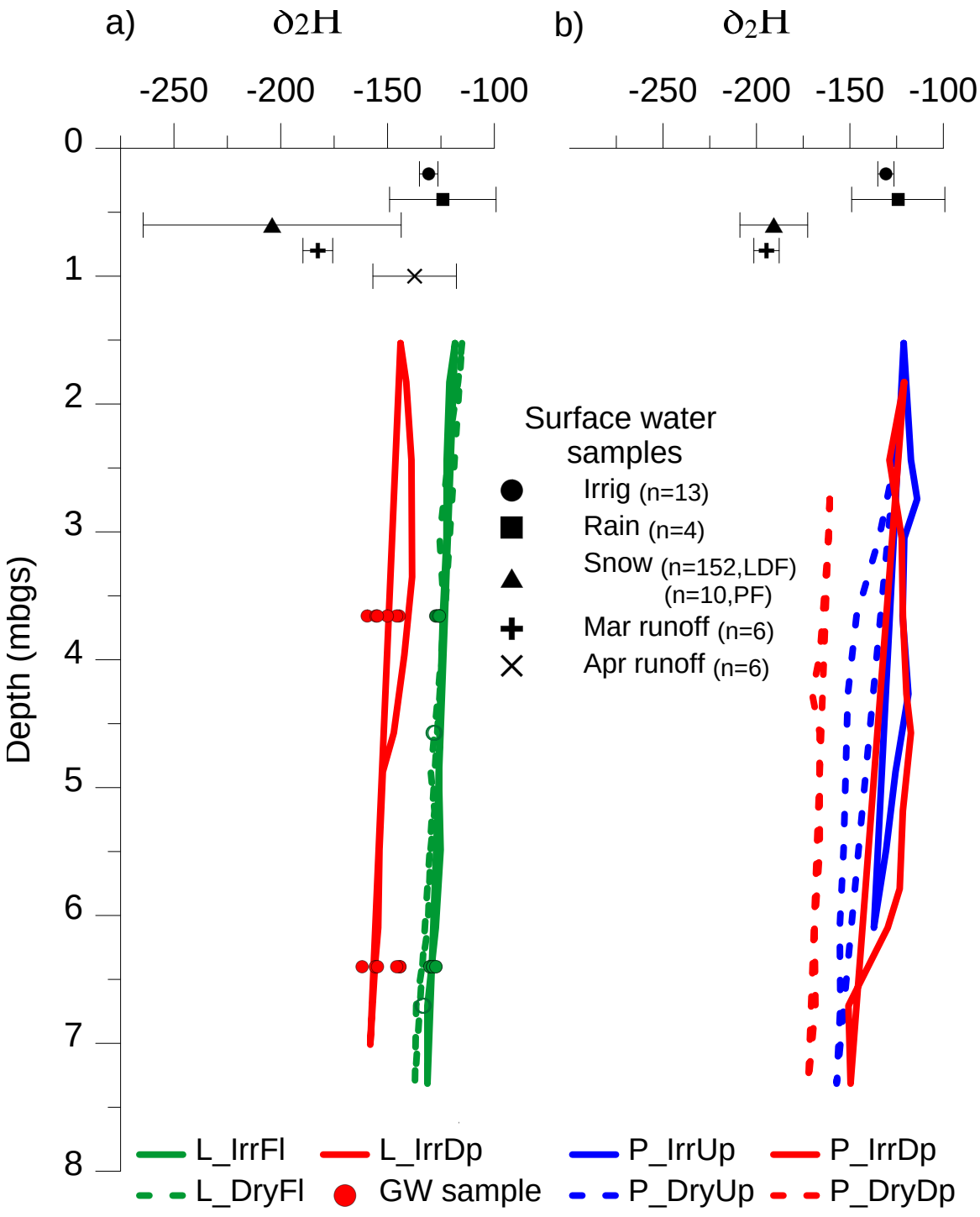

Figure F-1. Results from stable isotope analyses showing δ^2H for porewater extracts from LDF (a) and PP (b) borehole samples, groundwater samples from LDF, and snow, rain, irrigation and runoff samples from both study sites. Number of samples (n) is shown in the legend.

APPENDIX G: WATER BALANCE ERROR ANALYSIS

Uncertainty in recharge estimates obtained using the water balance method was quantified using standard error propagation analysis. A short description of the estimated error in each component of the water balance is given below.

The error in precipitation (*P*) was taken to be 1% full-scale (http://geonor.com/datasheets/geonor-t200b-series-all-weather-precipitation-gauges.pdf). The error in irrigation (*I*) was taken to be 2% (https://www.hydrologicalusa.com/products/rain-gauges/tb3-tipping-bucket-rain-gauge/). The error in evapotranspiration (*ET*) was calculated based on the method suggested by Hayashi et al. (2010) using:

$$\delta \mathrm{ET} = \frac{|Q_{L_{EB}} - Q_L|}{2} \tag{G.1}$$

where δET is the error in *ET*, Q_{L_EB} is the energy-balance-corrected value of *ET* (which overestimates) and Q_L is the raw value of *ET*, uncorrected for energy balance and determined from eddy-covariance measurements (which underestimates). Since the energy balance error was found to be 0.68 at the LDF site (section 2.3.1.1), equation G.1 can be simplified to:

$$\delta ET = Q_{L\_EB} \times 0.16 \tag{G.2}$$

Water balance calculations for the overwinter period required daily vapour flux estimates obtained using the Versatile Soil Moisture budget model (section 2.3.1.1) (Noorduijn et al., 2018; Hayashi et al., 2010). An uncertainty of 20% the simulated vapour flux value was assumed (a slightly higher uncertainty than was used for ET calculations). The error in the net change in water content ($\Delta\theta$) was calculated according to a soil moisture sensor accuracy of ± 0.04 m^3/m^3 found by Muenchrath (2018) and a soil profile length of 2.0 m (2000 mm), using the following equations:

$$\Delta\theta = (\theta_f \pm 0.04\ \frac{m^3}{m^3}) - (\theta_i \pm 0.04\frac{m^3}{m^3}) \quad \text{(G.3)}$$

$$\delta\Delta\theta = \sqrt{\left(0.04\frac{m^3}{m^3}\right)^2 + \left(0.04\frac{m^3}{m^3}\right)^2} \quad \text{(G.4)}$$

$$= 0.05657\frac{m^3}{m^3} \times 2000\ mm$$

$$= 113.1\ mm$$

where θ_i and θ_f are the initial and final average water contents of the profile, respectively in m^3/m^3. The estimated error for each water balance component and the resultant recharge are shown in Table 2.5.

APPENDIX H: CALIBRATION WATER CONTENT RESULTS

Simulated volumetric water content over the calibration period (August 10-September 30, 2018) either over- or under-estimated compared to observed values as shown in Figure H-1. However, the timing and magnitude of changes in water content was similar for simulated and observed values, with simulated values simply shifted to either higher or lower water content.

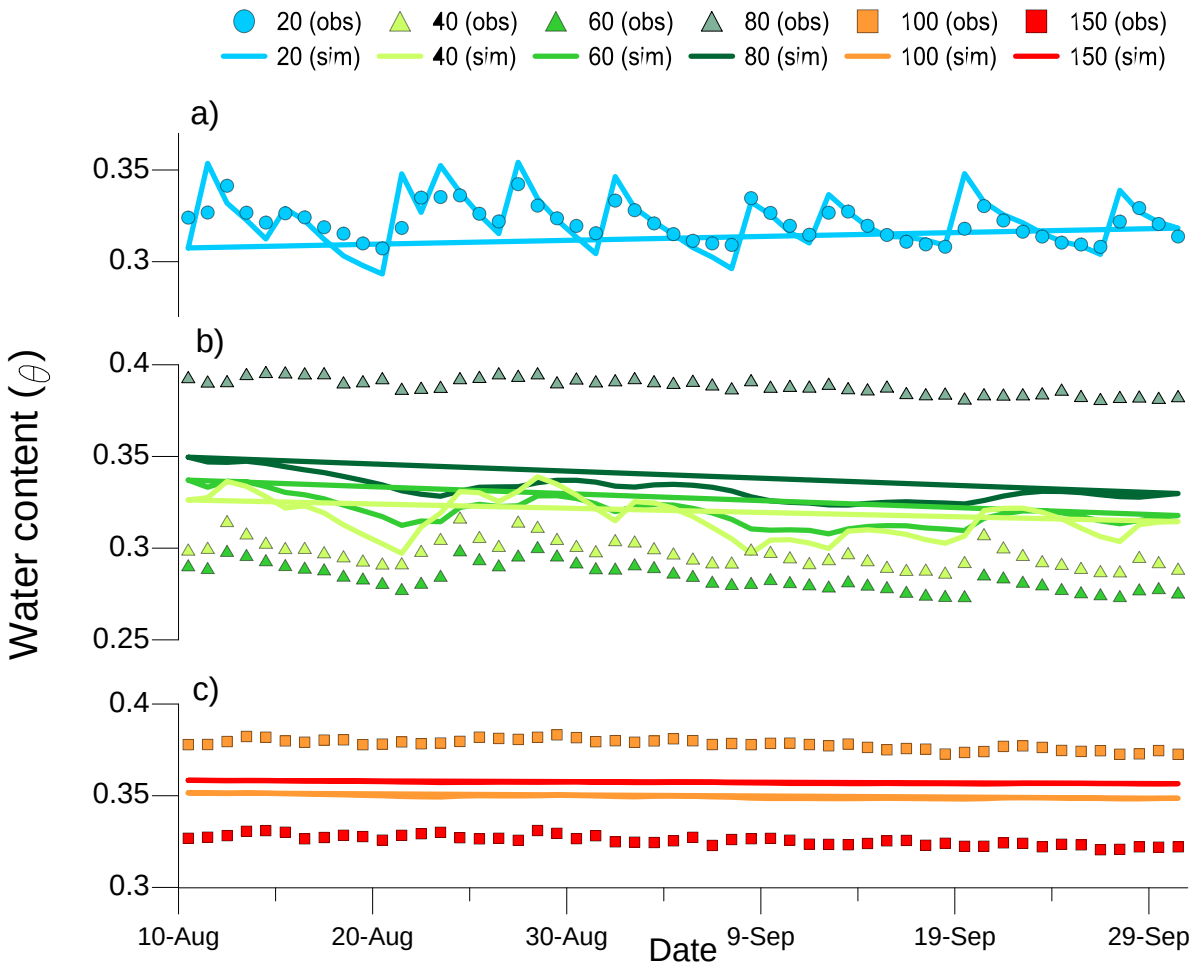

Figure H-1. Simulated volumetric soil water content results from the calibrated model (solid lines) plotted alongside field-measured water contents (symbols) from L_IrrFl. The model was divided into three layers: Layer 1 (a) from 0 to 35 cm, Layer 2 (b) from 35 to 85 cm and Layer 3 (c) from 85 to 200 cmbgs. The calibration period was August 10-September 30, 2018.